CELLULAR MECHANISMS OF LOW-THRESHOLD MECHANORECEPTOR RECEPTIVE FIELD DEVELOPMENT

By

Matthew B. Pomaville

A DISSERTATION

Presented to the Cell and Developmental Biology Graduate Program
and the Oregon Health & Science University
School of Medicine
In partial fulfillment of the requirements for the degree of

Doctor of Philosophy

September 2022

TABLE OF CONTENTS

Acknowledgements

There is no way to properly thank the large number of incredible people who have helped me along my graduate school journey, but I'm going to take this opportunity to express what thanks I can to the people who made this possible.

First, I want to thank Dr. Kevin Wright for being a wonderful graduate school mentor. I can't express how grateful I am for his guidance and support throughout graduate school. Whether through formal one-on-one meetings or our frequent casual discussions around the lab he has helped me become a more critical reader, a more thoughtful planner, and an all-around better scientist. His willingness to help me pursue questions I found interesting has helped me become the independent researcher I am today. Thank you for all the guidance, mentorship, teaching, and friendship you have provided over the years.

Next, I would like to thank my dissertation committee. Dr. Alex Nechiporuk, Dr. Tianyi Mao, and Dr. John Brigande for all their helpful advice during the completion of this project. Without their expertise and support over the years multiple aspects of this dissertation would not have been possible. I would also like to thank my outside reader, Dr. Swetha Murthy for her generosity in providing her expertise in the somatosensory system to my committee. All your contributions to this project and to my development as a scientist have strengthened my future independence.

I would like to thank all the members of the Wright lab that I've had the pleasure of working with over the years. You have all helped make the lab a place I looked forward to working in each day, even when my experiments weren't going as well as I'd have liked. In particular I would like to thank Dr. Pat Kerstein for the countless hours of

mentorship and scientific conversations throughout our time in the lab, and Dr. Alejandra Fernandez for being my partner on “team DRG” and always being my wild experiment sounding board.

I would also like to thank Dr. Philip Copenhaver and Lola Bichler for their support and help throughout the years. Whether it was navigating registering for classes, helping choose a lab, or applying to defend my dissertation you both were always ready and willing to jump in and solve problems that came up.

Before starting graduate school, I had multiple mentors who steered me onto the track I am on today. First, I would like to thank Dr. David Lent at Fresno State for giving me my first research experience. He took a freshman undergrad with no idea what he was getting into under his wing and allowed me to pursue my own arm of research in his lab. Without his mentorship and guidance, I don’t know that I would have gone to graduate school or chosen to pursue science as a career. Second, I would like to thank Drs. Brian O’Roak and Rebecca Barnard who mentored me as an undergraduate intern. You gave me my first exposure to “big science” and inspired me to come back to OHSU as a graduate student.

Last but not least, I want to thank all my friends and family who have provided me support along the way. To Jim Cameron and Adam Nalchajian, I want to say thank you for being the best friends a man could ask for. To Kylee Rosette, thank you for being a warm and welcoming person and bringing me into your group of friends here in Portland. To my other friends in Portland, in Fresno, and elsewhere: thank you for all the support over the years. It means so much to have a network of people I know I can count on to help me whenever I need it. My parents, Dave and Fran Pomaville, have

truly been the foundation upon which my entire life has been built, providing me with all the support, love, guidance, and independence I have needed throughout my life. You are both my heroes and without your values and your encouragement to achieve my goals I would not be here today. Finally, I want to thank my wife, Amanda Pomaville. There really aren't words that can express all the love and support you've given me throughout graduate school. I have truly appreciated getting to take this journey of life with you by my side and I look for our future together.

List of Tables

Chapter 1

Chapter 2

Chapter 3

Chapter 4

List of Figures

Chapter 1

Chapter 2

Chapter 3

Chapter 4

Abstract

We live in a world filled with nearly constant tactile stimuli, and our perceptions of and responses to these stimuli shape our many interactions. Processing the incredible diversity of tactile stimuli requires a wide array of specialized sensory neurons in the skin which pattern their peripheral receptors and central connections in a highly organized manner. The faintest stimuli we encounter are detected by a category of sensory neurons called follicle-innervating low-threshold mechanoreceptors (LTMRs). These specialized neurons form mechanosensory endings around hair follicle shafts in the skin, detecting hair movement, skin stroking, and skin indentation. In mice, these neurons are divided into three families based on their response to stimuli, their conduction velocity, and more recently, their expression of various molecular markers. Each family of LTMR neuron forms a receptive field in the skin, innervating a constrained number of hair follicles in adult animals. Recent work on these neurons has shown that all three subtypes of follicle-innervating LTMR tile in a pattern which prevents multiple same-subtype neurons from innervating the same hair follicle. This spatially tiled organization is essential for localization of stimuli on the body and for the receptive tuning of these neurons, but no mechanism exists which explains how neighboring same-subtype LTMR receptive fields interact to determine the hair follicles innervated by each neuron's receptive field.

Studies from invertebrate and non-mammalian animals have suggested dermal and epidermal innervation patterning is regulated through multiple molecular pathways and self-recognition signals. This results in a balance of attractive and repulsive cues which restrict neurons to innervating a constrained region of the body.

In this dissertation, I use a suite of molecular and conditional genetic tools to explore the development of follicle-innervating LTMR neurons in mice. I also address the hypothesis that LTMR receptive fields tile homotypically through a mechanism that is linked to population density. Using a neural overpopulation model driven by knockout of the pro-apoptotic protein *Bax* I assessed the changes in the number of hair follicles innervated by each LTMR neuron. I show that follicle-innervating LTMR neurons are present in the skin shortly after birth and develop their follicle-innervating nerve endings during the first two postnatal weeks. Additionally, I show that knockout of *Bax* increases the population of DRG neurons and that some follicle-innervating LTMR neurons adjust their receptive fields to accommodate this increase in populations, while others may not. In performing these experiments, I also developed a comprehensive series of protocols for immunofluorescence and histological staining of mouse skin in section and whole mount preparations. Finally, I present preliminary data suggesting a role for the cell adhesion molecule Teneurin transmembrane molecule 3 in the somatotopic organization of sensory neuron central projections into the spinal cord. Collectively, these results suggest that the organization and patterning of follicle-innervating LTMR receptive fields is regulated by a complex series of molecular interactions, and that some mechanism exists for homotypic exclusion of neurons from hair follicles in the developing skin.

Chapter 1: Introduction

Chapter Preface, General Somatosensory Anatomy

Somatosensation, or the sense of touch is an indispensable component of an animal's interactions with its environment. This sense is provided by multiple diverse families of neurons which detect stimuli through a combination of mechanically, chemically, or thermally gated ion channels and specialized, morphologically distinct receptive endings. In mammals, the bulk of the somatosensory neurons have their cell bodies located in the Dorsal Root Ganglia (DRGs), clusters of neurons and glia on either side of each spinal cord segment (Fig. 1). A single axon extends from the cell body of each neuron and bifurcates, extending one projection centrally, through the dorsal root and into the spinal cord. The other projection of the bifurcated axon extends peripherally, through the spinal nerve and into the skin and connective tissues (Rice and Albrecht, 2008). The centrally-projecting axon branch of each neuron forms synapses with interneurons and ascending neurons in the dorsal horn of the spinal cord which project to various brainstem nuclei (Gray and Carter, 2010). The peripherally-projecting axon branch of each neuron follows the spinal nerve into the periphery where it forms a specialized sensory ending containing ion channels. Activation of these ion channels causes an influx of cations and - if the stimulus exceeds the activation threshold of the neuron - depolarizes the neuron causing propagation of an action potential along the axon and into dorsal horn of the spinal cord.

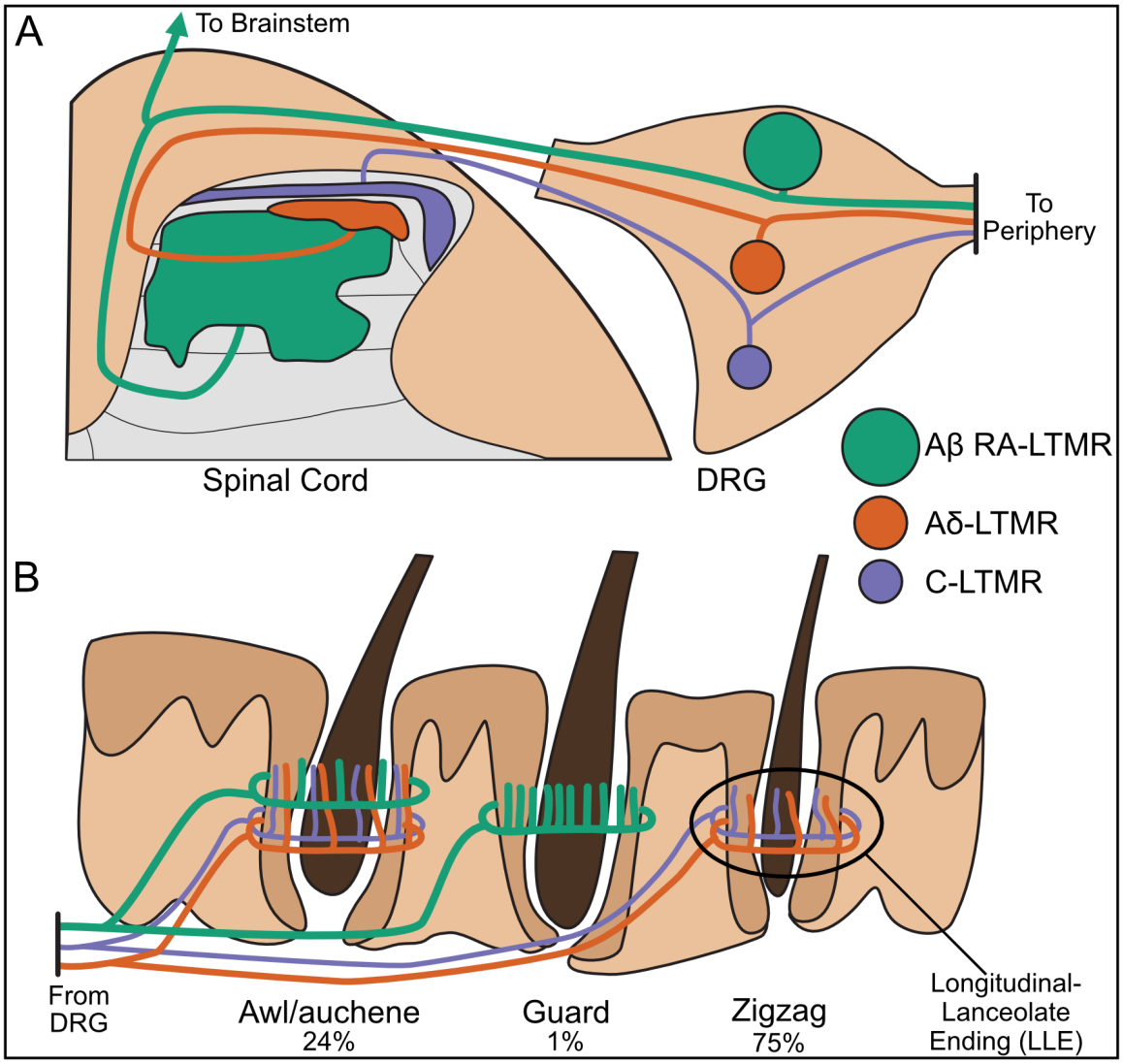

Figure 1 - Follicle-innervating LTMR neurons originate in the DRG and project to the spinal cord and skin.

A) Follicle-innervating LTMR neuron cell bodies in the DRG extend a single bifurcated axon which projects centrally to innervate specific laminae in the spinal cord dorsal horn.

B) The LTMR peripheral axon branch projects to the skin where it elaborates, forming LLEs around specific populations of hair follicles. The three hair follicle subtypes and their relative proportions in the skin are shown.

One of the most specialized populations of somatosensory neurons is the follicle-innervating low-threshold mechanoreceptors (follicle-innervating LTMRs). Neurons in this family form characteristic receptive fields of specialized endings, called longitudinal lanceolate endings (LLEs), around a constrained number of hair follicles in the skin (Li et al., 2011). Each LLE encircles a single hair follicle, extending several "palisade-like" protrusions towards the epidermis, parallel to the hair shaft. These protrusions contain mechanosensitive ion channels, such as PIEZO2, and use the hair shaft they surround like an antenna to amplify the faintest mechanical stimuli in the environment (Coste et al., 2010; Ranade et al., 2014). There are three genetically, functionally, and morphologically distinct populations of LLE-forming LTMRs in mice, the Aβ RA-LTMRs, Aδ-LTMRs, and C-LTMRs. These three populations were initially identified by their axonal conduction velocities and firing responses to skin indentation and hair follicle deflection. Modern molecular biology approaches have identified molecular and genetic identifiers for each of these neuronal populations allowing further exploration into their function and development (Sharma et al., 2020; Usoskin et al., 2015).

Our understanding of the somatosensory system has evolved significantly over time. While the concept of the five "major" senses – smell, sight, taste, touch, and hearing – dates back at least as far as Aristotle's *De Anima* (ca. 350 BCE), the first modern studies of somatosensation were undertaken by doctors and anatomists in the 18th and 19th centuries (Pacini, 1835; Polansky, 2009). As our collective understanding of biology has advanced so has our understanding of the sensory nervous system: first through the gross examination of discrete mechanosensory organs in the skin, then to the functional classification of sensory neurons by their response properties and

conduction velocities, and finally the identification of discrete, genetically defined populations of skin innervating neurons. This modern, genetically-based understanding of skin innervating neurons has opened many new avenues of research including detailed examination of the development and organization of somatosensory neurons and the structures with which they interact. One major finding to arise from the genetic dissection of somatosensory neurons is the spatial organization of skin innervation, and specifically hair follicle innervation, into discrete receptive fields which tile in a manner excluding neighboring neurons (Bai et al., 2015; Kuehn et al., 2019; Li et al., 2011; Rutlin et al., 2014; Wu et al., 2012). This discrete organization is essential for the localization of physical stimuli on the body, the proper tuning of neuronal responses tostimuli, and the coordination of an animal's reaction to stimuli. The objective of this dissertation is to explore how these follicle-innervating sensory neurons develop and organize their receptive fields in a tiled manner. Ultimately, a thorough understanding of the molecular mechanisms by which somatosensory neurons organize and self-regulate during development will inform our understanding of human conditions such as autism spectrum disorder, mechanical allodynia, and sensory processing disorders.

Mammalian Somatosensory Research in The Pre-Genetics Era

The beginnings of our modern understanding of somatosensation, where distinct modalities of touch sensation are conveyed by specialized populations of neurons, arise from the work of multiple individuals in the 19th century. Physiologists and anatomists Filippo Pacini, Georg Meissner, and Friedrich Sigmund Merkel, among others, described the first identified cutaneous nerve endings, the Pacinian or lamellar corpuscle, Meissner's or tactile corpuscle, and Merkel cells or tactile disks(Merkel, 1875; Pacini, 1835; Wagner and Meissner, 1852). This work was followed by that of

Magnus Blix, Alfred Goldscheider, and Henry Donaldson who, in independent studies, showed that stimulation of different regions of the skin with an electrical current could elicit hot or cold sensations, and that these same regions were specifically sensitive to either hot or cold temperature stimulation (Norrsell, 2000; Pearce, 2005). In 1894, Maximilian von Frey proposed that skin innervation could be broken into four separate senses: warmth, cold, touch, and pain; and that each of these senses was detected by discrete spots in the skin (von Frey, 1894; von Frey, 1896). This was notable as the first proposal of pain as functionally separate from other somatosensory modalities (Pearce, 2005).

As the 20th century began a new branch of study into skin innervation emerged, making use of an amplifier and recording electrode to directly measure the electrical discharges in a carefully prepared segment of skin with an attached nerve bundle (Adrian, 1926). This system allowed detailed measurements of nerve fiber characteristics to be made and set the stage for multiple decades of study into peripheral nerves. Early work using this skin-nerve preparation in both frog and cat skin showed a direct correlation between nerve fiber diameter, conduction velocity, and the magnitude of the voltage spike when the skin preparation was mechanically stimulated (Zotterman, 1939). Joseph Erlanger and Herbert Spencer Gasser used these conduction velocity and fiber diameter correlations to define electrophysiological categories of peripheral nerve fibers. The largest and fastest conducting nerve fibers were classified as Group A nerve fibers, while the narrower and slower conducting fibers were classified as Group B and C nerve fibers. The Group A fibers were further subdivided into Group Aα, Aβ, Aγ, and Aδ in descending order of size and velocity

(Gasser and Erlanger, 1927). It was later shown that these differences in conduction velocity were a result of myelination, neurons with thicker myelination have significantly higher conduction velocities than those with thin or no myelination (Huxley and Stämpfli, 1949; Tasaki, 1939). As more studies on conduction velocity and nerve fiber diameter were performed these categories were refined and it was shown that conduction velocity and nerve fiber diameter increase after birth, suggesting the postnatal maturation of both somatosensory axons and their myelination (Blair and Erlanger, 1933; Hursh, 1939). These classifications, which are still in use in the modern somatosensory neuron nomenclature, provided a foundational idea that multiple populations of somatosensory neurons with distinct physiological properties existed and play specific sensory roles, mirroring the work of von Frey and others.

Using the axon diameter and conduction velocity categories laid out by Gasser and Erlanger multiple groups began working towards describing more electrophysiological and morphological characteristics of somatosensory neurons. Due to their large size, distinct morphology, and innervation by a single neuron, the Pacinian corpuscle was one of the first cutaneous structures to be described in physiological detail. Work by Alvarez-Buylla, de Arellano, and Loewenstein showed Pacinian corpuscles to be responsive only to direct mechanical stimulus of the corpuscle ending, trigger action potentials only at the onset and offset of pressure and conduct these action potentials at the rate of an Aβ neuron (Alvarez-Buylla and de Arellano, 1952; Loewenstein, 1961). A number of studies followed, using similar techniques to analyze cutaneous innervation in rabbits, cats, and primates, and providing detailed physiological definitions, including stimulus type, receptive field area, innervation target,

conduction velocity, and stimulus response adaptation for 12 distinct subtypes of Group A somatosensory neurons (Brown and Iggo, 1967; Burgess et al., 1968; Iggo and Muir, 1969; Perl, 1968). Separately, nonmyelinated C neurons were identified and recordings from isolated neurons were made by Ainsley Iggo (Iggo, 1960).

The first clear descriptions of sensory neurons specifically innervating hair follicles also appear during this period. By recording from nerve bundles while stimulating the hair shaft without disturbing the surrounding skin it was shown that hair follicles functioned as sensory receptors independent of other skin innervating neurons (Weddell et al., 1955). Histological studies of neurons innervating hair follicles in human and cat skin described two groups of nerve fibers around the follicle: an outer group encircling the follicle perpendicular to the direction of hair growth, and an inner group which runs parallel to the hair shaft and terminates near the dermal/epidermal boundary (Winkelmann, 1959). These studies also showed that larger hair follicles (referred to as tylotrich or later, guard hairs) were innervated by more nerves than smaller hair follicles (Bonnet, 1878). Further electrophysiological work revealed three distinct populations of hair follicle innervating sensory neurons based on conduction velocity and stimulus response properties. First, a large population of neurons innervating primarily non-tylotrich hairs (later classified as awl/auchene and zigzag hairs) with a rapidly-adapting response to stimulus, a small receptive field, and a conduction velocity in the range of Aδ sensory neurons was described (Burgess et al., 1968; Hunt and McIntyre, 1960; Perl, 1968). Later, another population (initially thought to be two separate populations) innervating the sparse tylotrich (guard) hairs was identified (Tuckett et al., 1978). This population of neurons formed large receptive fields, responded only to hair follicle

movement, and had a conduction velocity range consistent with Aβ neurons. (Burgess et al., 1968; Perl, 1968). These two populations of neurons became known as the Aδ-LTMR and Aβ RA-LTMRs in later work. The final population of LLE forming LTMR neurons to be described were unmyelinated, had a conduction velocity range consistent with C neurons, required larger stimuli than the Aβ- and Aδ-LTMR populations, and had small receptive fields. Despite not being shown to specifically innervate hair follicles until 2011, these C-LTMR neurons were shown to be an independent population of sensory neurons from the higher threshold C-nociceptive free nerve endings through electrophysiological studies relatively early in the development of the field (Iggo, 1960; Li et al., 2011).

These functional and electrophysiological definitions of the three populations of LLE forming, follicle-innervating LTMRs remain, relatively unchanged, as the working classifications for follicle-innervating neurons. The next major leap in the field of cutaneous sensory innervation would come with the rise of molecular biology and the discovery of molecular markers which could define these populations of neurons in live tissue through non-electrophysiological means and in fixed tissue.

The Genetic Era of Somatosensory Research

The dawn of the genetic era of biology brought a new direction to the study of somatosensory neurons: finding molecular markers that could uniquely identify the neuronal subtypes that had been described through physiological and morphological studies. Since the 1980s, most somatosensory neuron subtypes have been defined either by single molecular identifiers or through combinatorial labeling approaches. The first molecules shown to have the potential to serve as markers for specific somatosensory neuron populations were the canonical neurotrophins and their

receptors. Shortly after the receptor tyrosine kinases *trkA*, *trkB*, and *trkC* were shown to be the canonical high affinity receptors for *NGF*, *BDNF*, and *NT-3,* respectively, multiple labs identified that cell bodies in the developing DRG show differential expression of the trk-family receptors (Carroll et al., 1992; Lamballe et al., 1991; Squinto et al., 1991). Knockout of the canonical NGF receptor *trkA* caused a 70-90% reduction in DRG cell bodies at multiple spinal cord levels. Examination of the remaining cell bodies showed this reduction was primarily driven by the loss of neurons with cell bodies with cross sectional area smaller than 175 μm^2 (Smeyne et al., 1994). Depletion of NGF through *in utero* administration of anti-NGF serum caused a nearly complete loss of *trkA* expressing neurons in the DRG while leaving the *trkB* and *trkC* populations unchanged (Carroll et al., 1992). Knockout mice for NGF confirmed these findings, showing a nearly complete loss of small cell body, peptidergic neurons in the DRG (Crowley et al., 1994). Mice with homozygous mutations in *trkB* or its ligands *BDNF* and *NT-4* both show significant reductions in DRG neurons, specifically loss of medium size myelinated neurons (Ernfors et al., 1994a; Jones et al., 1994; Klein et al., 1993). Interestingly, deletion of *NT-4* caused a less severe loss of neurons in the DRG than deletion of *BDNF*, suggesting *BDNF* may compensate for the loss of *NT-4* in some neurons but not others (Conover et al., 1995; Liu et al., 1995). Deletion of *trkC* or its binding partner *NT-3* resulted in loss of 50-80% of DRG neurons and a significant reduction in the myelinated area of the dorsal root (Fariñas et al., 1996; Klein et al., 1994). *NT-3* knockout mice also showed a complete lack of proprioceptive endings in the muscle, motor coordination deficits and abnormal movements, and a loss of cell bodies positive for a proprioceptive neuron marker (parvalbumin) but no change in the population of

peptidergic and nociceptive cell bodies in the DRG (Ernfors et al., 1994b). A comprehensive analysis of the effects of knockout of the canonical neurotrophins and their receptors on hairy skin innervation revealed follicle-innervating LLEs to be reduced in *NGF/trkA* and *BDNF/trkB* knockout animals, while knockouts of *NT-3*, *NT-4*, *trkC*, and *p75-NTR* showed no effect on follicle innervating LTMR neurons (Fundin et al., 1997b).

The work defining somatosensory neuron populations by their expression of neurotrophin receptors was paralleled by studies examining molecular markers related to the specific modalities detected by each population. Nagy and Hunt identified markers which divided the small-diameter C fibers into two populations: those expressing the neuropeptides calcitonin-gene related peptide (CGRP) and substance P, and those which did not express neuropeptides but instead contained fluoride-resistant acid phosphatase and could be labeled with Isolectin-B4 (IB4), a lectin extracted from *Griffonia simplicifolia* (Nagy and Hunt, 1982; Silverman and Kruger, 1990). Following the identification of these labels, these two populations were shown to be functionally distinct through electrophysiological experiments, with peptidergic (CGRP/substance P expressing) neurons showing a larger response to heat than non-peptidergic (IB4 positive) neurons (Stucky and Lewin, 1999).

The heat response in peptidergic C fibers was driven by the capsaicin-sensitive ion channel TRPV1, identified in 1997, marking the first population of sensory neurons to be labelled by a specific ion channel related to its function (Caterina et al., 1997). As other *Trp*-family genes were identified their expression in DRG neurons was examined. TRPM8, a menthol activated channel sensitive to cold stimulus, was expressed in a population of peptidergic DRG neurons which had minimal overlap with TRPV1

expressing neurons (Bautista et al., 2007; Dhaka et al., 2008; McKemy et al., 2002). Finally, TRPA1 (previously called ANKTM1) was identified as a chemosensory channel which detects isothiocyanate and thiosulfinate compounds like those found in mustard, garlic, and onions (Bandell et al., 2004; Bautista et al., 2005; Story et al., 2003). TRPA1 was found to be expressed in a subpopulation of TRPV1 neurons but not in TRPM8 neurons, suggesting a role in sensitization of heat sensitive neurons after exposure to inflammatory or irritating chemical compounds (Bautista et al., 2006). This work clearly defines the peptidergic nociceptors as the population directly responsible for the detection of temperature stimuli and a potential major component of the inflammatory pain pathway.

In parallel with the identification of the *Trp*-family proteins and their roles in the peptidergic nociceptors, the Mas-related G protein-coupled receptor (*Mrgpr*) protein family was identified and two of its members, *MrgprA3* and *MrgprD*, were found to identify unique populations of non-peptidergic IB4-expressing nociceptors (Dong et al., 2001). *MrgprA3* labels a population of neurons responsive to chemically-induced itch but that does not trigger a pain response when stimulated at a high threshold (Han et al., 2013; Liu et al., 2009). *MrgprD* labels a population of pain and itch sensitive neurons which may play a role in modulating other mechanosensory and thermosensory nociceptors (Liu et al., 2012; Shinohara et al., 2004). Other *Mrgpr*-family proteins have been shown to have complex roles in modulating nociception, but none have been shown to identify distinct populations of neurons in the DRG, nor do they appear to be involved in the primary sensory function of the neurons (Green, 2021).

The final group of somatosensory neurons to have a defined molecular mechanism of action identified were the mechanoreceptors. While mechanoreceptive neurons were the first members of the somatosensory system to be described, it was not until 2010 that the ion channels responsible for translating mechanical force into electrical impulses, *Piezo1* and *Piezo2,* were identified and cloned (Coste et al., 2010). Prior to this discovery, molecular identifiers that could uniquely identify some LTMR subpopulations were identified. Work by Pablo Brumovsky showed that a population of small diameter DRG neurons express tyrosine hydroxylase (TH). These TH-positive neurons rarely colocalize with CGRP or IB4 labeling and do not express other components of the noradrenergic synthesis pathway like Dopamine β-hydroxylase (DBH) or dopamine transporter (DAT) (Brumovsky et al., 2006). Further examination of the TH-positive cells showed they do not express common markers for peptidergic or non-peptidergic nociceptors. Skin-nerve preparation recordings from these neurons showed they are C fibers which respond to low-threshold mechanical stimulation of the skin, identifying TH as a molecular label for C-LTMR neurons (Li et al., 2011). Based on studies showing loss of Aδ fibers in mice lacking the TrkB ligand NT-4 it was hypothesized that TrkB could be used as a marker for the Aδ-LTMRs. Using a TrkB-GFP knock-in mouse, it was shown that TrkB is expressed in a population of medium diameter DRG neurons which did not overlap with labeling for C-LTMRs (TH), non-peptidergic nociceptors (IB4), or Aβ RA-LTMRs (Ret). Recordings from TrkB-GFP-positive neurons showed Aδ conduction velocities and a response to gentle touch, confirming TrkB as a unique marker for the Aδ-LTMR neurons (Li et al., 2011).

Further identification and research into LTMR neurons would rely heavily on the inducible Cre^{ER}/Cre^{ERT2}-*loxP* genetic driver system. This system uses a modified form of a bacterial recombinase protein *Cre*, which recognizes and cuts DNA at a 34-mer sequence called a *loxP* site (Fig. 2) (Sauer and Du, 1987; Sauer and Henderson, 1988). By inserting the *Cre* gene at a specific locus the expression of the targeted locus can be assessed using Cre-dependent reporters. In the Cre^{ER} and Cre^{ERT2} systems *Cre* recombinase is fused to a modified form of the mammalian estrogen receptor (Metzger and Chambon, 2001). This sequesters *Cre* outside the nucleus until the estrogen modifying drug tamoxifen is administered, allowing both temporal and genetic control over the expression of a reporter in cells.

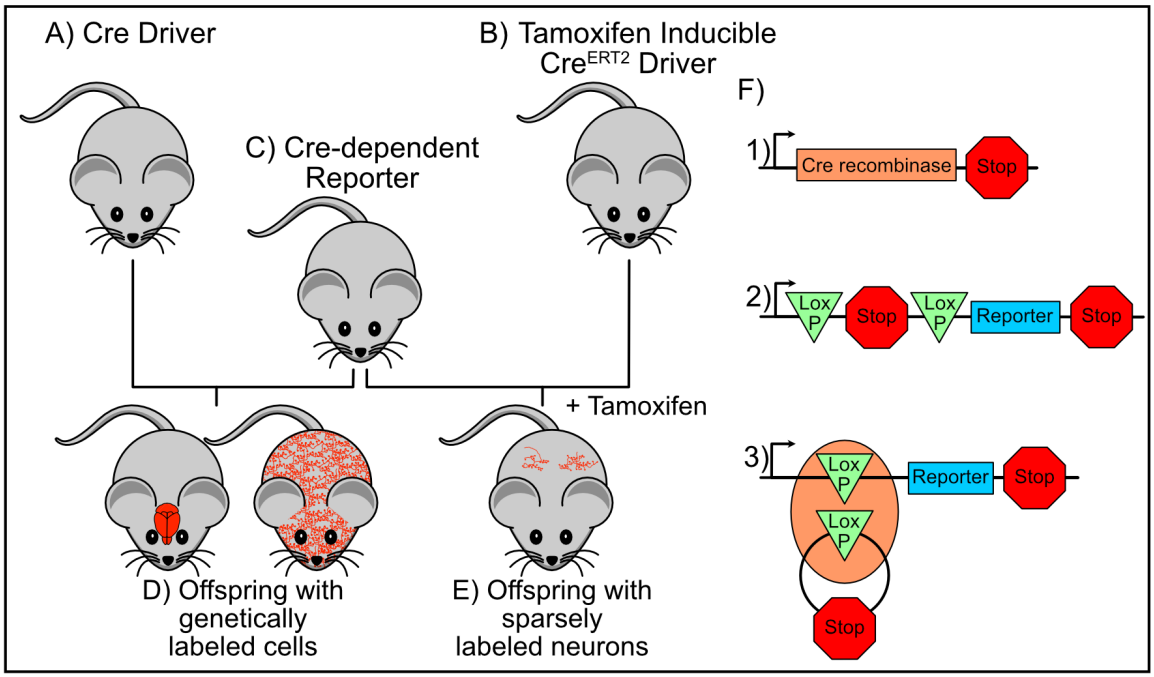

Figure 2 - The Cre-Lox recombination allows temporal and genetic control of cell labeling.

A-E) By combining a Cre driver under control of a chosen promoter (A) with a Cre-dependent reporter line (C) cells expressing proteins under control of the chosen promoter can be labeled (D). By using a Cre^{ERT2} driver (B) the frequency and timing of expression of the reporter (C) can be controlled by administration of tamoxifen to achieve sparse labeling (E).

F) Schematic illustrations of standard genetic cassettes for 1) Cre drivers, 2) Cre-dependent reporters, and 3) a recombined (active) Cre-dependent reporter where Cre-recombinase (orange) has excised a stop codon allowing expression of the reported (blue).

The Cre^{ERT2}/*loxP* system was essential in the discovery of subtype specific markers for the Aβ RA-LTMR neurons. These neurons were known from electrophysiological studies to innervate hair follicles in hairy skin and innervate Meissner and Pacinian corpuscles in glabrous skin. Unlike the Aδ-LTMRs and C-LTMRs which are dependent on TrkB and TrkA during development, the Aβ RA-LTMRs show no loss of cells due to deletion of any canonical neurotrophin or Trk-family receptor. It is known from previous work looking at the expression of non-*Trk* growth factors in the DRG that three of the four members of the GFR family (*GFRα1*, *GFRα2*, and *GFRα3*) were expressed in DRG neurons during development (Luo et al., 2007). These GFR-

family of receptors bind members of the glia-derived neurotrophic factor (GDNF) family, and signal internally through the receptor tyrosine kinase Ret (Durbec et al., 1996; Trupp et al., 1996). This suggested that GFR/Ret signaling plays a role in Aβ RA-LTMR development and may be a target for identifying these cells. In adult mice, Ret is expressed in approximately 60% of DRG neurons, but during development Ret is primarily expressed in two sequential waves, one beginning before embryonic day 11.5 (E11.5) and marking early-born, large diameter neurons, and another beginning at E15.5 and marking small and medium diameter neurons (Luo et al., 2007; Marmigère and Ernfors, 2007; Molliver et al., 1997). It was shown that by using the inducible genetic driver *Cre^{ERT2}* expressed from the *Ret* locus and early prenatal (E10.5-12.5) administration of tamoxifen the Aβ RA-LTMR neurons could be labeled (Luo et al., 2009). It was later shown that a reporter driven by the gene locus for Neuropeptide Y receptor 2 (Npyr2) also specifically labeled Aβ RA-LTMR neurons, and that this population showed no overlap with markers for C-LTMRs or Aδ-LTMRs (Li et al., 2011).

The advent of single cell RNA sequencing brought about a new approach to classify cells into distinct types using unsupervised clustering algorithms to group cells based on similar transcriptional profiles. The first single cell transcriptomic study of DRG neurons was published in 2015 on approximately 800 cells collected from adult mouse DRGs (Usoskin et al., 2015). Cluster analysis of transcriptomes from these cells revealed 5 major clusters: non-neuronal cells; cells containing transcripts for neurofilament heavy chain (*Nefh*) and parvalbumin (*Pvalb*) thought to be myelinated neurons; cells containing transcripts from genes associated with peptidergic nociceptors (*Tac1* [substance P], *Ntrk1* [TrkA], and *Calca* [CGRP]); cells containing transcripts from

genes associated with nonpeptidergic nociceptors (*Mrgprd* and the purinergic receptor *P2rx3*); and cells containing transcripts for tyrosine hydroxylase (*Th*). Subclustering of each of the main neuronal clusters revealed five myelinated neuron clusters, three nonpeptidergic neuron clusters, and two peptidergic neuron clusters. The major cluster containing *Th* could not be subclustered. From analysis of these subclusters it was clear that the Aβ RA-LTMRs and Aδ-LTMRs grouped into clusters distinct from each other, and from other myelinated neurons while the C-LTMR neurons remained indistinguishable from the C-nociceptor neurons. These data also provided additional markers for Aδ-LTMRs (*Necab2*) and Aβ RA-LTMRs (*Calb*), both calcium binding proteins. Another single cell RNA sequencing study, this one sequencing less cells (~200) but at a higher read depth to capture low expression transcripts, was published in 2017. The findings largely align with those of the 2015 study regarding the follicle-innervating LTMRs, but suggests more complexity lies within the nociceptor populations than had been previously reported (Li et al., 2016).

These molecular studies on somatosensory neurons both confirm and expand upon the early anatomical and electrophysiological studies of skin innervation. Molecular identifiers have been defined for most populations of neurons reported in early studies, and recent analyses of transcriptomic data have suggested even more complexity in the nociceptive neuron populations than was previously thought. The genetic and molecular labeling tools developed for the follicle-innervating LTMRs have proven essential for continuing research into these neurons on a cellular level.

LTMR Neuron Class	Protein Markers	Genetic Markers
Aβ RA-LTMRs	Calbindin	Npy2R (transgenic), Ret (embryonic)
Aβ SA-LTMRs	Unknown	TrkC (embryonic)
Aδ-LTMRs	TrkB, NECAB2	TrkB (embryonic)
C-LTMRs	TH, Vglut3	Th (postnatal)

Table 1: Summary of Genetic and Protein markers for LTMR neuron subtypes

Anatomy and Functional roles of follicle-innervating LTMR neurons

The identification of unique genetic and molecular markers for each follicle-innervating LTMR neuron subtype has greatly expanded research into the function and anatomy of these neurons. The three subtypes of LLE forming follicle-innervating LTMRs share a similar pseudounipolar anatomy, originating in the DRG and extending a bifurcated axon into the skin and spinal cord dorsal horn. In the skin this axon elaborates, forming LLEs – finger-like projections parallel to the hair shaft – around a constrained number of hair follicles in the skin. Each LTMR subtype selectively forms endings around two out of the three populations of hair follicles on the mouse: Aβ RA-LTMRs form endings around guard and awl/auchene hair follicles (~26% of hair follicles), while Aδ-LTMRs and C-LTMRs form endings around zigzag and awl/auchene hair follicles (~99% of hair follicles) (Kuehn et al., 2019; Li et al., 2011). The LLE projections from different LTMR subtypes interdigitate when multiple LTMR neurons are present at a single hair follicle forming a complex receptive ending (Li et al., 2011). These endings are associated with a specialized glial cell, called a Terminal Schwann Cell (TSC) which partially ensheaths the LLE projections and form an interface between the LLE and the epithelial cells of the hair follicle (Li and Ginty, 2014). These TSCs are necessary for the maintenance of LLE projections as ablation of TSCs in adult animals led to degeneration of follicle-innervating nerve endings within 2-3 weeks, while

axotomy leading to hair follicle denervation did not affect TSC morphology over the same period (Li and Ginty, 2014).

In addition to targeting different populations of hair follicles, each follicle-innervating LTMR subtype has distinct responses to stimuli and receptive field morphologies. Several studies have leveraged Cre^{ER}/*loxP* and other genetic labeling systems to sparsely label individual neurons from LTMR populations to examine these differences in detail. Experiments using the inducible genetic driver $Ret^{CreERT2}$ and the genetically driven fluorescent reporter *Npyr2-GFP* showed that Aβ RA-LTMRs form large receptive fields with sparse LLEs, innervating approximately 20 hair follicles over 0.75 mm^2 of skin in adult animals (Meltzer et al., 2022b preprint). *In vivo* and *ex vivo* skin-nerve preparation recordings from Aβ RA-LTMRs have on average conduction velocity greater than 26 m/s, respond to skin indentation by firing short action potential bursts at the onset and offset of light pressure (0.07 mN), and fire in response to hair follicle deflection caused by skin stroking (Bai et al., 2015; Li et al., 2011).

The expression of TrkB in Aδ-LTMRs and their dependence on BDNF signaling for survival has led to several important findings about this population of LTMRs. Using the $TrkB^{CreERT2}$ genetic driver line to sparsely label receptive fields in the skin showed that Aδ-LTMRs form compact receptive fields, innervating approximately 35 hair follicles over 0.4 mm^2 of skin (Meltzer et al., 2022b; Rutlin et al., 2014). Skin-nerve preparation recordings from Aδ-LTMRs, done using a *TrkB-GFP* knock-in mouse line, have shown them to conduct action potentials with a velocity greater than 5 m/s but slower than 30 m/s, and like the Aβ RA-LTMRs fire short bursts of action potentials at the onset and offset of light pressure to the skin (Koltzenburg et al., 1997; Li et al., 2011). Further work

on Aδ-LTMR neurons has shown preferential firing of action potentials in response to skin stroking and hair follicle deflection rostrally, against the direction of hair growth. This is primarily due to the formation of LLE projections on only the caudal side of each hair follicle, unlike the Aβ RA-LTMRs and C-LTMRs which form projections symmetrically around the hair shaft. This asymmetrical structure arises due to BDNF expression only on the caudal side of the follicle and is necessary for the direction selective activity (Rutlin et al., 2014).

Sparse labeling studies using the *TH*^{CreER} genetic driver showed, for the first time, that C-LTMR neurons formed LLEs around hair follicles, not just free nerve endings as had been previously described (Li et al., 2011). The C-LTMRs form the smallest LTMR receptive fields, innervating approximately 18 hair follicles over 0.3 mm^2 of skin (Bai et al., 2015; Li et al., 2011). Skin-nerve preparation and patch clamp recordings indicate C-LTMRs have the slowest conduction velocity of the follicle-innervating LTMRs (<2 m/s) and fire action potentials continuously during the application of skin pressure and skin stroking, suggesting a more intermediate or slow adapting physiology than the other LTMR subtypes (Li et al., 2011; Seal et al., 2009).

While the Aβ RA-LTMR and Aδ-LTMR populations appear to have straightforward roles as detectors of gentle skin stimulation, the unique physiology of the C-LTMRs has led to speculation about their possible role in injury-induced hypersensitization and pleasurable touch signaling. In addition to selectively expressing tyrosine hydroxylase, C-LTMRs uniquely express *Vglut3*, a vesicular glutamate transporter (Seal et al., 2009; Usoskin et al., 2015). *Vglut3* knockout mice show no change in sensitivity to heat, cold, and gentle mechanical stimuli (e.g., brushing or

stroking), but do show reduced sensitivity to high threshold mechanical stimuli (e.g., tail and toe pinch), inflammatory pain hypersensitivity, and post-injury hypersensitivity (Seal et al., 2009). In addition to this role in hypersensitization of nociceptors after injury, C-LTMRs have also been suggested as the mechanosensory neurons responsible for encoding pleasurable touch. A population of C-LTMRs expressing *Mrgprb4* contain the mechanosensitive ion channel PIEZO2 and respond to brushing but not pinch stimuli, though it remains unclear if this population of neurons innervates hair follicles with LLEs like the follicle-innervating LTMR neurons (Liu et al., 2007; Vrontou et al., 2013; Yamaguchi and Otsuguro, 2017). Chemogenetic activation of these neurons with Designer Receptors Exclusively Activated by Designer Drugs (DREDDs) done in a three-chamber place preference assay did show a significant increase in time spent in the MRGPRB4 activating chamber compared to the control chamber (Vrontou et al., 2013). This suggests increased activity of MRGPRB4 neurons may be associated with pleasurable and attractive stimuli.

Tiling in the Somatosensory Nervous System

One of the key components of a functional somatosensory nervous system is its ability to transmit the precise location of a stimulus on the body. For stimuli to be accurately located on the body a sensory neuron must have two morphological features: it must innervate a discrete and constrained area, and it must be able to communicate its location relative to other neurons and body structures. In the mammalian follicle-innervating LTMRs this first requirement is met through the non-overlapping tiled arrangement of peripheral axonal arbors (Kuehn et al., 2019). Using subtype-specific genetic drivers for each population of follicle-innervating LTMRs and a genetically driven multi-fluorophore system to label neurons with one of three fluorophore combinations

LTMR receptive fields were shown to tile homotypically with varying degrees of exclusivity. The Aδ-LTMR neurons tile nearly exclusively with less than 20% of hair follicles innervated by an Aδ-LTMR receiving endings from more than one neuron. The C-LTMRs also showed exclusive tiling, with less than 30% of innervated follicles showing innervation by more than one neuron. The Aβ RA-LTMRs overlapped receptive fields the most, with more than half of the Aβ RA-LTMR innervated hair follicles receiving innervation by more than one neuron, and approximately 10% of hair follicles innervated by three or more neurons. There were no differences in receptive field overlap across body regions, but Aβ RA-LTMR innervation did differ across hair follicle types. Receptive fields innervating awl/auchene and zigzag hairs showed more exclusivity than those innervating guard hairs, suggesting different roles for Aβ RA-LTMRs innervating these two groups (Kuehn et al., 2019).

In addition to homotypic tiling, where neurons exclude other same-subtype neurons from forming endings at hair follicles in their receptive field, the Aδ-LTMRs and Aβ RA-LTMRs show considerable isoneuronal tiling, where neurons only innervate a hair follicle with a single axon branch. In both populations less than 15% of follicles have LLEs composed of more than one axon branch. This contrasts with the C-LTMRs in which over 70% of hair follicles were innervated by multiple axon branches (Kuehn et al., 2019).

Our understanding of tiling in the mammalian somatosensory system is built on an extensive literature exploring tiling in the somatosensory nervous systems of non-mammalian animals, in particular *Drosophila* larvae and leeches. Early experiments on the neurons innervating the body wall of the leech showed epidermally innervating

neurons formed repeated patterns in each segment and formed stereotyped receptive fields with little isoneuronal overlap (Blackshaw, 1981; Yau, 1976). Despite these neurons not exhibiting exclusive tiling behavior in their receptive fields the fields of touch sensitive neurons expanded when neighboring neurons were ablated (Blackshaw et al., 1982).

The larval *Drosophila* dendritic arborization (DA) neurons have long been considered the archetypal example of tiled somatosensory neurons. Each central larval body segment is innervated by two mirrored arrangements of 15 DA neurons clustered with other sensory neurons into 4 groups per hemisegment (Bodmer and Jan, 1987). Through a series of landmark studies from the Jan lab at UCSF it was shown that the DA neurons could be divided into four classes based on their morphology and that each class of DA neuron exhibited differing degrees of homotypic and isoneuronal tiling behavior. Using the Mosaic Analysis with a Repressible Marker (MARCM) system to sparsely label DA neurons with fluorescent reporters, detailed descriptions of each DA neuron class were constructed (Grueber et al., 2002; Lee and Luo, 1999). The three Class I DA neurons formed the simplest dendritic arbors with single dorsally extended primary dendrites and multiple secondary branches in the anterior-posterior direction. The four Class II DA neurons primarily innervate the ventral body wall, and often show bifurcated primary dendrites with second-order branching but few higher order branches. The five Class III DA neurons collectively innervate approximately 70% of each hemisegment and show significantly more complex arbors than those of Class I and II neurons, with long primary and secondary dendrites and substantial higher-order branching. Finally, the three Class IV DA neurons collectively cover 100% of each

hemisegment, forming highly complex dendritic arbors with as many as 900 terminal branches. Dendritic arbors from neurons of different classes arrange independently of one another, but Class II, III, and IV DA neurons show no homotypic overlap, showing signs of repulsion when neighboring arbors approach each other (Fig. 3B) (Grueber et al., 2002).

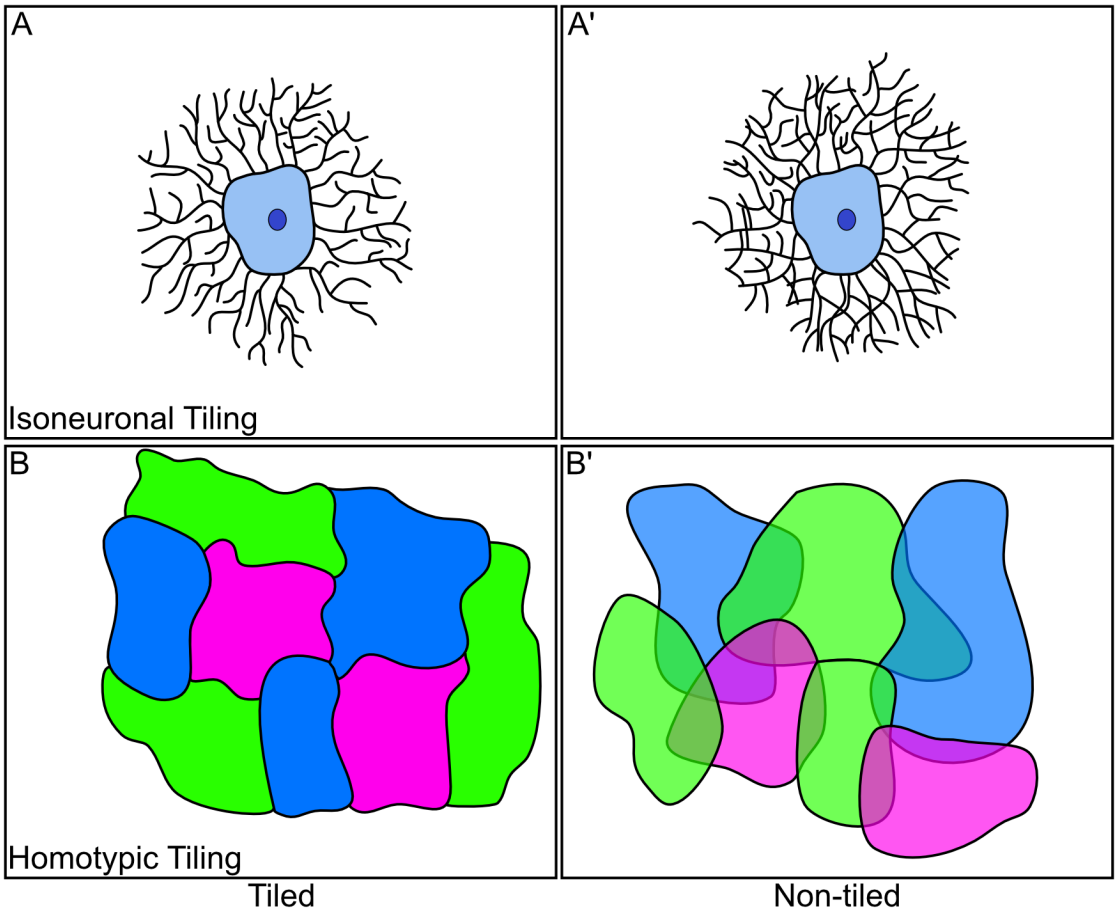

Figure 3 - Examples of Isoneuronal and Homotypic Tiling

A-A') Examples of isoneuronal tiling of dendrites. The neuron illustrated in A) shows tiled dendrites, where there is no crossing-over of dendrite branches and no poly-innervation of a given region of space by dendrites from the same neuron. The neuron in A') shows non-isoneuronally tiled dendrites which cross-over and poly-innervate the same space.

B-B') Examples of homotypic neuron receptive field tiling. Illustration B) demonstrates 8 neighboring receptive fields arranged in a homotypically tiled manner. No neuron innervates the same area as a neighboring same-subtype neuron. Illustration B') demonstrates 7 non-homotypically tiled receptive fields. Each receptive field overlaps with those of neighboring neurons to varying degrees.

This work was followed up with a mechanistic study examining the effects of sparse ablation or duplication of DA neurons. By using laser ablation to remove Class IV DA neurons from late-stage embryos remaining Class IV DA neurons will extend their arbors to fill in for missing neighbors, even crossing segments and the dorsal-ventral midline, suggesting the tiling phenotype seen in these neurons is entirely cell-intrinsic. When extra Class IV DA neuron were present in larvae receptive field tiling was maintained, and the arbors of each DA neuron shrank to accommodate the extra neighbor. Similar experiments using mutations which caused duplications of Class I, II, and III DA neurons showed Class I and II neurons readily overlap their arbors rather than shrinking their arbors to maintain tiling, while Class III DA neurons readily overlap their major dendrites, but show exclusive tiling of their higher-order branches (Fig. 3A) (Grueber et al., 2003). The combination of self-avoidance and tiling seen in DA neurons functions to ensure the body wall is fully innervated as efficiently as possible, and that each DA neuron arbor innervates a constrained area for stimulus localization.

The molecular mechanisms behind neuronal tiling interactions have been extensively studied in *Drosophila* but remain relatively unexplored in vertebrates. Experiments in *Drosophila* DA neurons suggest that homotypic tiling of receptive arbors and isoneuronal self-avoidance are controlled through two separate molecular mechanisms (Grueber et al., 2003). The axon guidance molecule Down's Syndrome Cell Adhesion Molecule (*Dscam*) is both necessary for maintaining dendrite self-avoidance, and sufficient to cause heterotypic avoidance not seen in wild-type neurons when a single isoform was expressed across all neurons (Soba et al., 2007). *Dscam* is a highly spliced cell adhesion molecule with over 38.000 potential isoforms that shows a

high degree of repulsion between identical isoforms and plays a role in the patterning of multiple neural systems in *Drosophila* (Schmucker et al., 2000; Wojtowicz et al., 2004). *Dscam* is conserved in mammals, though with greatly reduced splice variation, and functions as a recognition/repulsion molecule with demonstrated roles in patterning retinal dendrites and regulating neuronal lamination in the midbrain, in both cases acting through masking/inhibiting members of the cadherin cell adhesion molecule family (Agarwala et al., 2001; Arimura et al., 2020; Garrett et al., 2018).

The molecules regulating the homotypic tiling of DA neurons are less well understood than those regulating isoneuronal self-avoidance. Multiple molecular pathways have been proposed as important for homotypic tiling, including *Hippo*, *Tricornered/Furry* (*Trc/Fry*), and portions of the *target of rapamycin complex 2* (TORC2) which can activate *Trc* (Emoto et al., 2004; Emoto et al., 2006; Koike-Kumagai et al., 2009). While these molecular pathways do appear to have a role in regulating homotypic tiling, multiple recent studies have suggested that the tiling phenotypes seen in *Trc/Fry* and TORC2 mutants are caused by failure of dendrites to properly adhere to the extracellular matrix (ECM) due to reduced integrin function (Han et al., 2012; Kim et al., 2012). This implies that the tiling seen in DA neurons may be primarily caused by steric restrictions rather than canonical axon guidance adhesion and repulsion interactions.

The mechanisms behind homotypic tiling of neuronal arbors have been explored in multiple vertebrate systems, though none to the same degree as the *Drosophila* DA neurons. Experiments examining the development of zebrafish trigeminal neurons showed remarkable isoneuronal self-avoidance and exclusive homotypic tiling of arbors

at the midline which was theorized to be dependent on repulsive cues from the contralateral neurons (Sagasti et al., 2005). In mice, the mechanisms regulating tiling are most well studied in the various cell populations of the retina. Retinal bipolar cells form dendritic fields which innervate all available photoreceptor synapses while excluding synapse formation from neighboring homotypic neurons. In wild-type mice, these dendritic fields are sensitive to changes in both photoreceptor and bipolar cell population size, adjusting their dendritic field size to a fixed range of synaptic contacts (Reese et al., 2005). In studies examining an overpopulation of bipolar cells caused by knockout of the pro-apoptotic Bcl-2 associated X-protein (*Bax*) the entire population of bipolar cells shrank their receptive fields to accommodate the increased number of neighboring cells (Lee et al., 2011). Examination of dendritic tiling of multiple bipolar cell subtypes in a sparse *Dscam* knockout model showed bipolar cell tiling is dependent on *Dscam* expression (Simmons et al., 2017). In contrast to the exclusive dendritic field forming bipolar cells, many retinal amacrine cells exhibit little tiling behavior. In Bax-driven overpopulation studies multiple amacrine cell subtypes maintain their dendritic field size, instead increasing the amount of field overlap between homotypic neurons (Farajian et al., 2004; Keeley et al., 2020; Lee et al., 2011). This variability in tiling phenotypes seen in the retina suggests that there may be multiple molecular mechanisms at play, regulating tiling behavior in other mammalian sensory systems.

Central Projections of LTMR Neurons

While the peripheral endings of mechanoreceptive neurons were some of the first structures in the somatosensory system to be described, it was not until the advent of specific genetic labeling tools that the central axonal projections of LTMRs could be studied in detail. It is known from anatomical and lesioning studies that DRG central

projections enter the spinal cord through the posterolateral tract, also called Lissauer's tract, before turning caudally or rostrally, traveling one to two spinal segments and forming a complex synaptic glomerulus with spinal cord interneurons in the dorsal horn (Nolte, 2009). Recent comparisons of LTMR neurons innervating the back and abdominal skin showed neurons innervating the back skin nearly exclusively project their central axons rostrally, while abdominally innervating neurons nearly exclusively project their central axons caudally before forming their synaptic glomerulus (Kuehn et al., 2019). The dorsal horn interneurons project rostrally through the anterior and lateral spinothalamic tracts, eventually forming synapses in various thalamic nuclei. Aβ-LTMRs also send projections directly to the dorsal column nuclei in the brainstem through the dorsal column tracts in addition to forming synapses with dorsal horn interneurons (Johnson and Hsiao, 1992). Initial theories about somatosensation followed the labeled line hypothesis, the idea that each somatosensory modality was projected relatively independently into the sensory cortex of the brain where the signals were integrated. This hypothesis has since been superseded by the population coding hypothesis, the idea that somatosensory neurons have signaling crosstalk, both directly and through interneurons, throughout the central nervous system and that signals from multiple somatosensory modalities are integrated well before the sensory cortex (Reviewed in Ma, 2010).

The dorsal horn of the spinal cord is classically described as being separated into five distinct laminae, initially based on cell density, and later shown using molecular markers (Abraira et al., 2017; Rexed, 1952; Rexed, 1954; Todd, 2010). Central projections from follicle-innervating LTMRs primarily innervate the deeper laminae of the

dorsal horn, with C-LTMRs innervating the deep portion of lamina II (lamina IIiv), Aδ-LTMRs innervating the bulk of lamina III with some projections into lamina IIiv, and Aβ RA-LTMRs innervating laminae IIiv, III, and IV (Abraira et al., 2017; Li et al., 2011). Lamina I and the superficial portion of lamina II (IIi) primarily receive peptidergic and non-peptidergic nociceptive inputs respectively. Careful analysis of LTMR synaptic partners in the dorsal horn showed that not only do the different populations of LTMR neurons overlap their target regions, they also frequently form synapses onto the same interneurons, though with differing frequencies and distributions (Abraira et al., 2017). This work was expanded upon in 2018 by an extensive single-cell RNA sequencing analysis of the spinal cord dorsal horn. Cluster analysis of approximately 1500 dorsal horn interneurons from adult mice showed 30 molecularly distinct clusters of interneurons exist in the dorsal horn, 15 clusters of GABAergic neurons and 15 clusters of glutamatergic neurons (Häring et al., 2018). Spatial analysis of these clusters using a combination of immunofluorescence and *in situ* hybridization revealed stark differences in the distributions of GABAergic and glutamatergic clusters. Glutamatergic interneuron clusters are frequently constrained to one or two adjacent dorsal horn laminae, while GABAergic interneurons are more widely distributed. This suggests excitatory dorsal horn interneurons may play more modality specific roles in signal integration and transmission, while inhibitory interneurons may play a more widespread role in signal intensity regulation.

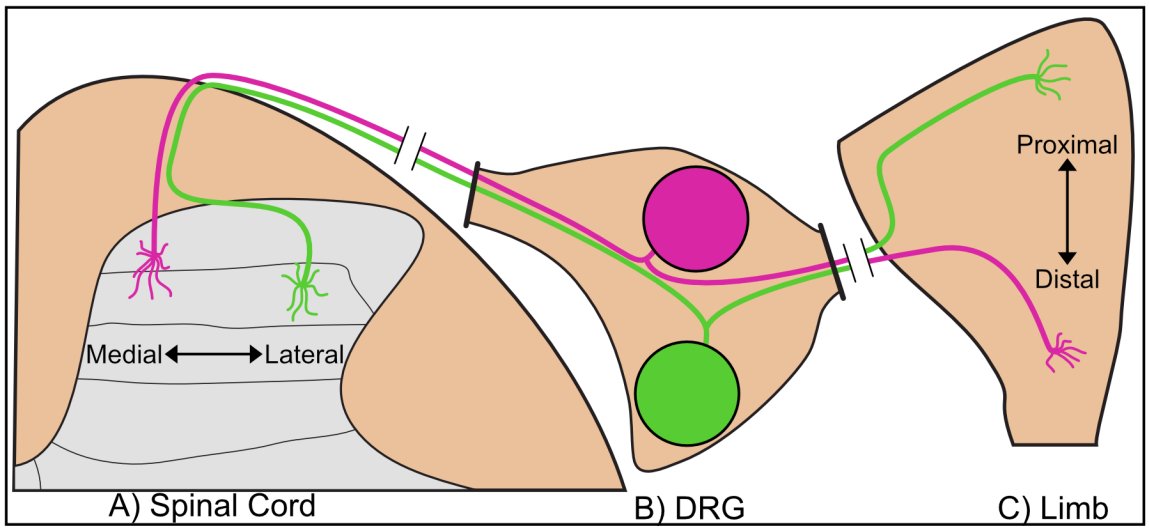

Figure 4 - The dorsal horn of the spinal cord is somatotopically organized. A-C) Axons from neurons originating in the DRG (B) project peripherally into the limb (C) where they innervate a constrained area of skin. The central projections of these neurons arrange somatotopically in the dorsal horn (A), with the central projections of proximally-innervating neurons (green) forming columns in the lateral dorsal horn, and the central projections of distally-innervating neurons (magenta) forming columns in the medial dorsal horn.

In addition to the dorsal-ventral lamination of the dorsal horn, early work on the sensory projections to the spinal cord showed mediolateral somatotopic organization of inputs. Tracing experiments done using horseradish peroxidase showed that skin innervating neurons form a wedge-shaped synaptic field in the dorsal horn, and that the mediolateral position of these wedges correlated inversely with the mediolateral position of the associated peripheral fields (Fig. 3) (Brown and Fuchs, 1975; Woolf and Fitzgerald, 1986). Multiple studies using injections of retrograde neural tracers into glabrous and hairy skin demonstrated the precise nature of sensory neuron somatotopic organization. Adjacent microinjections of Choleratoxin subunit B (CTB) tagged with different fluorophores into the hairy skin of young adult mice revealed adjacent columns of dorsal horn innervation which scaled in rostro-caudal length with the labeled area of the skin (Li et al., 2011). Simultaneous injection of retrograde tracers which preferentially label either large diameter neurons (CTB) or non-peptidergic nociceptors

(wheat-germ agglutinin, WGA) showed that the somatotopically arranged dorsal horn columns extended across somatosensory neuron subtypes (Odagaki et al., 2018; Shehab and Hughes, 2011). There has been limited exploration into the development of somatotopic organization in the dorsal horn, or into molecular cues which may regulate and refine somatotopy. Retrograde labeling of somatosensory neurons in rat embryos suggests that central projections begin to arrange somatotopically as soon as they enter the spinal cord dorsal horn and undergo little refinement during development (Silos-Santiago et al., 1995). More recent work has expanded on this finding, showing that central projections of one somatosensory neuron population refine significantly before their peripheral arbor is mature, suggesting that the somatotopic arrangement of sensory neurons in the skin may be either cell intrinsic or derived from cues present in the dorsal horn at the time of central axon innervation (Olson and Luo, 2018).

LTMR Differentiation and The Role of Developmental Cell Death in the Peripheral Nervous System

The sensory neurons in the DRG derive from a population of neural precursor cells (NPC) which, in mice, migrate off the neural crest between E8.5 and E10.5 and progress down the ventral midline forming clusters on either side of the neural tube (Serbedzija et al., 1990; Weston, 1970). These clusters of NPCs begin dividing off immature neurons in two major waves, the first driven by Neurogenin 2 (*Neurog2*) from E9.5-E11.5 which primarily gives rise to the large diameter DRG neurons (Aβ-LTMRs, Aδ-LTMRs, and proprioceptors) and the second driven by Neurogenin 1 (*Neurog1*) from E10.5-E13.5 which primarily gives rise to medium and small diameter DRG neurons (C-LTMRs, and nociceptors) (Landy et al., 2021; Lawson and Biscoe, 1979; Ma et al., 1999). This two-wave model of differentiation is further supported by single-cell RNA

sequencing time course experiments examining DRG development revealing two clusters of developing cells which acquire neuronal identity approximately 24 hours apart (Faure et al., 2020; Sharma et al., 2020). By E15.5 all the non-nociceptive DRG neuron populations have acquired unique molecular identities, and by birth every population of DRG neurons that is present in adult animals has differentiated (Sharma et al., 2020). The LTMR neurons arise through a complex cascade of transcription factor expression and neurotrophin receptor activation. Aβ-LTMRs and Aδ-LTMRs both originate in the *Neurog2*-positive first wave of differentiation, and express runt-related transcription factor 3 (*Runx3*) early after specification then downregulate this expression and upregulate *Ret* (Aβ-LTMRs) and *TrkB* (Aδ-LTMRs) beginning at E11.5 and continuing until adulthood (Kramer et al., 2006; Li et al., 2011; Luo et al., 2009). The C-LTMRs derive from the *Neurog1*-positive population and are their differentiation is dependent on runt-related transcription factor 1 (*Runx1*) and zinc finger protein 521 (*Zfp521*) signaling in an incoherent feed forward loop where *Runx1* upregulates both *Zfp521* multiple downstream targets inhibited by *ZFP521* (Lou et al., 2013; Lou et al., 2015).

An important element of LTMR development and maturation is the effect of developmental cell death on the LTMR population. Many neuronal populations go through some level of programmed or developmental cell death to ensure an appropriate population density of neurons is present in adult animals or to ensure neurons have innervated their intended targets (Oppenheim, 1991). In DRG populations neurotrophin supply is a major driver of developmental cell death, resulting in a loss of approximately 50% of DRG neurons during embryonic development (Lentz et al., 1999;

Sun et al., 2003; Vogelbaum et al., 1998). This cell death can be rescued through knockout of the proapoptotic protein *Bax* and results in a 100% increase in the number of DRG neurons in adult animals (Deckwerth et al., 1996; Vogelbaum et al., 1998). The cell bodies and axons of sensory neurons in *Bax* deficient animals are atrophied compared to wild-type counterparts, suggesting a lack of developmental trophic support in these neurons (Kinugasa et al., 2006; Patel et al., 2000; Sun et al., 2003; Suzuki et al., 2010). A study examining the effects of *Bax* knockout on specific DRG neuron populations demonstrated that blocking developmental cell death increases the population size of nociceptor and proprioceptor populations by 50%-75% and that the cell bodies of these neurons were smaller than in wild-type animals (Suzuki et al., 2010). Surprisingly, only the peptidergic nociceptors, the population exhibiting the least cell body atrophy, showed increased innervation density in the skin suggesting that these neurons may have been able to receive sufficient trophic support despite a 75% increase in population size, and that neurons from the other populations did not extend axons into their target regions. This may be a result of two different trophic supply schemes being present in cutaneous neurons. One used in epidermally-innervating free nerve endings wherein trophic factors are present relatively ubiquitously throughout the dermis and epidermis and extra neurons are able to be supported without issue. The other, used in structure-innervating neurons like proprioceptors where trophic factors are derived from a discrete structure and a limited number of neurons are able to be supported.

Dissertation Overview

The overarching goal of this dissertation is to further our understanding of the mechanisms which regulate the organization of follicle-innervating LTMR receptive

fields. Previous work showed LTMR receptive fields are highly stereotyped in adult mice, with each subtype of neuron forming a field of distinct size and innervating a discrete number of hair follicles. these receptive fields pattern in a tiled manner, innervating hair follicles while excluding nerve endings from other same-subtype neurons. Based on these pieces of data I hypothesized that the size of LTMR receptive fields is determined through competitive interactions for hair follicles during early development of skin innervation. In Chapter 2 I present a comprehensive series of protocols for the immunofluorescent and histological staining and imaging of hairy and glabrous skin in both section and whole mount preparations, as well as protocols for genetically-driven sparse labeling of various skin innervating neuron populations. In Chapter 3 I use these protocols to characterize the development of follicle-innervating LTMR neurons during the first postnatal month and use a neural overpopulation model driven by knockout of the pro-apoptotic protein *Bax* to assess the role of competition for hair follicles on LTMR receptive field size. This work shows that one population of follicle-innervating LTMR neurons, the Aδ-LTMRs, adjust their receptive field size to accommodate an increase in the number of skin innervating neurons, while another population, the C-LTMRs, do not. This suggests that, at the hair follicle level, there is competition between neighboring Aδ-LTMR neurons for innervation targets, and that this competition is essential for the formation of constrained receptive fields. In Chapter 4 I present preliminary data exploring the role of cell adhesion proteins in the DRG and spinal cord dorsal horn in somatotopic patterning of sensory neuron central projections.

Chapter 2: Immunohistochemical and genetic labeling of hairy and glabrous skin innervation

Matthew B. Pomaville & Kevin M. Wright, Ph.D.

Manuscript published in Current Protocols May 5, 2021

Available at: https://doi.org/10.1002/cpz1.121

Significance Statement:

In mammals, the skin is a highly innervated and structurally complex organ. The development of skin innervation requires many genetically distinct populations of sensory neurons to extend axons over large distances to form complex endings at specific structures. This process involves multiple biological mechanisms including axon pathfinding, target recognition, and developmental pruning. Analysis of skin innervation is also applicable to translational research questions. Peripheral neuropathy and sensory nerve damage are symptoms of many neurodegenerative conditions and side effects of many drugs. Understanding the mechanisms by which these conditions and drugs damage neurons requires the ability to examine skin innervation in high detail. This series of protocols outlines techniques for comprehensive analysis of mouse skin innervation applicable to many research contexts.

Abstract:

Cutaneous innervation is an essential component of the mammalian sensory nervous system. During development, genetically and morphologically diverse subtypes of sensory neurons use distinct molecular pathways to innervate end organs or form free nerve endings in glabrous and hairy skin. Peripheral neurons can be damaged by acute injury or degenerate due to chronic conditions including diabetes and chemotherapy, leading to peripheral neuropathy. Analysis of skin and cutaneous innervation can be applied to many research endeavors, from developmental neuroscience to pharmaceutical testing. Due to its natural hydrophobicity and heterogenous makeup (dense, keratinized cells as well as sparse, ECM-bound cells), histological analysis of the skin presents unique challenges compared to many other tissues. This series of protocols describes histological methods for generalized immunohistochemistry and

subtype-specific genetic labeling of sensory neurons in mouse skin in both whole mount and section formats. I provide detailed methodology of tissue preparation for hairy and glabrous skin, labeling, and counting of hair follicles in flat-mounted mouse skin.

Introduction:

The skin serves as both an essential environmental barrier and a highly complex sensory organ. Based on genetic, functional, and morphological analyses there are at least 11 distinct populations of skin innervating somatosensory neurons in the mouse, providing a full range of touch, temperature, and pain sensation (Abraira and Ginty, 2013; Sharma et al., 2020; Usoskin et al., 2015). Skin innervating somatosensory neurons can be broadly divided into two classes based on the type of skin they target, hairy or glabrous (non-hairy). In mice, glabrous skin is innervated by three major populations of sensory neurons: (1) Aβ rapidly adapting (RA) type 1 neurons which innervate Meissner corpuscles, (2) Aβ slowly adapting (SA) type 1 neurons which innervate Merkel cells, and (3) free nerve endings. Hairy skin is also innervated by three major sensory neuron populations: (1) Aβ SA type 1 neurons terminating at Merkel cells, (2) 4 types of follicle-innervating low-threshold mechanoreceptors (LTMRs), and (3) free nerve endings (Abraira and Ginty, 2013; Jenkins and Lumpkin, 2017). The follicle innervating LTMR neurons were originally classified based on their conduction velocity and response to stimuli. These subtypes are the Aβ RA-LTMRs which innervate guard and Awl/Auchene hairs, the Aδ-LTMRs which innervate zigzag and Awl/Auchene hairs, the C-LTMRs which also innervate zigzag and Awl/Auchene hairs, and the circumferential endings which innervate all three hair types (Bai et al., 2015; Koltzenburg et al., 1997; Li et al., 2011; Millard and Woolf, 1988; Olson et al., 2016; Wu et al., 2012). Recent work has identified unique markers for many of the skin innervating

somatosensory neuron populations, including Calbindin, Tyrosine Hydroxylase, and the Trk-receptor family proteins. These markers allow detailed analysis of the development and organization of these neurons, and their responses to pharmacological and genetic treatments (Sharma et al., 2020; Usoskin et al., 2015). This opens many avenues for detailed study into the biology of skin innervating neurons and their associated structures.

Traditionally, analysis of skin innervation has been done using thin sections (20-50 μm) labeled with antibody markers for various cell populations and structures. While this approach provides high detail in the skin depth axis, it sacrifices spatial information which is maintained in whole-mount tissue samples. Combining immunohistochemistry with sparse genetic labeling through inducible recombinases or viral vectors allows for detailed analysis of single neuron morphology in combination with population-wide patterning and density measurements.

Basic protocol 1 outlines the fixation, sectioning, and immunolabeling of cryosections from mouse hairy skin. It includes an alternate protocol to improve the morphology of fine nerve endings in sectioned skin. These sections can be used to quantify the density of hair follicles, the innervation of hair follicles, or the innervation of intra-follicle skin. Basic protocol 2 outlines the fixation, section, and immunolabeling of cryosections from mouse glabrous (paw) skin. Sections from this protocol can be used for measuring changes in paw innervation in models of peripheral neuropathy or sensory neuron development. Basic protocol 3 outlines the preparation and immunolabeling of whole mount mouse hairy skin. While this protocol has much more stringent timing requirements than the protocols for preparing sections from hairy skin, it

preserves the skin morphology in an intact manner, yielding a more complete picture of the skin innervation environment. Basic protocol 4 outlines the sparse labeling of cutaneous innervation using inducible *Cre*^{ER} mouse lines and a *Cre*-dependent alkaline phosphatase reporter. This is a powerful technique for generating morphological data on individual neurons from a large population. Basic protocol 5 outlines the use of Oil Red O, a lipophilic dye, to selectively stain hair follicles in mouse skin. This technique can be used to assess changes in hair density and patterning in a rapid and robust manner.

Strategic Planning

With proper planning, the skin from a single animal can be used for all the procedures in this protocol. This provides the potential for a comprehensive analysis of multiple aspects of skin innervation while reducing the number of experimental animals required. A flow chart illustrating how a single skin sample from one mouse can be used for multiple processing steps is shown below (Fig 1). The following protocols take between 2 and 14 days to complete, not including time for image analysis. Much of this time is “hands-off”, including overnight fixation and antibody incubation steps. Samples labeled with fluorescent reporters and cleared in Benzyl alcohol-Benzyl benzoate (BABB) begin to suffer from fluorescent signal loss within hours of clearing and should be imaged immediately after clearing when possible. In contrast, the signal in tissue samples stained with chromogenic stains such as Alkaline Phosphatase and Oil Red O are much more stable and can be stored long-term in appropriate conditions with little degradation of signal.

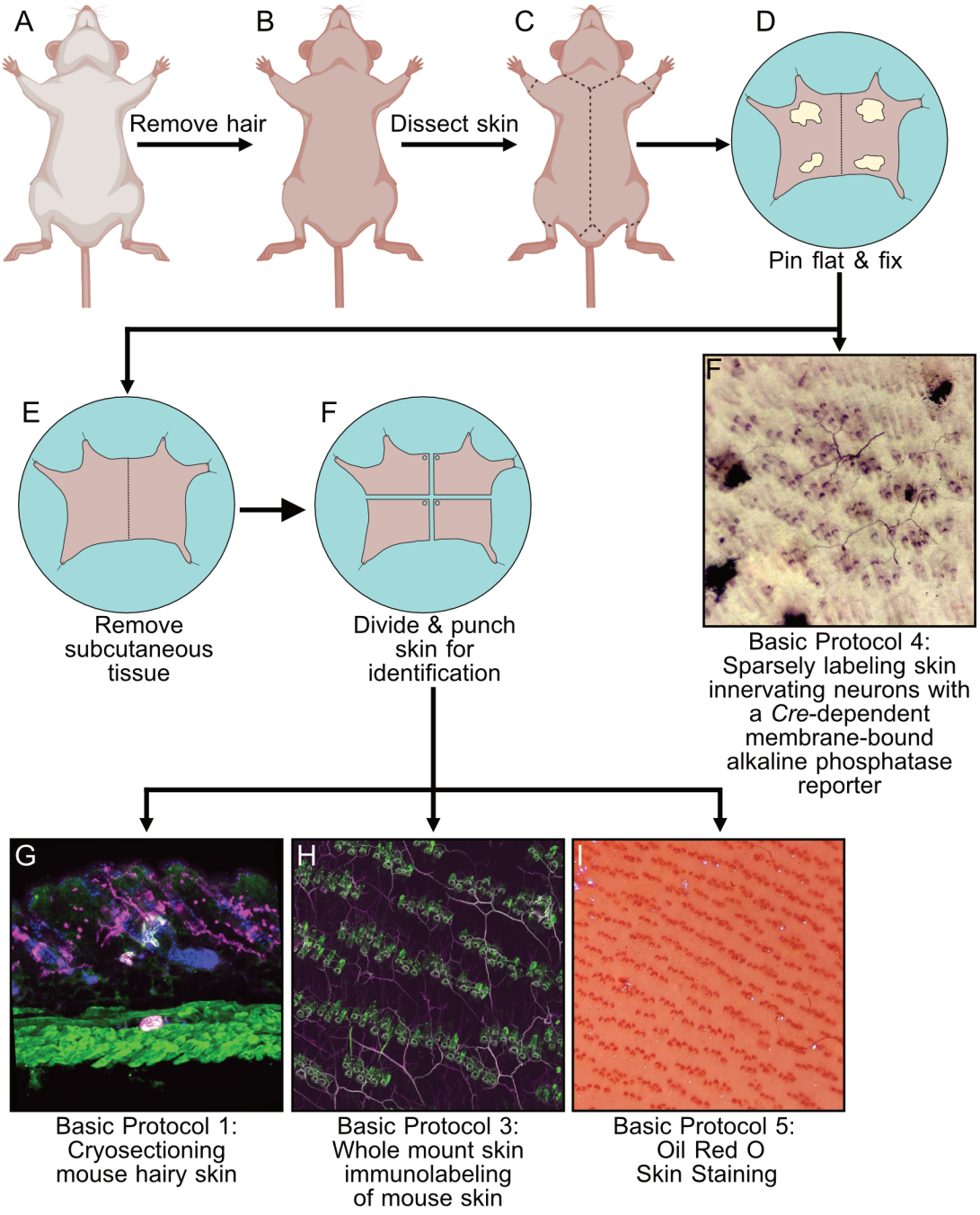

Figure 1 - Summary of skin processing protocols
A-C) Depilation and removal of skin. D-F) Initial skin processing, fixation, and division for parallel processing of multiple forms of analysis (cyrosectioning, whole mount immunolabeling, and Oil Red O) from one animal. For cryosectioning, the skin is further cut into ~1cm strips perpendicular to the AP axis. G-H) Example images generated from Basic Protocol 1 (H), Basic Protocol 3 (I), Basic Protocol 4 (G), and Basic Protocol 5 (J). Not shown: Protocol 2: Processing and imaging of glabrous skin cryosections.

Basic Protocol 1: Cryosectioning mouse hairy skin

Introductory paragraph:

Sections of hairy skin can be used for detailed examination of dermal and epidermal innervation, measurement of hair follicle density, and examination of end organ innervation by sensory neurons. Sections are useful for examining a wider range of ages and are faster to process than whole skin samples but sacrifice spatial information beyond tissue depth. This protocol outlines tissue preparation, freezing, sectioning, and immunofluorescent labeling of both free-floating sections and slide mounted sections. In general, slide mounted sections thicker than 50 μm will suffer from incomplete antibody penetration. Floating sections work well up to 100 μm, showing thorough tissue penetration with most antibodies. Sections thicker than 100 μm begin to suffer from diffraction issues during imaging, obscuring deeper labeling. Thicker sections can be imaged using confocal microscopy. Zamboni's fixative can be substituted for 4% Paraformaldehyde to help reduce background fluorescence in the 488 nm range and increase labeling of fine nerve endings in the skin but may suffer from antibody incompatibility issues.

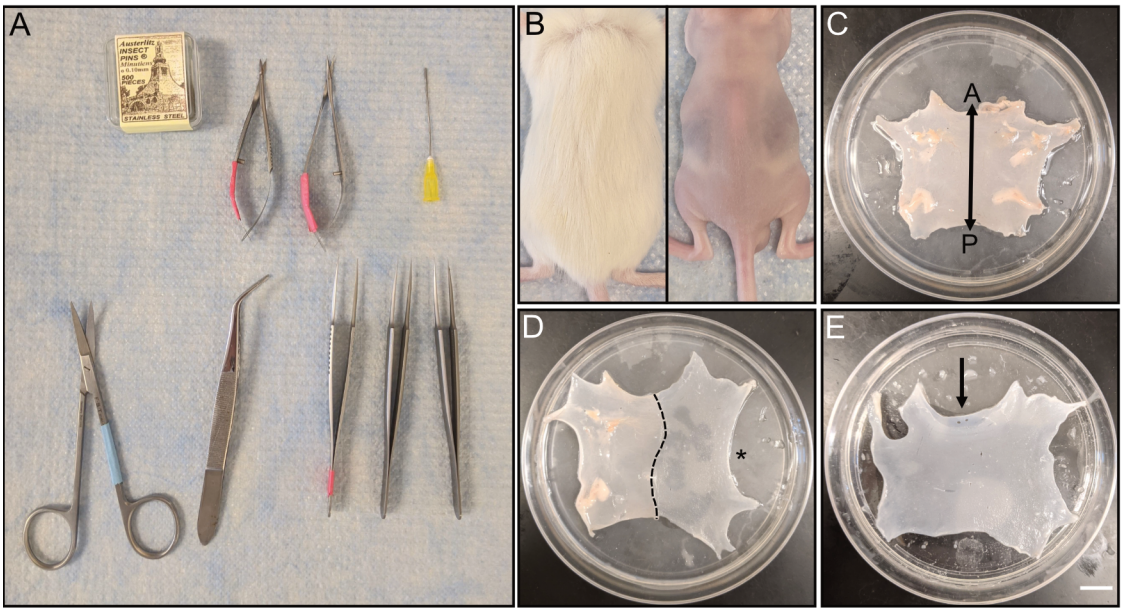

Figure 2 - Dissection tools and initial preparation steps

A) Tools used in skin dissection and preparation. From top left, clockwise: Fine insect pins, straight spring scissors, curved spring scissors, 20 gauge metal gavage needle with rubber tip removed, fine forceps (Dumont #5, Dumont #2, and Dumont #55), 45° forceps, curved scissors.

B) Mouse skin before (left) and after (right) hair removal with commercial depilatory cream.

C) Mouse skin pinned to a silicone bottomed dish, subcutaneous side up. Line indicated anterior/posterior axis.

D) Fixed skin partially scraped to remove subcutaneous tissue. Dashed line indicates the boundary between scraped and unscraped tissue, asterisk indicates scraped side of tissue.

E) Fully scraped mouse skin on silicone bottomed dish. Arrow indicates identification holes punched in the tissue. Scale bar – 1 cm

Materials:

Laboratory mice (see Critical Parameters for age and genetic background considerations)

Phosphate buffered saline (PBS) (see recipe)

4% Paraformaldehyde (PFA) in PBS, 4°C (see recipe)

Blocking buffer (see recipe)

30% w/v sucrose in PBS

Commercial hair remover (Nair)

Hand soap (Fisher #04-355-17)

Insect pins

Fine forceps

- Straight tip (Dumont #5)
- Bent/angled tip (Dumont #45)

Spring scissors

- Large, straight blade
- Small, curved blade

Single edge razor blades

Dissecting stereoscope

Silicone bottomed dish (A standard 10 cm cell culture dish with 3-4 mm Sylgard 182 poured into the bottom)

Optimal Cutting Temperature (OCT) Media (Richard Allen Scientific Neg-50, Fisher # 22-110-617)

Tissue embedding molds (Fisher #22-19)

Immedge Pen (Fisher #NC9545623)

Fluoromount G (Fisher # OB100-01)

12-well tissue culture plate

Dry ice

2-Methylbutane, -80°C

Hoechst 33342 (Fisher # BDB561908)

Glass slides

#1.5 Coverslips

Clear nail polish (Sally Hansen #800 “Crystal Clear”)

Flat glass or plastic plate (used Western blot cassette)

Slide staining tray or slide box lined with damp paper towels

Metal gavage needle (Fisher # 01-208-87, plastic tip removed) or small (1-2mm) dermal punch or mouse ear punch (Fisher # 13-820-063)

Kimwipes

Paper towels

Protocol steps — Step annotations:

Tissue preparation and fixation

1. Euthanize mouse in accordance with IACUC approved protocols.
2. Wash mouse with water and mild soap such as Bac-Down hand soap (Fisher #04-355-17).
3. Generously apply commercial hair remover (Nair) to wet mouse

   Work hair remover into the hair/skin very well. The better/more thoroughly it is worked in, the more complete the hair removal will be.
4. After 5 minutes check for hair removal by wiping a small section of skin with a Kimwipe or paper towel (Fig. 1B, Fig. 2B).

   If hair removal is complete, bare skin will be exposed, progress to step 5.

   If hair removal is not complete, let hair remover sit for another minute.
5. Wash skin thoroughly under cool water, scrubbing off any remaining hair and hair remover.
6. On the abdominal side, make an incision from the neck to the region just above the genitals with sharp scissors, being careful to only cut through the skin,

leaving the subcutaneous fascia intact. This will ease removal of the skin in step 8 (Fig. 1C).

7. Make incisions around the limbs and tail, such that the skin can be removed in a single piece, leaving the limb skin behind.
8. Gently separate the skin from the body being careful to not tear the skin or the subcutaneous fascia/muscle.
9. Place directly into chilled PBS in a petri dish (Fig. 1D).

    Smaller skin sections can be taken if whole body analysis is not needed. (For sections, local labeling, etc.)

10. Pin skin to a silicone coated petri dish with a small amount of PBS, subcutaneous side up, using insect pins and forceps. Get the skin as flat as possible without overstretching or distorting it (Fig. 1D, Fig. 2D).
11. Use bent forceps and curved spring scissors to remove as much subcutaneous fat as possible without damaging the skin.
12. Use a dermal punch or metal gavage needle to punch an identification hole (or series of holes) near the centerline on the caudal end of the skin if needed (Fig. 1F).
13. Pour off PBS and add cold 4% PFA to cover the tissue.
14. Fix overnight at 4°C with gentle, rocking agitation.
15. Remove PFA and wash skin 3x30 minutes with PBS.
16. Store at 4°C in PBS with 0.01% sodium azide until ready to section.

Cryosectioning

1. Make a single cut along the A-P midline of the skin using a sharp blade. One half of the skin will be used for cryosections, the other can be saved for future sections or used for whole mount immunolabeling (Fig. 1F).
2. Cut skin into multiple approximately 1 cm wide strips perpendicular to the A-P axis. If only processing tissue from one animal, make a small cut (1-2 mm) into the midline face of the strip.

    If processing tissue from multiple animals, punch a series of identification holes using the gavage needle/dermal punch/ear punch. This will mark the cutting face of the tissue sample in later steps.
3. Trim lateral side of each strip to form a rectangle 1 cm wide and slightly shorter than your embedding mold.
4. Transfer skin blocks to a 10% sucrose/0.01% NaN_3/PBS solution and incubate at room temperature for 2 hours.
5. Replace 10% sucrose solution with 15% sucrose/0.01% NaN_3/PBS solution and incubate overnight at 4°C with rocking.
6. Dry tissue samples by gently blotting both sides on a paper towel and embed in Optimal Cutting Temperature Media (OCT) with the subcutaneous side up. Adjust sample until it is centered in the OCT and level on both axes. Mark the cutting face of the mold (the midline face of the skin block which was marked in step 2) (Fig. 3A).
7. Freeze by immersion in 2-methylbutane chilled to -80°C on dry ice for 2-3 minutes.

8. Move blocks to cryostat with chamber temperature set to -20°C and object temperature set to -18°C. Allow samples to equilibrate for 30 minutes before mounting and cutting.
9. Mount tissue blocks to mandrel/chuck using OCT with the cutting face facing away from the plate. Adjust block before OCT hardens to square cutting face to the mounting plate. Mount block with epidermal face of skin facing down (so it hits the blade first).
10. Trim block until skin segment begins to show (Fig. 3B).
11. Take a test 50 µm section on a slide to adjust orientation. Tilt block until hair follicles are running vertically through the section (Fig. 3C).
12. *For floating sections:* Cut ten to fifteen 50-100 µm sections and place into a well of a 12-well plate with PBS.
13. *For slide mounted sections:* Cut one section and pick-up directly on a room temperature slide. Repeat in series for the number of needed slides.
14. Every 10-20 sections, check the sections and adjust block angle to keep follicles running vertically through the section.
15. *For slide mounted sections:* Allow tissue to dry on slides 4 hours to overnight before moving to 4°C for short term storage (up to 1 week), or -20°C for longer term storage (longer than 1 week).
16. *For floating sections*: Gently agitate sections at room temperature for 1 hour, making sure none are stuck to the sides of the well. Replace the PBS with fresh PBS containing 0.01% sodium azide and store at 4°C for up to 1 month.

Immunolabeling floating sections

1. Wash sections 3x10 minutes in PBS at room temperature with gentle agitation to remove excess OCT.
2. Incubate sections in blocking buffer for 1 hour at room temperature with agitation.

   Normal donkey serum (NDS) or Normal goat serum (NGS) blocking buffer is used as appropriate for secondary antibody compatibility. NDS is used with secondary antibodies raised in donkeys, while NGS is used with secondary antibodies raised in goats.
3. Primary Incubation: Incubate with primary antibodies in appropriate blocking buffer overnight at 4°C with agitation. Be sure to use enough antibody/buffer that the samples can freely move without clumping.
4. Wash sections 4x15 minutes in PBS at room temperature with agitation.
5. Secondary Incubation: Incubate 4 hours at room temperature with agitation with secondary antibodies in appropriate blocking buffer. Protect the slides from light from this point forwards.
6. Stain with Hoechst 33342 diluted at 1:5000 in PBS for 10 minutes at room temperature.
7. Wash sections 4x15 minutes in PBS at room temperature with agitation.
8. Move sections to slides with a paintbrush/pair of sharp forceps and gently flatten/unroll. Use a drop of PBS to help flatten difficult sections.
9. Blot off excess PBS with a Kimwipe.
10. Coverslip using Fluoromount G.

a. Use 20-30 µl Fluoromount G per slide, applied in a bead along one long side of the slide. Apply the coverslip from the side with the Fluoromount G to the other, being sure to allow air bubbles to escape.

11. Let slides dry >1 hour at room temperature then seal with clear nail polish.

Immunolabeling slide mounted sections

1. Allow slides to come to room temperature if stored at 4°C or -20°C.
2. Outline sections on slide with an Immedge pen.
3. Wash sections 3x10 minutes in PBS at room temperature, tapping off PBS between washes.
4. Incubate sections in blocking buffer for 30 minutes at room temperature.

   Normal donkey serum (NDS) or Normal goat serum (NGS) blocking buffer is used as appropriate for secondary antibody compatibility. NDS is used with secondary antibodies raised in donkeys, while NGS is used with secondary antibodies raised in goats.
5. Primary Incubation: Incubate with primary antibodies in appropriate blocking buffer overnight at 4° C.
6. Wash sections 3x10 minutes in PBS at room temperature, tapping off PBS between washes.
7. Secondary Incubation: Incubate 4 hours at room temperature with secondary antibodies in appropriate blocking buffer. Protect the slides from light from this point forwards.

8. Stain with Hoechst 33342 diluted at 1:5000 in PBS for 10 minutes at room temperature.
9. Wash sections 4x15 minutes in PBS at room temperature, tapping off PBS between washes.
10. Tap slides on slide box to remove excess PBS, then tap again on a paper towel to dry sections more.
12. Coverslip using Fluoromount G.
    a. Use 20-30 µl Fluoromount G per slide, applied in a bead along one long side of the slide. Apply the coverslip from the side with the Fluoromount G to the other, being sure to allow air bubbles to escape.
13. Let slides dry >1 hour at room temperature then seal with clear nail polish.

Alternate Protocol 1: Alternate preparation and fixation protocol for mouse hairy skin

The fixation and tissue preparation protocol listed in Basic Protocol 1 preserves gross tissue morphology but may impair/reduce labeling of fine innervation (ex. free nerve endings). This alternative protocol helps preserve fine innervation labeling for robust antigens but may sacrifice signal for other targets by using a short fixation and forgoing chemical hair removal in favor of trimming hair with electric clippers. Empirical testing of both protocols is recommended to determine the preparation and fixation protocol that is optimal for each experimental. As with Basic Protocol 1, Zamboni's fixative may be substituted for 4% paraformaldehyde to help reduce background fluorescence in the 488 nm range but may have antibody/antigen compatibility issues.

Materials:

Laboratory mice (see Critical Parameters for age and genetic background considerations)

Phosphate buffered saline (PBS) (see recipe)

4% Paraformaldehyde in PBS, 4°C (see recipe)

Small electric hair clippers (beard trimmer)

Insect pins

Fine forceps

- Straight tip (Dumont #5)
- Bent/angled tip (Dumont #45)

Spring scissors

- Large, straight blade
- Small, curved blade

Single edge razor blades

Dissecting stereoscope

Silicone bottomed dish (A standard 10 cm cell culture dish with 3-4 mm Sylgard 182 poured into the bottom)

Optimal Cutting Temperature (OCT) Media (Richard Allen Scientific Neg-50, Fisher # 22-110-617)

12-well tissue culture plate

Tissue embedding molds (Fisher #22-19)

Dry ice

2-Methylbutane, -80°C

Metal gavage needle (Fisher # 01-208-87, plastic tip removed) or small (1-2mm) dermal punch or mouse ear punch (Fisher # 13-820-063)

Kimwipes

Paper towels

Protocol steps—Step annotations:

Tissue preparation and fixation

1. Euthanize mouse in accordance with IACUC approved protocols.
2. Carefully trim hair using electric hair trimmers. Working both with and against the direction of hair growth and keeping the clippers flat to the skin remove as much hair as possible without damaging the skin. Generally, only a small portion of the skin needs to be clipped to get enough tissue to prepare many sections (approximately 1.5 cm x 1.5 cm).
3. Wash the mouse using warm water and hand soap to remove all clipped hair.
4. Cut out clipped section of skin, being careful to not cut through subcutaneous fascia if possible. Make sure one edge of the skin section being removed is parallel to the direction of hair growth to ensure a good cutting face later.
5. Gently begin to separate the skin from the body being careful to not tear the skin or the subcutaneous fascia/muscle.
6. Place directly into chilled PBS in a petri dish.
7. Trim removed section of skin to approximately 1.5 cm x 1.5 cm using a razor blade and punch an identification hole on the side of the skin to become the cutting face (one of the sides parallel to the hair growth direction) using a metal gavage needle or dermal punch.

8. Pin skin to a silicone coated petri dish with a small amount of PBS, subcutaneous side up, using insect pins and forceps. Get the skin as flat as possible without overstretching or distorting it.
9. Use bent forceps and curved spring scissors to remove as much subcutaneous fat as possible without damaging the skin.
10. Pour off PBS and add cold 4% PFA to cover the tissue.
11. Fix 15 minutes at room temperature with agitation.
12. Remove PFA and wash skin 3x30 minutes with PBS.
13. Wash skin overnight with PBS at 4°C.
14. Store at 4°C in PBS with 0.01% sodium azide until ready to section.

Cryosectioning

1. Remove tissue samples from Sylgard plates and dry by gently blotting both sides on a paper towel. Embed in OCT with the subcutaneous side up. Adjust sample until it is centered in the OCT and level on both axes. Mark the cutting face of the mold (the marked face of the skin block in step 7 of the tissue preparation and fixation section) (Fig. 3A).
2. Freeze by immersion in 2-methylbutane chilled to -80°C on dry ice for 2-3 minutes.
3. Move blocks to cryostat with chamber temperature set to -20°C and object temperature set to -18°C. Allow samples to equilibrate for 30 minutes before mounting and cutting.
4. Mount tissue blocks to mandrel/chuck using OCT with the cutting face facing away from the plate. Adjust block before OCT hardens to square cutting face to

the mounting plate. Mount block with epidermal face of skin facing down (so it hits the blade first).

5. Trim block until skin segment begins to show (Fig. 3B).
6. Take a test 50 μm section on a slide to adjust orientation. Tilt block until hair follicles are running vertically through the section (Fig. 3C).
7. *For floating sections:* Cut ten to fifteen 50-100 μM sections and place into a well of a 12-well plate with PBS.
8. *For slide mounted sections:* Cut one section and pick-up directly on a warm slide. Repeat in series for the number of needed slides.
9. Every 10-20 sections, check the sections and adjust block angle to keep follicles running vertically through the section.
10. *For slide mounted sections:* Allow tissue to dry on slides 4 hours to overnight before moving to 4°C for short term storage (up to 1 week), or -20°C for longer term storage (longer than 1 week).
11. *For floating sections*: Gently agitate sections at room temperature for 1 hour, making sure none are stuck to the sides of the well. Replace the PBS with fresh PBS with 0.01% sodium azide and store at 4°C for up to 1 month.

Immunolabeling

See Basic Protocol 1: Immunolabeling slide mounted sections and Immunolabeling floating sections

Basic Protocol 2: Sectioning mouse paw glabrous skin

Introductory paragraph:

This protocol uses many of the same steps as Basic Protocol 1 to generate slide mounted cryosections of mouse paw glabrous skin for immunolabeling. The key differences come in the tissue fixation and preparation. In brief, paws are collected from euthanized animals, and the palmar skin is dissected away and fixed in Zamboni's fixative. Zamboni's fixative contains picric acid, which improves the immunolabeling of some skin innervation and reduces background fluorescence in the 488nm range. If Zamboni's fixative is incompatible with target antigens 4% paraformaldehyde can be substituted at the cost of potentially increased background signal in the 488nm range. Shorter fixation times (30 minutes at room temperature) can improve the labeling of fine nerve endings with robust antibodies against stable antigens (neurofilaments, cytoskeletal components, etc.), but may cause loss of signal with less stable antibodies/antigens. Testing both long and short fixation periods is recommended to determine the best procedure for specific experimental goals.

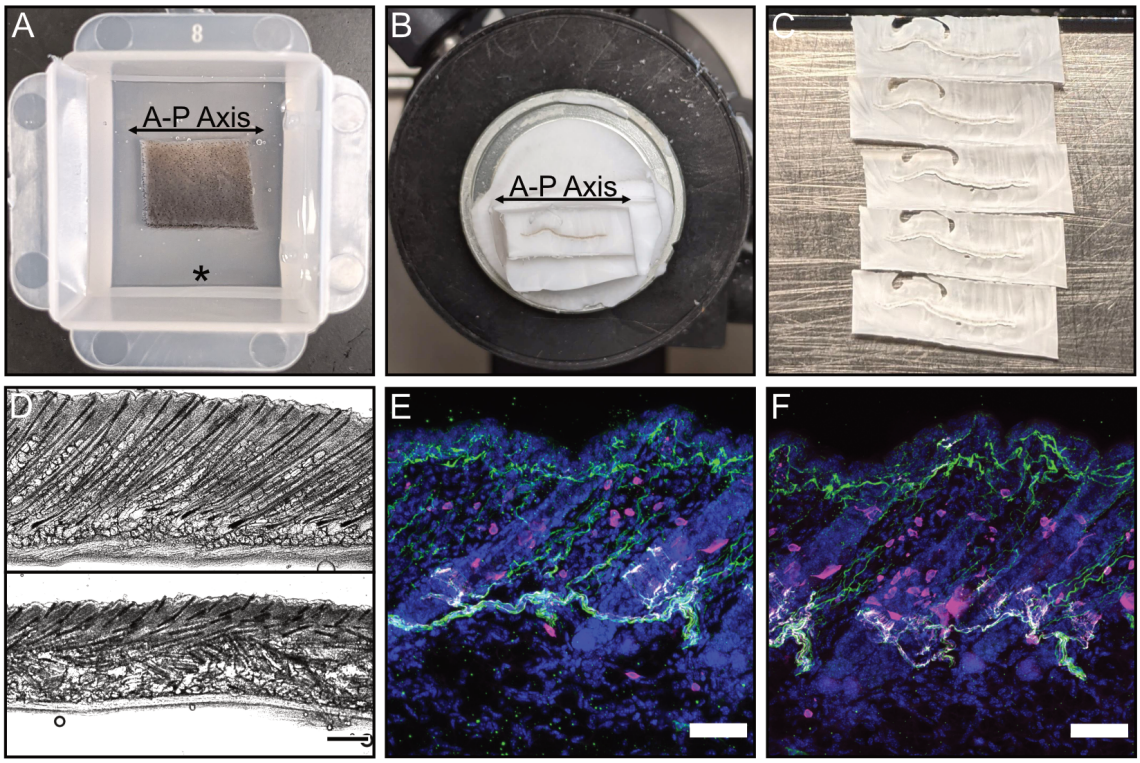

Figure 3 - Preparation of hairy skin cryosections

A) Sample of mouse skin in cutting media in a 22 mm x 22 mm cutting mold. Asterisk indicates cutting face, horizontal arrow indicates anterior-posterior axis.

B) Skin sample frozen in cutting media and mounted to cryostat chuck. Skin is visible on cut face. Arrow indicates anterior-posterior axis orientation.

C) 5 section long ribbon of 50 µm skin cryosections. Skin is visible in the center of each section. An air bubble is visible in the upper left of each section.

D) Examples of properly oriented (top) and improperly oriented (bottom) sections from P14 mouse hairy skin. The properly oriented skin section shows the full length of the hair shaft and follicle passing through the skin, while the improperly oriented section shows partial hair shafts scattered throughout the section. Brightfield, Scale bar – 200 µm.

E) Representative image of cryosectioned hairy skin taken on a Zeiss AxioImager.M2 with a 20x objective and an ApoTome.2 structured illumination module. Green – βIII-Tubulin, Magenta – *Vglut3*^{Cre}-TdTomato, Blue – Hoechst 33258. Scale bar – 50 µm

F) Representative image of cryosectioned hairy skin taken on a Zeiss LSM900 with a 20x objective. Green – βIII-Tubulin, Magenta – *Vglut3*^{Cre}-TdTomato, Blue – Hoechst 33258. Scale bar – 50 µm

Materials:

Phosphate buffered saline (PBS) (see recipe)

Zamboni's fixative (see recipe)

Blocking buffer (see recipe)

30% (w/v) sucrose in PBS

Hand soap

Sturdy scissors

Single edge razor blades

Dissecting stereoscope

Silicone bottomed dish (A standard 10 cm cell culture dish with 3-4 mm Sylgard 182 poured into the bottom)

Optimal Cutting Temperature (OCT) Media (Richard Allen Scientific Neg-50, Fisher # 22-110-617)

Tissue embedding molds (Fisher #22-19 for adult paw tissue or Ted Pella Inc. #27181 for juvenile paw tissue)

Dry ice

2-Methylbutane, -80°C

Hoechst 33342 (Fisher # BDB561908)

Immedge Pen (Fisher #NC9545623)

Fluoromount G (Fisher # OB100-01)

Glass slides

#1.5 Coverslips

Slide staining tray or slide box lined with damp paper towels

Kimwipes

Paper towels

Protocol steps—Step annotations:

Tissue Preparation and fixation

1. Euthanize mice in accordance with IACUC approved protocols.

2. Use sturdy scissors to remove paws above the wrist/ankle joint.
3. Carefully dissect palmar surface of paw and digits off the subcutaneous tissue. Curved spring scissors with the tips pointed towards the subcutaneous tissue will help with the intact removal of the paw and digit skin (Fig. 4A-B).

    Note: Paw skin from neonatal mice (<P3) may be difficult to dissect off for fixation and sectioning. Due to the incomplete calcification of the paw bones at this age and the small size of the tissue, the paw can be drop fixed and sectioned intact rather than dissecting away the palmar surface. The following steps can be followed without modification in this case.
4. Pin to a Sylgard bottomed container with insect pins, subcutaneous side up (Fig. 4C).

    If desired, the paw and digit surfaces can be separated at this point, and the tissues fixed free-floating in tubes.
5. Fix overnight in Zamboni's solution at 4°C with gentle agitation.
6. Remove fixative and wash paws 4x30 minutes with PBS at 4°C with gentle agitation.
7. Store at 4°C in PBS with 0.01% sodium azide until ready to section, up to 1 month.

Cryosectioning

1. Incubate paws in 10% sucrose solution at room temperature until tissue sinks in solution.
2. Replace 10% sucrose solution with 15% sucrose solution and incubate until tissue sinks. Repeat with 20% sucrose solution.

3. Dry samples by blotting both sides on a paper towel and embed in OCT with the dorsal side up. Adjust sample until it is centered in the OCT and level on both axes. Mark the cutting face of the mold (the digit end of the paw) (Fig. 4D).

    If paw and digit skin portions were fixed separately, freeze tissues in silicone embedding molds. A small portion of fixed retina or similar tissue can be used to help inform sectioning depth.

4. Freeze by immersion in 2-methylbutane chilled to -80°C on dry ice for 2-3 minutes.
5. Move blocks to cryostat with chamber temperature set to -20° C and object temperature set to -18°C. Allow samples to equilibrate for 30 minutes before mounting and cutting.
6. Mount tissue blocks to mandrel using OCT with the cutting face facing away from the plate. Adjust block before OCT hardens to square cutting face to the mounting plate. Mount block with palmar face of the paw facing down (so it hits the blade first).
7. Trim block until the digits or palmar surface are reached.
8. Take a test 50 µm section on a slide and adjust the block orientation.
9. Cut one 50 µm section and pick-up directly on a warm slide. Repeat in series for the number of needed slides.
10. Every 10-20 sections, check the sections and adjust block angle to keep the tissue square to the cutting blade.
11. Allow tissue to dry on slides overnight before moving to 4°C for short term storage (up to 1 week), or -20°C for longer term storage (longer than 1 week).

Immunolabeling slide mounted sections

1. Label as with **Basic Protocol 1**.

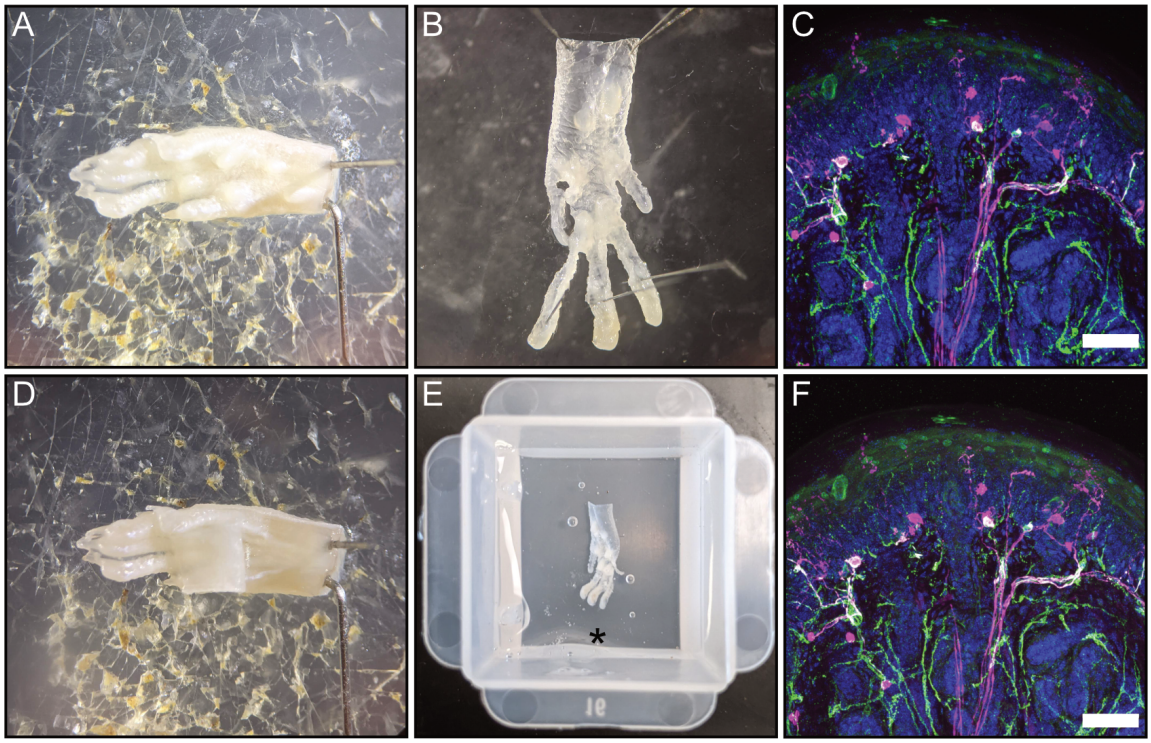

Figure 4 - Preparation of glabrous skin cryosections

A) Mouse paw pinned to silicone bottomed dish, palmar surface up.

B) Palmar skin partially dissected off of paw.

C) Palmar skin pinned to silicone bottomed dish, palmar surface down.

D) Fixed mouse paw in cutting media in 22 mm x 22 mm mold. Asterisk indicates cutting face.

E) Representative image of cryosectioned mouse forepaw pad taken on a Zeiss AxioImager.M2 with a 20x objective and an ApoTome.2 structured illumination module. Green – βIII-Tubulin, Magenta – *Vglut3*^{Cre}-TdTomato, Blue – Hoechst 33258. Scale bar – 50 μm

F) Representative image of cryosectioned mouse forepaw pad taken on a Zeiss LSM900 with a 20x objective. Green – βIII-Tubulin, Magenta – *Vglut3*^{Cre}-TdTomato, Blue – Hoechst 33258. Scale bar – 50 μm

Basic Protocol 3: Whole mount immunolabeling of mouse skin

Introductory paragraph:

Compared with sections, analysis of whole flat-mounted skin yields increased spatial information and allows for analysis of more skin area in the same imaging time. However, this comes at the cost of imaging resolution and antibody selection. Whole mount skin labeling also limits analysis timepoints to telogen and early anagen (see critical parameters in the Commentary section for details on hair cycle determination). Due to its natural hydrophobic properties, skin is highly resistant to antibody penetration. Penetration is increased through the removal of subcutaneous connective tissue and extensive washing with Triton X-100, a common nonionic detergent. This technique can be used with antibody labeling and can be combined with *Cre*-dependent fluorescent reporters and *Cre*-driver lines to provide genetically specified labeling, or inducible *Cre*-drivers or viral reporters for sparse labeling of innervation in the skin.

Notes: Skin autofluorescence occurs in the 488 nm/GFP/FITC range and obscures fluorescence detection of antibodies. This is reduced by post-labeling methanol dehydration and clearing in BABB but will still obscure a weak antibody signal. BABB is a skin irritant, breaks down nitrile gloves with prolonged exposure, and can etch/destroy microscope objectives. Use with caution and dispose of properly. Clean all items used with BABB thoroughly with hot water and dish soap then with 70% EtOH. Be sure to only use glass/polypropylene supplies, as BABB dissolves polystyrene (ex. cell culture dishes).

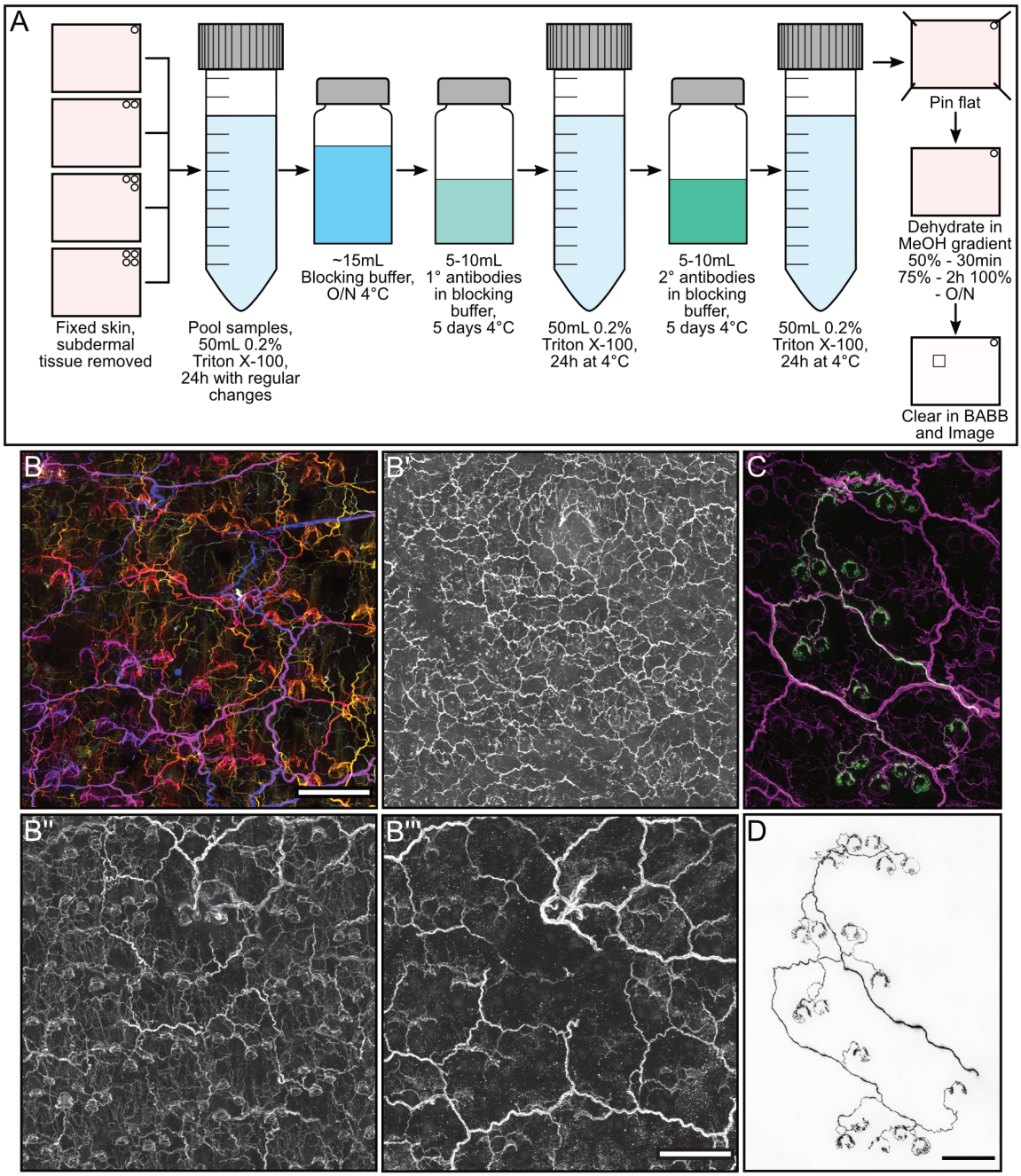

Figure 5 - Preparation of whole mount hairy skin

A) Summary graphic of whole mount immunohistochemistry processing steps.

B) βIII-Tubulin labeling of skin innervating neurons in whole mount hairy skin, false colored by tissue depth. Blue – Subcutaneous, Yellow – Superficial. Scale bar – 200 μm.

B'-B'") βIII-Tubulin labeled skin innervating neurons in whole mount hairy skin segmented by depth. B') Superficial innervation and free nerve endings. B'') Longitudinal lanceolate endings. B'") Deep cutaneous nerves and nerve plexus. Scale bar – 200 μm

C-D) Single fluorescently labeled Aδ-LTMR peripheral receptive field from a *TrkB*^{CreERT2}*;Ai140* mouse(C, green) with βIII-Tubulin labeling (C, magenta) in cleared mouse skin and isolated receptive field image (D). Scale bar – 100 μm.

Materials:

Laboratory mice (see strategic planning for age and genetic background considerations)

Phosphate buffered saline (PBS) (see recipe)

4% Paraformaldehyde in PBS, 4°C (see recipe)

Blocking buffer (see recipe)

0.2% (v/v) Triton X-100 in PBS

Commercial hair remover (Nair)

Hand soap

Insect pins

Fine forceps

- Straight tip (Dumont #5)
- Bent/angled tip (Dumont #45)

Spring scissors

- Large, straight blade
- Small, curved blade

Single edge razor blades

Dissecting stereoscope

50 mL conical tube or 20 mL glass scintillation vial

5 mL centrifuge tube

Silicone bottomed dish (A standard 10 cm cell culture dish with 3-4 mm Sylgard 182 poured into the bottom)

Glass petri dish or other non-polystyrene dish

Flat glass or plastic plate (*Ex. one side of a used Western blot cassette*)

Slide staining tray or slide box lined with damp paper towels

Metal gavage needle (Fisher #01-208-87, plastic tip removed) or small (1-2 mm) dermal punch or mouse ear punch (Fisher #13-820-063)

Kimwipes

Paper towels

Methanol

BABB (see recipe)

Protocol steps—Step annotations:

Tissue fixation and preparation

1. Euthanize mice in accordance with IACUC approved protocols.
2. Wash mice with water and soap in lab sink.
3. Generously apply commercial hair remover (Nair) to wet mice.

   Work hair remover into the hair/skin very well. The better/more thoroughly it is worked in now the more complete the hair removal will be.
4. After 5 minutes check for hair removal by wiping a small section of skin with a Kimwipe or paper towel.

   If hair removal is complete bare skin will be exposed, progress to step 5.

   If hair removal is not complete let hair remover sit another minute
5. Wash skin thoroughly under cool water, scrubbing off any remaining hair and hair remover (Fig. 1B, Fig. 2B).
6. Make an incision from the neck to the naval with sharp scissors, being careful to only cut through the skin, leaving the subcutaneous fascia intact. This will ease removal later.

7. Make incisions around the limbs and tail, such that the skin can be removed in a single piece, leaving the limb skin behind (Fig. 1C).
8. Gently begin to separate the skin from the body being careful to not tear the skin or the subcutaneous fascia/muscle.
9. Place directly into chilled PBS in a petri dish.
10. Pin skin to silicone bottomed dish being careful to not stretch or distort skin (Fig 1D, 2D).
11. Punch identification holes on the caudal midline of the skin if taking skin from multiple animals.
12. Remove PBS from step 9 and replace with 4% PFA in PBS.
13. Fix overnight in 4% PFA at 4°C with gentle agitation.
14. Wash skin in PBS 3x30 minutes.
15. Flatten fixed and washed skin on a smooth, flat surface such as a used Western blot cassette, subcutaneous side up (Fig. 2C).
16. Make an extremely shallow cut into the subcutaneous connective tissue on the medio-lateral midline of the skin using a sharp razor blade or scalpel.

    The goal is to cut through the clear subcutaneous tissue while leaving the skin layers intact.
17. Using a Kimwipe to anchor the tissue with one hand, scrape the subcutaneous connective tissue off the skin starting at the midline cut by holding a razor blade at a 45°- 90° angle to the skin. The subcutaneous tissue should begin to peel away from the skin.

18. Continue scraping until the subcutaneous tissue is removed from the entire skin sample. The skin should now be much thinner and much more pliable (Fig. 2E).
19. Cut the skin into approximately 1cm^2 sections and punch the top right corner to identify the caudal-midline for identification and orientation of the sample later.
20. Wash skin samples in PBS 3-5x for 30 minutes at room temp or 4°C.

Immunolabeling and tissue clearing

1. Pool skin segments from multiple animals after punching and wash for >8 hours with 20-50mL 0.2% Triton-X100/0.01% NaN_3/PBS at room temperature with agitation. Change the wash buffer every hour for the first 3-4 hours (Fig 5A).
2. Wash overnight at 4°C in appropriate blocking buffer.

   Normal donkey serum (NDS) or Normal goat serum (NGS) blocking buffer is used as appropriate for secondary antibody compatibility. NDS is used with secondary antibodies raised in donkeys, while NGS is used with secondary antibodies raised in goats.

3. *Primary Incubation:* Incubate with antibodies in appropriate blocking buffer for 3-5 days at 4°C with agitation.

   Be sure to use enough antibody/blocking buffer mixture that the samples can freely move without clumping (at least 2 mL for two to three 1 cm^2 samples). Table 1 has a list of validated antibodies and their effective concentrations.

4. Wash 4-5 hours in 20-50 mL 0.2% Triton X-100/0.01% NaN_3/PBS at room temperature with agitation. Change the wash buffer every hour.
5. *Secondary Incubation:* Incubate 2 days at 4°C with agitation with secondary antibodies in appropriate blocking buffer.

Be sure to use enough antibody/buffer that the samples can freely move without clumping (at least 2 mL for two to three 1 cm^2 samples).

Progression of secondary incubation can be evaluated at this point using a fluorescence dissecting microscope. It is difficult to increase labeling intensity after washing out excess antibodies and impossible after clearing the tissue in BABB.

6. Wash 4-5 hours in 20-50 mL 0.2% Triton X-100/0.01% NaN_3/PBS at room temp with agitation. Change the wash buffer every hour.
7. Dehydrate in serial MeOH dilutions at room temperature with agitation:
    a. 25% MeOH in PBS - 30 minutes
    b. Pin skin samples flat after dehydration in 25% MeOH to avoid curling later in processing.
    c. 50% MeOH in PBS - 1 hour
    d. 75% MeOH in PBS - 2 hours
    e. 100% MeOH - Overnight at 4°C
8. Warm samples in MeOH back to room temperature before clearing.
9. Clear samples by submersion in BABB (1:2 Benzyl Alcohol:Benzyl Benzoate) in a glass or polypropylene dish. Tissue should be optically clear in 30-45 minutes. Mount on slide, subdermal side up and coverslip with a small amount of BABB. Image as soon after clearing as possible as extended time in BABB can reduce fluorescence intensity.

Basic Protocol 4: Sparsely labeling skin innervating neurons with a Cre-dependent membrane bound alkaline phosphatase reporter

Introductory paragraph:

Due to its dense innervation, analysis of single neuron morphology in skin is impossible using traditional immunofluorescent labeling techniques. By combining *Cre*^{ERT2} driver lines and *Cre*-dependent reporter lines, sparse neuronal populations can be labeled for precise analysis of their morphology (Abraira and Ginty, 2013; Bai et al., 2015; Li et al., 2011). While fluorescent labeling has become the most common method for genetic labeling, the use of chromogenic reporters has many advantages over fluorescent labeling for assessing skin innervation. Labeling of neurons with chromogenic reporters like Alkaline Phosphatase allows for more rapid, sensitive, and permanent staining of tissue than immunofluorescent antibody labeling. Chromogenic labeling reagents are also less expensive per reaction and stained tissues have less stringent storage requirements. The main drawback of chromogenic reporters is their inability to be used for multi-color labeling and high-resolution three-dimensional imaging. In this protocol, a *Cre*-dependent, membrane-bound placental alkaline phosphatase is used to label follicle innervating low-threshold mechanoreceptors because of its labeling sensitivity and rapid spread through growing neurons (Badea et al., 2003). Tamoxifen induction timing and dosage to achieve sparse labeling of the target cells must be determined empirically for each *Cre*^{ERT2} driver line. The minimum time for signal to be detectable after induction will also need to be determined empirically and will be highly dependent on the promotor driving the reporter construct and the size of the structure to be labelled - small cells and structures close to the cell body will label quicker than structures far from the cell body.

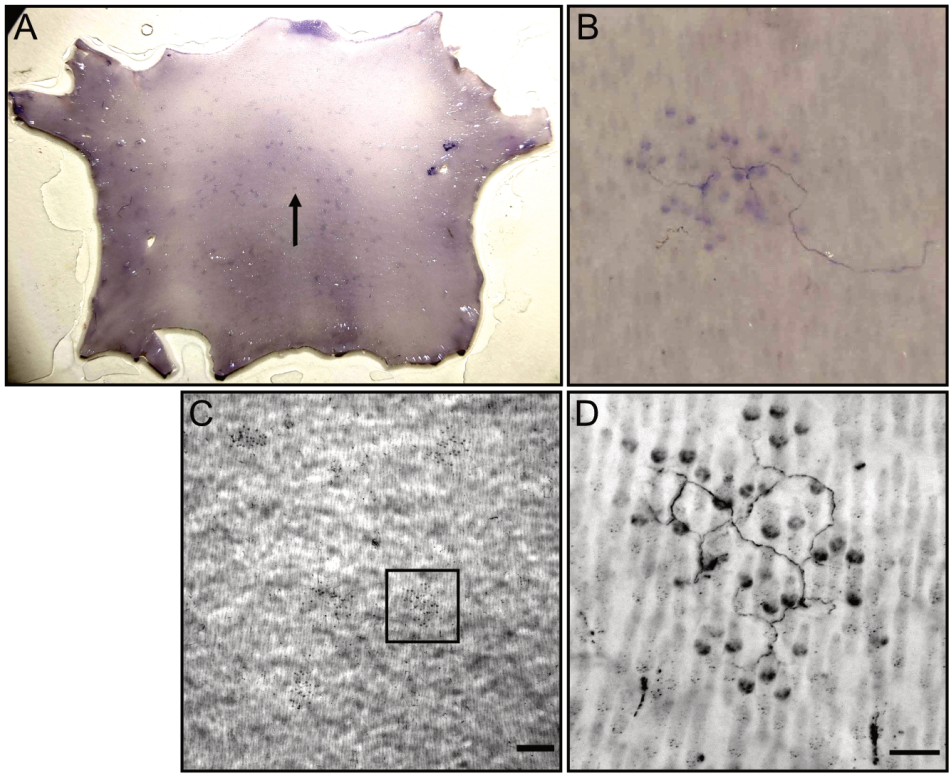

Figure 6 - Sparse neuron labeling with *Cre*-driven alkaline phosphatase

A) Whole uncleared skin from a P21 *TrkB*^{CreERT2}*; R26*^{iAP} mouse after alkaline phosphatase reaction. The arrow highlights an isolated cutaneous low-threshold mechanoreceptor receptive field, shown in B.

B) An isolated cutaneous low-threshold mechanoreceptor receptive field in uncleared skin.

C) Cleared alkaline phosphatase stained mouse skin. The box highlights an isolated receptive field shown in D. Scale bar – 500 µm.

D) High magnification image of the receptive field highlighted in C. Scale bar – 100 µm

Materials:

Laboratory mice (see strategic planning for age and genetic background considerations)

Phosphate buffered saline (PBS) (see recipe)

4% Paraformaldehyde in PBS, 4°C (see recipe)

PLAP development buffer (see recipe)

Levamisole hydrochloride (Fisher #ICN15522810)

$MgCl_2$, 1 mM in H_2O

5-Bromo-4-chloro-3-indolyl phosphate (BCIP) (Roche Applied Science #11383221001)

Nitro blue tetrazolium chloride (NBT) (Roche Applied Science #11383213001)

Commercial hair remover (Nair)

Hand soap

Insect pins

Fine forceps

- Straight tip (Dumont #5)
- Bent/angled tip (Dumont #45)

Spring scissors

- Large, straight blade
- Small, curved blade

Single edge razor blades

Dissecting stereoscope

50 mL conical tube or 20 mL glass scintillation vial

Silicone bottomed dish (A standard 10 cm cell culture dish with 3-4 mm Sylgard 182 poured into the bottom)

Glass petri dish or other non-polystyrene dish

Flat glass or plastic plate (used Western blot cassette)

Slide staining tray or slide box lined with damp paper towels

Metal gavage needle (Fisher # 01-208-87, plastic tip removed) or small (1-2 mm) dermal punch or mouse ear punch (Fisher # 13-820-063)

Kimwipes

Paper towels

Methanol

BABB (see recipe)

Protocol steps—Step annotations:

Tissue preparation and fixation

1. Follow protocol in Basic Protocol 3: Whole mount immunostaining of mouse skin, Tissue preparation and fixation subsection

Placental alkaline phosphatase stain development

1. Heat inactivate endogenous alkaline phosphatase in skin samples by incubating samples in 1 mM $MgCl_2$ in PBS at 70°C for 90 minutes with regular agitation.
2. Add BCIP/NBT in development buffer: 16.6 µg/mL BCIP and 33.3 µg/mL NBT

   This is a 1:3000 reagent:buffer ratio when using 50 mg/mL BCIP and 100 mg/mL NBT stock solutions as supplied by Roche

   Adding levamisole (2.5 mM, 0.5 mg/ml) will help reduce nonspecific staining due to non-inactivated alkaline phosphatases.
3. Develop at room temperature 4-48 hours until a satisfactory level of staining is reached as determined by observation under a dissecting microscope (Fig. 6A, B).

   Samples can be stored at 4°C overnight as needed to slow reaction and avoid overdevelopment.

   Staining solution should be replaced after 24 hours.

   Some NBT precipitate will wash out during MeOH dehydration and BABB clearing steps, reducing the staining intensity. Allowing the reaction to

progress past the bare minimum level of staining to visualize your structures is recommended to ensure stability.

4. Once a satisfactory level of staining intensity is reached, stop the staining reaction by washing 3x20 minutes at room temperature in 0.1% Tween-20/PBS and incubating samples in 4% PFA for 2-3 hours at room temp or 4°C.
5. Wash out PFA 3x10 minutes at room temperature with PBS.
6. Tissue can be dehydrated in MeOH (Clearing and imaging section, step 1) and stored at -20°C until ready to clear and image.

   Tissue should be dehydrated as soon after staining is complete as possible to reduce the development of excess background staining.

Clearing and imaging PLAP stained skin

1. Dehydrate in serial MeOH dilutions at room temperature with gentle agitation:
   a. 25% MeOH in PBS - 30 minutes
   b. 50% MeOH in PBS - 1 hour
   c. 75% MeOH in PBS - 2 hours
   d. 100% MeOH - Overnight at room temperature
   e. Note: Pin skin samples flat after dehydration in 25% MeOH to avoid curling later in processing.
   f. If not clearing tissue immediately, move to fresh 100% MeOH in a 50mL conical tube and store at -20°C until ready to image.
2. If samples were stored at -20°C, bring samples back to room temperature before clearing. Tubes should warm on bench in 20-30 minutes.

3. Clear samples in BABB (1:2 Benzyl Alcohol:Benzyl Benzoate). Tissue should be optically clear in 5-15 minutes. Mount on slide, subdermal side up and coverslip with a small amount of BABB (Fig. 6C-D).

   A small amount of NBT precipitate may dissolve in the BABB, tinting it purple. Move the samples to fresh BABB before imaging.

   Extended storage (> 8 hours) in BABB may reduce staining intensity significantly.

4. After imaging is complete, samples can be “un-cleared” in 100% MeOH, before moving to fresh 100% MeOH for long term storage at -20°C. Stained skin samples can be stored this way indefinitely with little loss of signal.

Basic Protocol 5: Oil Red O Skin staining

Introductory paragraph:

Oil Red O is a lipophilic dye that selectively labels sebaceous glands in skin. It can be used to measure hair follicle density more quickly and cost effectively than antibody labeling, at the cost of performing any other labeling/staining. Due to its lipophilic nature, Oil Red O staining is not compatible with tissue clearing methods that use delipidation (e.g., BABB, CLARITY, iDISCO).

Note: Oil Red O is an extremely persistent dye. The dry powder and the dye formed when it is mixed with isopropanol will permanently stain most surfaces that are not glass or metal, including most plastics, clothes, benchtops, etc. Dedicated equipment and a lab coat are recommended when working with Oil Red O. Metal tools can be cleaned with dish soap and water followed by an ethanol rinse.

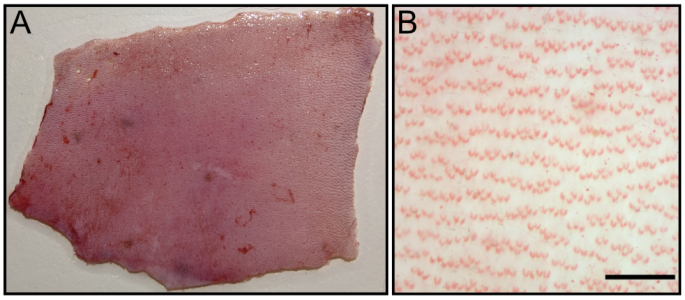

Figure 7 - Oil Red O staining of hair follicles
A) P21 mouse skin stained with oil red O after staining and washout.
B) High magnification image of skin in A. Scale bar – 500 μm

Materials:

Laboratory mice (see critical parameters for age and genetic background considerations)

Phosphate buffered saline (PBS) (see recipe)

4% Paraformaldehyde in PBS, 4°C (see recipe)

0.5% (w/v) Oil Red O in 100% isopropyl alcohol (see recipe for preparation)

60% (v/v) isopropyl alcohol in H_2O

0.2 µm syringe filter

30 mL syringe with Luer lock

Commercial hair remover (Nair)

Hand soap

Insect pins

Fine forceps

- Straight tip (Dumont #5)
- Bent/angled tip (Dumont #45)

Spring scissors

- Large, straight blade
- Small, curved blade

Single edge razor blades

Dissecting stereoscope

50 mL conical tube or 20 mL glass scintillation vial

Silicone bottomed dish (A standard 10 cm cell culture dish with 3-4 mm Sylgard 182 poured into the bottom)

Glass petri dish or other non-polystyrene dish

Flat glass or plastic plate (used Western blot cassette)

Metal gavage needle (Fisher # 01-208-87, plastic tip removed) or small (1-2 mm) dermal punch or mouse ear punch (Fisher # 13-820-063)

Kimwipes

Paper towels

Protocol steps—Step annotations:

Tissue preparation and fixation

1. Follow protocol in Basic Protocol 3: Whole mount immunostaining of mouse skin, Tissue preparation and fixation subsection
2. In addition to scraping/removing the subdermal connective tissue, gently scrape the outside of the skin. This helps remove the stratum corneum and reduces the amount of background staining.

Oil Red O Skin staining

1. Wash 10 minutes in 60% Isopropanol in water at room temperature with agitation.
2. Prepare 0.3% Oil Red O/60% Isopropanol by diluting 0.5% (w/v) Oil Red O in Isopropanol with water at a mixture of 3 parts dye to 2 parts water.

   The mixture will turn opaque.
3. Run the prepared 0.3% Oil Red O dye through a 0.2 µm syringe filter to remove any particles of undissolved dye.

   The suspended particles make filtering this solution difficult. Be careful to not apply too much pressure to the syringe during filtering as this may cause the filter to burst. The filtering step may take 5-10 minutes if a large volume (>25 mL) is needed.

4. Stain skin samples in 0.3% Oil Red O in 60% Isopropanol at room temperature for 30 minutes to 3 hours. Monitor the staining reaction to avoid overstaining of the skin, which will lead to high background (Fig. 7 A-B).

    As staining occurs the sebaceous glands adjacent to hair follicles will darken gradually with red pigment.

5. Wash with 60% Isopropanol in water 2x10 minutes at room temperature with agitation.
6. Wash/store in water at 4°C until ready to image.

    If storing tissue longer than one week, add 0.01% sodium azide to the water to inhibit microbe growth.

Reagents and Solutions:

1x Phosphate Buffered Saline (PBS)

For 1 L 10x PBS stock solution:

Dissolve in 800mL distilled H_2O:

80 g NaCl (1.37 M final)

2 g KCl (26.8 mM final)

14.4 g Na_2HPO_4 (101.4 mM final)

2.4 g KH_2PO_4 (17.6 mM final)

Adjust pH to 7.4, adjust volume to 1L with distilled H_2O.

10x stock solution is stable at room temp for ≥6 months. Recheck pH before using old stock solution.

For 1L 1x PBS:

Dilute 100mL 10x PBS stock in 900mL distilled H_2O. Check pH and adjust to 7.4 if necessary.

1x PBS is shelf stable at room temperature for 2-3 months.

4% Paraformaldehyde in PBS

From dry paraformaldehyde stock:

1. Add 400mL of 1x PBS to a beaker on a heat plate with a stir bar in a fume hood. Heat to 60°C.
2. Weigh out 20g paraformaldehyde powder (Fisher #A1131336) in a fume hood and add to heated PBS.
3. Add 10M NaOH dropwise to paraformaldehyde/PBS mixture until all PFA granules are in solution.

4. Allow solution to cool to room temperature and filter through a Whatman #1 filter or a coffee filter to remove any residual PFA granules.
5. Adjust pH to 7.4 using dilute (5M or 1M) HCl. Note: This will contaminate a pH electrode with PFA. If this is a concern, use pH test strips (VWR #10BDH3171).
6. Adjust final volume to 500mL using reserved 1x PBS and re-check/adjust pH.
7. Aliquot into 40mL volumes and freeze for up to 6 months at -20°C.

From 16% electron microscopy grade liquid paraformaldehyde:

1. Carefully snap open one 10mL ampule of 16% EM grade PFA (Fisher #50-980-487) in a chemical fume hood. Wrapping the ampule in a paper towel will protect your hands from the occasional glass flake during opening.
2. Empty ampule contents into a 50mL conical vial.
3. Rinse ampule with 10mL freshly made PBS (from 10x PBS stock) and add to 50mL conical vial.
4. Add an additional 20mL fresh PBS to the conical vial to a total volume of 40mL 4% PFA.
5. Store on ice until use. Leftover stock can be stored at -20°C until used. Avoid freeze-thawing PFA stocks.

IHC Blocking Buffer

For 15 mL of blocking buffer (enough for approximately 60 slides or approximately 5-10 whole skin samples):

750 µL (5% v/v) DMSO

375 µL (2.5% v/v) Triton X-100

375 µL (2.5% v/v) Normal Donkey Serum or Normal Goat Serum (as appropriate for primary/secondary antibodies) (Jackson ImmunoResearch #017-000-121 (NDS) or #005-000-121 (NGS))

7.5 µL (0.05% v/v final concentration) Sodium Azide from a 2% w/v Sodium Azide in water stock solution

Adjust volume to 15 mL with 1x PBS

Blocking buffer can be stored at 4°C for up to 1 month. Discard if solution becomes cloudy or develops an odor. A base mixture excluding serum can also be made in bulk (150 mL) quantities and stored at room temperature up to 6 months, adding serum to smaller aliquots before use.

Zamboni's Fixative

For 50 mL fixative:

6.25 mL 16% w/v Paraformaldehyde, MeOH and RNase free (EMS #15710)

7.5 mL saturated picric acid solution (Fisher #SP920050)

36.25 mL 1x PBS

Adjust pH to 7.4 with 10M NaOH

Zamboni's fixative can be stored at 4°C indefinitely but should be carefully disposed of if a precipitate forms. *Dry picric acid is shock sensitive and explosive. While saturated solutions are relatively safe be sure to clean all storage containers and wash any equipment used with picric acid thoroughly. Do not use metal equipment with picric acid. Use pH test strips to avoid contamination of pH meter electrode with paraformaldehyde. As with any paraformaldehyde solution, handle in a fume hood to avoid inhaling fumes.*

PLAP Development Buffer

For 1 L buffer:

Dissolve in 800mL distilled H2O:

12.1 g Tris Base (0.1 M final)

5.84 g NaCl (0.1 M final)

4.5 g $MgCl_2$ (50 mM final)

Adjust pH to 9.5

Adjust volume to 1 L with distilled H_2O

Add Levamisole hydrochloride (Fisher ##ICN15522810) to 2.5 mM (12.5 mg in 50 mL) to volume to be used just before adding BCIP/NBT

Buffer solution without levamisole and BCIP/NBT is shelf stable indefinitely as long as no precipitate or odor forms. After adding levamisole, the buffer should be used within 2-3 days and stored at 4°C. BCIP/NBT should be added immediately before application to tissue.

0.5% w/v Oil Red O in isopropyl alcohol

Dissolve 500 mg Oil red O (Fisher #AAA1298914) in 100 mL isopropyl alcohol.

The Oil Red O powder is extremely fine and is a persistent dye. Measure carefully in a chemical fume hood and thoroughly clean any spillage to avoid contamination of surfaces with the dye.

Special Equipment

Silicone-bottomed dishes:

Uncoated 10 cm cell culture plates or glass 10 cm petri dishes

Sylgard 182 Elastomer Kit (Fisher #NC9897184)

Sylgard 182 silicone elastomer base

Sylgard 182 silicone elastomer curing agent

Disposable mixing container (plastic drinking cup)

Wooden popsicle stick or tongue depressor

1. Weigh an appropriate volume of Sylgard 182 base and **thoroughly** mix with Sylgard 182 curing agent at a 10:1 by weight ratio of base to curing agent. Use a disposable mixing container and wooden popsicle stick to mix. Mix for 3-5 minutes continuously, scraping container sides frequently to ensure complete incorporation of base and curing agent. Air bubbles will be introduced during mixing. These need to be removed before curing.

   A standard 10 cm cell culture dish requires approximately 25 mL total elastomer to coat the bottom. Due to its viscosity, precise volumetric measurement of Sylgard 182 base is difficult and unnecessary for most situations.

2. Pour silicone elastomer mixture into plates to coat bottoms 2-3mm deep.
3. Move plates to a vacuum bell jar and evacuate. Quickly release the vacuum to dispel air bubbles.

   Some bubbles may take multiple rounds of vacuum treating to remove. Sharply banging the plates on a benchtop can also help bubbles rise to the surface.

4. Cure plates overnight at an elevated temperature (37°C- 60°C).

   Supplies used in pouring the plates can also be cured to neutralize the elastomer components.

Commentary

Background Information

Detailed analysis of sensory neurons is an essential technique for many labs wishing to study the development and morphology of complex neuronal systems. Due to its hydrophobicity and heterogenous composition, analysis of skin innervation in both flat mount preparations and cryo-sections requires additional steps beyond those used in many other immunolabeling contexts. Sections of hairy and glabrous skin are useful for analysis of innervation density, innervation depth into the dermis, and detailed analysis of hair follicle innervating neurons. Thin sections (≤50 μm) can be labeled with a wider array of antibodies than whole-mount skin. Sections up to 100 μm can be labeled using the floating section immunolabeling steps in Basic Protocol 1 and can be imaged using a confocal fluorescence microscope without tissue clearing. This allows the analysis of approximately 2 hair shaft diameters depth of skin in each section. Flat mount skin can be used for analysis of single neuron receptive fields and innervation patterns when combined with sparse labeling approaches or can be used to assay general neuronal density when combined with population specific antibody labeling.

Critical Parameters:

The key parameter when planning experiments involving the histological analysis of mouse skin innervation is the stage of the hair follicle replacement cycle (Alonso, 2006; Müller-Röver et al., 2001; Sundberg et al., 2005). In brief, hairy skin goes through a series of three stages: anagen, the growth of a new hair shaft and loss of the old hair shaft; catagen, the transition from growth into resting phase where the stem cells responsible for hair growth undergo apoptosis; and telogen, the resting phase where a mature hair shaft and follicle are present waiting to be replaced. During this cycle, the

thickness of the skin varies, being thinnest during telogen and thickest during mid-late anagen. While the skin is thicker and contains more of the hair shaft, labeling and imaging becomes difficult or impossible due to limits on antibody penetration and light scattering induced by hair shafts. In most laboratory mouse strains hair development starts at approximately postnatal day 3 and reaches its first telogen between postnatal day 19 and day 21, making this the first window of opportunity for analysis of flat mounted skin (Müller-Röver et al., 2001). The hair cycle repeats every 20-40 days, becoming more desynchronized across the animal as time goes on. In older animals, hair cycle stage can be judged based on the color of the skin in pigmented mouse strains, or on the thickness of the skin in pigmentless mice (Müller-Röver et al., 2001). Experiment timing may have to be empirically determined based on mouse strains used and the effects of genetic manipulations, particularly manipulations of cell death and hair follicle specification pathways (Nowak et al., 2008).

Hair cycle stage is less important for imaging glabrous skin, and for processing and analysis of slide mounted hairy skin sections. Floating skin sections can be successfully prepared from tissue at all phases of the hair cycle, but samples from animals in catagen are much more difficult to flatten onto slides after labeling and are more prone to tissue damage during processing.

Troubleshooting:

Problem	Possible Cause	Solution
Skin sections fall apart during floating section labeling	Fungal/bacterial growth in labeling solution if cloudy	Dispose of blocking buffer stock and remake fresh stock; ensure NaN_3 is included in blocking buffer
Cryosections break apart or horizontal lines run through sections	Cryostat is too cold Block or blade is loose	Increase chamber temperature of cryostat 1-2°C Securely tighten all blade holder adjustments and add additional OCT to block/mandrel
Cryosections smear on blade or compress during cutting	Cryostat is too warm	Lower the chamber temperature 1-2°C.
Vertical lines running through cryosections	Debris on cryostat blade or anti-roll plate Cryostat blade is damaged/dull	Clean blade and anti-roll plate Replace blade
Large “clumps” of Oil Red O pigment collect on sample	0.3% Oil Red O solution not filtered before staining Skin is not in telogen Skin needs additional destaining washes in 60% isopropyl alcohol	Filter 0.3% Oil Red O solution after mixing Extend the 60% isopropyl alcohol wash step, image skin with the epidermal (outside) face up
Low signal intensity	Antibody concentration too low Poor tissue fixation Poor secondary antibody choice for microscope	Increase antibody concentration and repeat labeling Fix tissue with perfusion when possible Use fresh fixative when possible Choose fluorescent secondary antibodies carefully to balance background autofluorescence with brightness
Uneven labeling across sections or tissues	Poor or uneven tissue fixation Incomplete coverage of tissue with labeling solution	Re-attempt experiment using fixative perfusion rather than drop fixation Increase labeling solution volume and ensure samples are moving freely in tubes during incubation Ensure slides do not dry out during incubation, use a humidified slide staining chamber if possible.
Bright “clumps” in fluorescently labeled samples	Aggregation of secondary antibodies	Spin stock tubes of secondary antibodies at 5000 x g for 5 minutes at room

		temperature or 4°C and use only supernatant from the top of the tube or pass secondary antibody solution through a 0.45 µm syringe filter before application. Replace old secondary antibodies with fresh ones as needed.
Dehydrated whole mount skin does not fully clear within 30-45 minutes in BABB	Skin is not fully dehydrated (can occur if final wash did not run long enough or if final wash was not in 100% MeOH.)	Attempt to re-dehydrate skin samples by immersing in 100% MeOH at room temperature overnight. This may dramatically reduce signal intensity.
High background in skin sections	Natural autofluorescence in 488 nm/FITC/GFP range	Avoid 488 nm/FITC/GFP range when possible. Use only strongly fluorescent antibody labels on the 488 nm/FITC/GFP channel.

Table 1: Troubleshooting Guide

Understanding Results:

Expected results from fluorescently labeled skin and paw sections and flat-mount skin will depend heavily on the imaging modality used. Standard widefield fluorescence imaging can be used for general surveying of samples and for identification of gross changes to innervation, such as denervation. Widefield microscopy can also be used on hairy skin sections to examine the proportion of follicles innervated by a given neuronal subtype through follicle and nerve ending counting. Using structured illumination widefield microscopy, such as the Zeiss Apotome.2 system, optical sections can be taken allowing for tissue depth segmentation in flat-mount samples. This allows for more focused analysis of specific skin layers (i.e., free nerve endings vs. longitudinal-lanceolate endings) (Fig. 5C-E). Detailed analysis into changes in nerve ending density or morphology in both section and flat-mount preparations will generally require imaging on a confocal microscope equipped with a 40x oil-immersion objective. Examples of

image quality from structured illumination widefield and confocal microscopy in hairy and paw skin sections (Fig 3D-E, Fig 4E-F).

Imaging of Alkaline Phosphatase and Oil Red O stained skin is done using traditional brightfield microscopy. Alkaline Phosphatase stained and cleared skin can be imaged a brightfield capable upright microscope or a dissecting microscope capable of transmission illumination. Clearer images can be obtained using a color microscope camera to separate the natural purple-blue tint of the Alkaline Phosphatase precipitate from the natural tint of the cleared skin (Fig. 6B, D). Likewise, the intense red color of Oil Red O labeled hair follicles can be used to isolate stained areas for automated analysis if imaged on a color camera (Fig. 7B).

Time Considerations:

The protocol for sectioned hairy skin (Basic Protocol 1) can be run from start to finish in just over 3.5 days, including the two overnight incubation steps (fixation, sucrose, and primary incubation). The hands-on steps for this protocol require 6-8 hours spread over the 3.5 days, with the bulk of the hands-on time spent in the sectioning and imaging steps.

Alternate protocol 1 can be run from start to finish over 2 days if needed by omitting the overnight wash step and freezing/sectioning tissue on the same day it is collected. It is important that the tissue is allowed to dry on slides for at least 4 hours after sectioning and before immunolabeling to ensure good section adhesion. As with Basic Protocol 1, the bulk of the time in this protocol is spent sectioning and imaging and will increase as additional samples are added.

The protocol for sectioned glabrous skin (Basic Protocol 2) can be run from start to finish in 5.5 days, with multiple overnight steps and a 2-day incubation with no

interaction. Like Basic Protocol 1, the bulk of the hands-on time is spent in sectioning and imaging of the tissue.

The protocol for whole mount skin immunolabeling (Basic Protocol 3) can be run from start to finish in 7-14 days depending on the amount of time spent in primary incubation. This will need to be determined empirically for specific age/antibody combinations. The bulk of this time is hands-off, requiring 6-8 hours of hands-on time spread over the length of the protocol. The amount of time to complete the protocol does not increase significantly with additional samples.

The protocol for whole mount skin immunohistochemical labeling with a *Cre*-dependent placental alkaline phosphatase (Basic Protocol 4) can be run from start to finish in 3-5 days depending on the length of time spent in AP development. As with the other protocols much of this time is hands-off, requiring 6-8 hours over the length of the protocol.

The protocol for Oil Red O staining of whole skin samples (Basic Protocol 5) can be run from start to finish in 1.5 days including the one overnight fixation step. The staining and washing steps take 4-5 hours total, with approximately 45 minutes of hands-on time once all solutions are made.

Imaging and image analysis time for all these protocols will vary greatly based on the imaging methodology chosen and the specific analysis needs of the experiments. Imaging of Oil Red O and Alkaline Phosphatase-stained skin is much quicker than imaging of fluorescently labelled samples due to using brightfield microscopy rather than multi-color fluorescence, structured illumination, or confocal microscopy. Image analysis time can range greatly depending on the desired analysis. For example, hair

follicle density from Oil Red O stained skin samples can be quickly calculated manually using cell counting software included in Fiji and can be easily automated with cell/point counting programs. In contrast, detailed tracing of single neuron receptive fields in the skin can take upwards of 2 hours per neuron depending on the complexity and is a task which is difficult to automate using existing automated axon tracing programs.

Acknowledgements:

The authors would like to thank the Ginty, Badea, and Nathans labs for many of the mouse lines used in the preparation of this protocol, as well as the members of the Lumpkin lab for advice in developing the whole mount skin immunolabeling protocol. This work was supported by NIH grants R01NS091027 (KMW), T32GM071338 (MBP), and a Whitehall Foundation Research Grant (KWM).

Chapter 3: Follicle-innervating Aδ-low threshold mechanoreceptors organize through a population-dependent mechanism.

Matthew B. Pomaville & Kevin M. Wright, Ph.D.

Manuscript under review at Development and available on bioRxiv at:

https://doi.org/10.1101/2022.08.09.503379

Summary Statement

Aδ follicle-innervating low-threshold mechanoreceptor neurons form tiled receptive fields through competition for hair follicles during the early postnatal period.

Abstract

The mammalian somatosensory system is comprised of multiple neuronal populations that form specialized, highly organized sensory endings in the skin. The organization of somatosensory endings is essential to their functions, yet the mechanisms which regulate this organization remain unclear. Using a combination of genetic and molecular labeling approaches, Iexamined the development of mouse hair follicle-innervating low-threshold mechanoreceptors (LTMRs) and explored competition for innervation targets as a mechanism involved in the patterning of their receptive fields. Ishow that follicle innervating neurons are present in the skin at birth and that LTMR receptive fields gradually add follicle-innervating endings during the first two postnatal weeks. Using a constitutive *Bax* knockout to increase the number of neurons in adult animals, I show that two LTMR subtypes have differential responses to an increase in neuronal population size: Aδ-LTMR neurons shrink their receptive fields to accommodate the increased number of neurons innervating the skin, while C-LTMR neurons do not. Our findings suggest that competition for hair follicles to innervate plays a role in the patterning and organization of follicle-innervating LTMR neurons.

Introduction

Mammalian somatosensation relies on the proper development, organization, and integration of multiple highly specialized sensory neuron subtypes that reside in the dorsal root ganglia (DRG) (Rice and Albrecht, 2008). In mice, there are at least 10 identified subtypes of skin-innervating sensory neurons, which can be broadly

categorized as hairy skin-innervating or glabrous skin-innervating based on their terminal ending locations (Burgess et al., 1968; Cain et al., 2001; Halata, 1993; Iggo and Muir, 1969; Joong Woo Leem et al., 1993; Knibestöl, 1973; Lynn and Carpenter, 1982; Paré et al., 2002). Historically, these two groups of somatosensory neurons were subdivided based on their conduction velocity and responses to stimuli as measured by electrophysiological recordings (Brown and Iggo, 1967; Horch et al., 1977; Joong Woo Leem et al., 1993; Lewin and McMahon, 1991). In hairy skin, follicles are innervated by multiple populations of low-threshold mechanoreceptive neurons (follicle-innervating LTMRs). Each LTMR neuron extends a peripherally projecting axon into the skin, where it elaborates a receptive field containing highly specialized endings around hair follicles. A series of landmark studies identified tools to genetically label somatosensory neuron subtypes, including the Aβ rapidly adapting (RA)-LTMR, Aδ-LTMR, and C-LTMR neurons, populations that were previously distinguished only by their electrophysiological characteristics (Li et al., 2011; Luo et al., 2009; Rutlin et al., 2014; Wu et al., 2012). These tools have enabled the examination of LTMRs on a population specific and single neuron level, allowing for more detailed questions about receptive field patterning and organization mechanisms to be asked.

In adult mice, the follicle-innervating LTMR neurons form discrete and stereotyped receptive fields, innervating a constrained number of hair follicles in the skin (Bai et al., 2015). LTMR subtypes show remarkable selectivity in the populations of hair follicles that they innervate. Aδ-LTMRs and C-LTMRs innervate both zigzag hairs and awl/auchene hairs, which comprise approximately 74% and 25% of the total hairs in the skin, respectively. Aβ RA-LTMRs form receptive fields innervating awl/auchene hairs, as

well as guard hairs that comprise approximately 1% of the hairs in the skin (Kuehn et al., 2019; Li et al., 2011). Detailed electron microscopy studies also illustrated the ultrastructure of the longitudinal lanceolate ending (LLE), its ensheathing terminal Schwann cells, and their interaction with the hair follicle (Li and Ginty, 2014). These studies together laid the groundwork for molecularly driven exploration into the development and function of follicle-innervating neurons.

The strict organization of follicle innervating neurons into constrained receptive fields is essential for the proper localization of touch stimulus on the body. Recently, advancements in genetically driven multi-fluorophore reporter systems made it possible to examine the interactions between neurons of the same genetic subtype in adult mice. These studies showed that Aδ-LTMR and C-LTMR neurons form tiled receptive fields with minimal overlap between neighboring homotypic neurons. In contrast, Aβ RA-LTMR neurons form receptive fields that overlap with those of neighboring Aβ RA-LTMR neurons, resulting in LLEs from multiple Aβ RA-LTMR neurons at each guard hair (Kuehn et al., 2019). The mechanisms by which follicle-innervating LTMR neurons form exclusive receptive fields remains largely unexplored.

The homotypically tiled arrangement of Aδ-LTMRs and C-LTMRs in mice is reminiscent of the innervation patterns of dendritic arborization (DA) neurons in larval *Drosophila melanogaster* epidermis (Grueber et al., 2002). The four DA neuronal subtypes show differing capacities for homotypic receptive field arrangement. Class IV and III DA neurons tile the body wall with differing degrees of receptive field overlap, while Class I and II DA neurons show no repulsive response to homotypic neurons (Grueber et al., 2003). Tiled dendritic receptive fields have also been observed in

neurons innervating the epidermis in *Manduca sexta* and *Haementeria ghilanii* (Blackshaw et al., 1982; Grueber et al., 2001; Kramer and Kuwada, 1983). The paradigm of sensory neuron receptive field patterning is also present in vertebrate systems. *Danio rerio* trigeminal neurons arrange at the midline through repulsive mechanisms like those seen in *Drosophila* (Sagasti et al., 2005). In the mouse retina, multiple examples of dendritic tiling and population-based organization exist. Bipolar cell subtypes and horizontal cells tile to innervate all available photoreceptor terminals while excluding neighboring homotypic dendritic fields and can adjust their receptive field size to accommodate changes in population. (Huckfeldt et al., 2009; Reese et al., 2005). In contrast, some amacrine cells show substantial overlap of dendritic arbors with homotypic neighbors and maintain dendritic field size even when cell density is altered (Farajian et al., 2004; Keeley et al., 2020; Lee et al., 2011).

In this study, I closely examine the development and maturation of hair follicles and follicle-innervating LTMR neurons over the first three postnatal weeks in mice. I test the hypothesis that LTMRs tile their receptive fields through a process which responds to increases in neuronal population by generating smaller receptive fields. I show that follicle innervation and hair follicle maturation coincide during the early postnatal window (before postnatal day 7, P7), and that by P14, follicle-innervating LTMR receptive fields have similar numbers of mature LLEs as adult receptive fields. Finally, using genetic tools to sparsely label single follicle-innervating LTMR neurons, I show that they form receptive fields in part through homotypic competition during the early postnatal period.

Results

Mouse hair follicle maturation occurs during the early postnatal window

Follicle-innervating LTMR neurons are highly branched in the skin to form receptive fields of highly specialized LLEs around hair follicles. Each follicle-innervating LTMR subtype selectively innervates specific hair follicle subtypes (Fig. 1A). However, the process by which this occurs during development is poorly understood. To understand the temporal relationship between hair follicles and LTMRs during development, I first characterized the postnatal maturation of hair follicles. Previous literature characterizing hair follicle maturation demonstrated that hair follicles are established in multiple waves starting at embryonic day 15 (E15) and continue through P9, when all hair follicles have a mature structure, including a hair shaft emerging from the skin (Paus et al., 1999). To assess hair follicle density during the early postnatal period, back skin was collected from mice at time points between P0 and P60 (Fig. 1B-G). Hair follicles could be easily identified as cell-dense structures in skin sections by staining with the nuclear marker DAPI. Hair follicle density was calculated by counting the number of hair follicle structures (long DAPI-dense structures) present in a known length of skin. Hair follicle density initially remains stable from P1-P6, then decreases beginning at P14 as mice grow more rapidly (Fig. 1H, Table 1). This decrease in density corresponds with hair follicles completing their passage through the hair follicle cycle, as can be seen by the changes in dermal thickness over time (Müller-Röver et al., 2001).

I further analyzed the changes in hair follicle density by normalizing the density measurements for each timepoint to the average body length of a cohort of age-matched mice (Fig. S1A). This normalization supports the conclusion that hair follicle density decreases as mice grow, and that the density of hair follicles decreases more

than would be expected if mice were adding hair follicles at a rate that kept pace with animal growth (Fig. S1B). From these data, I conclude that hair follicle maturation occurs rapidly in the early postnatal window and that the rate of hair follicle addition decreases in maturing mice.

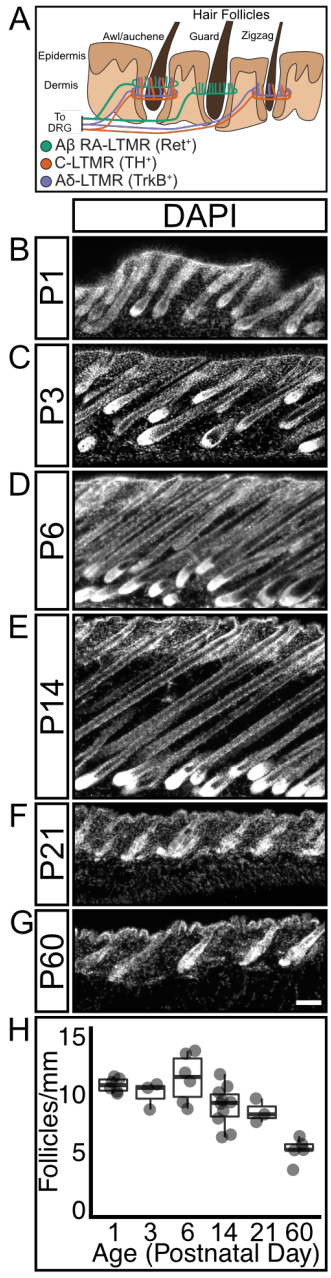

Figure 1 – Mouse hair follicle density decreases as mice age

A) Schematic showing hair follicle-innervating LTMR neuron subtypes projecting to the skin, where their axons branch and selectively innervate specific hair follicle types.

B-G) Sagittal sections of mouse back skin stained with DAPI to highlight hair follicle structures. Section height increases, then decreases as mice age and progress through the hair follicle life cycle. Scale bar – 50 μm

H) Hair follicle density remains stable for the first week of postnatal life, then decreases as mice grow. N= 6(P1), 3(P3), 6(P6), 10(P14), 3(P21), 5(P60)

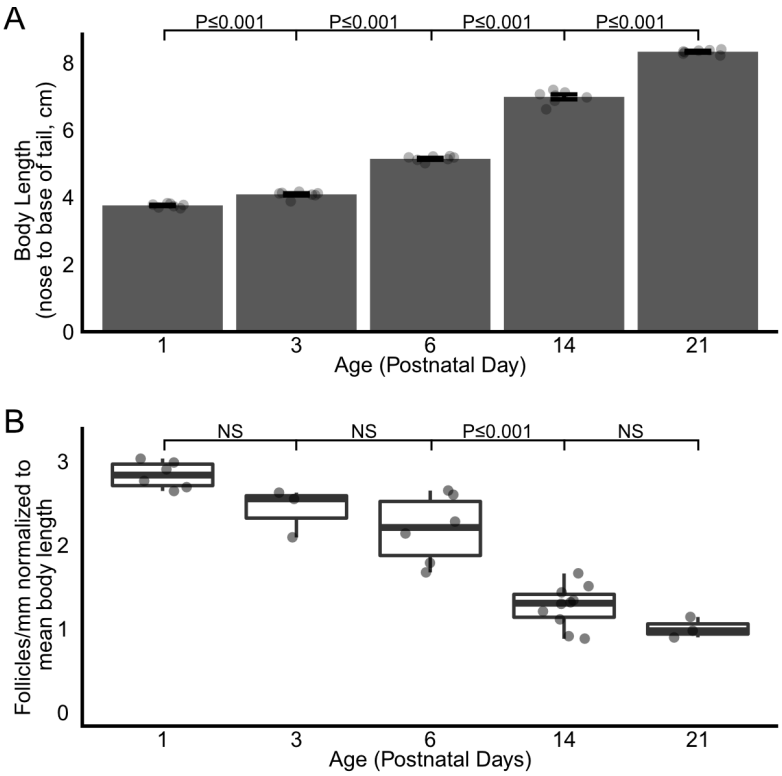

Supplemental Figure 1 – Hair follicle density decreases relative to body length as mice grow

A) Average body length (nose to base of tail) of an age-matched cohort of 10 wild-type mice in centimeters. Bars represent mean ± s.e.m. One-way ANOVA with Tukey's HSD post-hoc testing (ANOVA P≤ 0.001, P1-P3: P≤ 0.001, P3-P6: P≤ 0.001, P6-P14: P≤ 0.001, P14-P21: P≤0.001.

B) Quantification of mouse hair follicle density from Figure 1H normalized to the mean body length of a cohort of 10 same-age mice shown in (A). Bars represent mean ± s.e.m. One-way ANOVA with Tukey's HSD post-hoc testing (ANOVA P≤ 0.001, P6-P14 P≤ 0.001) N = 6(P1), 3(P3), 6(P6), 10(P14), 3(P21), 5(P60)

Sensory neurons form specialized endings concurrently with hair follicle maturation

I next examined the developmental time course of hair follicle innervation using the pan-neuronal marker β-III Tubulin. I quantified the proportion of hair follicles with a β-III Tubulin-positive nerve ending encircling the follicle at multiple developmental timepoints from P1-P60 (Fig. 2A-F). Axons are present in the dermis and epidermis at P1, but very few innervate hair follicles at this age (Fig. 2A, 2G). While axon branches are present at the expected depth for follicle-innervating LLEs (inset region, Fig. 2A), these neurite branches do not yet encircle the hair follicle. There is a significant

increase in the proportion of innervated hair follicles at P3, with over half of hair follicles encircled by a β-III Tubulin-positive axon (Fig. 2B, 2G). At P3 the encircling endings have not formed the LLE projections characteristic of follicle-innervating LTMRs. By P6 the innervation of hair follicles is nearly complete and the characteristic LLEs have appeared, projecting towards the epidermal surface along the hair shaft from the encircling neurite (Fig. 2C and inset, 2G). By P14, hair follicle innervation is complete, and the proportion of innervated hair follicles and LLE morphology remains unchanged at P21 and P60 (Fig. 2D-F, 2G, Table 1). These findings are largely in agreement with other studies and suggest that murine hair follicle innervation occurs during the early postnatal window, and that by the end of the first postnatal week hair follicle innervation has reached a grossly mature state (Meltzer et al., 2022b preprint; Peters et al., 2002).

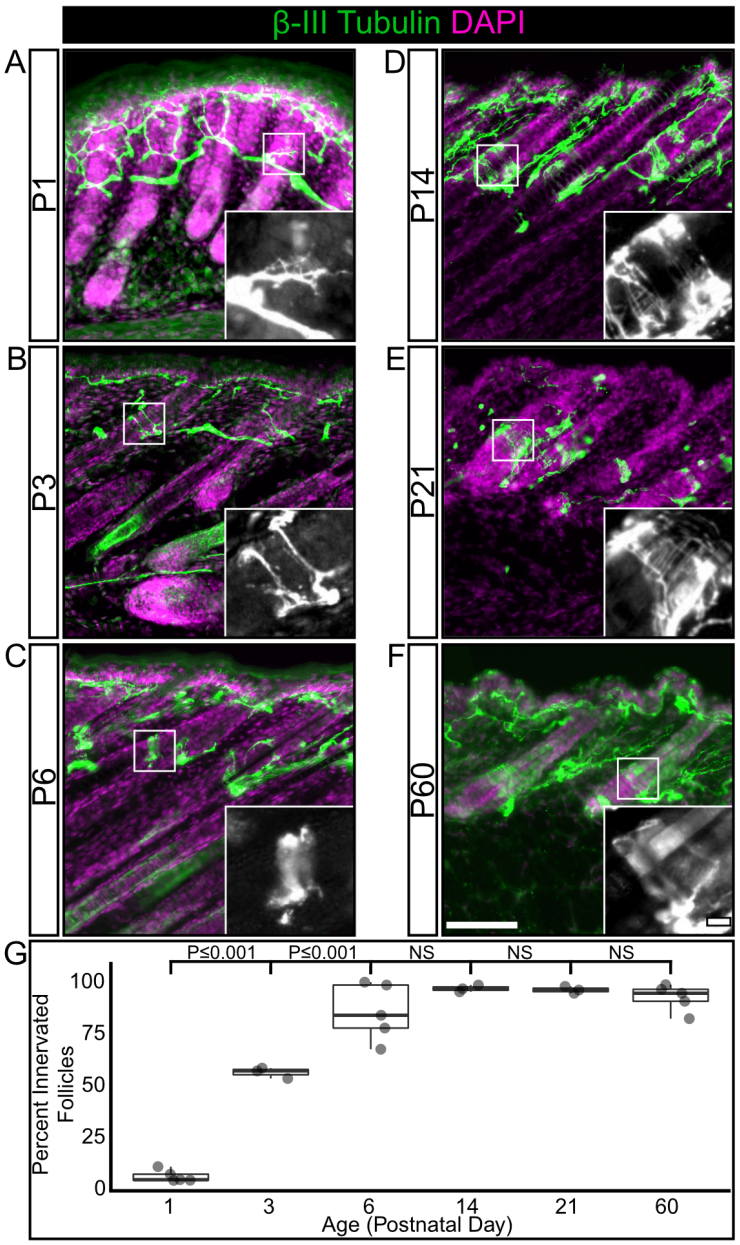

Figure 2 – The percentage of innervated hair follicles increases during the first postnatal week, then remains stable into adulthood.

A-F) Representative images of hair follicle innervation labeled with a pan-neuronal marker (β-III Tubulin, green) and DAPI (magenta). Mature longitudinal-lanceolate endings begin to appear by P6. Insets – Single channel images of follicle innervation. Scale bar – 50 μm, insets – 10 μm.

G) Quantification of the percentage of hair follicles innervated by a β-III Tubulin positive axon. One-way ANOVA with Tukey's HSD post-hoc testing (ANOVA P≤ 0.001, P1-P3 P≤ 0.001, P3-P6 P≤ 0.001) N= 5(P1), 3(P3), 5(P6), 3(P14), 3(P21), 5(P60)

Aβ RA-LTMR follicle innervation precedes C-LTMR and Aδ-LTMR follicle innervation

I next investigated whether there is a temporal hierarchy of hair follicle innervation between LTMR subtypes. To assess the development of hair follicle innervation by specific LTMR subtypes, I utilized three separate labeling strategies. Based on data from single-cell RNA sequencing performed on adult dorsal root ganglia neurons and previous studies examining LTMR development, I identified ubiquitous markers for Aβ RA-LTMRs (anti-Calbindin immunohistochemistry) and C-LTMRs (*Vglut3*^{iCre} driven *TdTomato* expression (*Ai9*)), and an inducible marker for Aδ-LTMRs (*TrkB*^{CreERT2} driven placental alkaline phosphatase (*R26*^{iAP}) reporter) (Badea et al., 2003; Lou et al., 2013; Rutlin et al., 2014; Seal et al., 2009; Sharma et al., 2020; Usoskin et al., 2015).

Calbindin^{+} Aβ RA-LTMRs innervate guard (tylotrich) hairs, which make up approximately 1% of the hair follicles in mouse skin, and awl/auchene hairs which make up approximately 25% of the follicles (Kuehn et al., 2019; Li and Ginty, 2014). At P1, there are very few Calbindin^{+} follicle-encircling nerve endings present (Fig. 3A, 3G), but by P3 the proportion of hair follicles with Calbindin^{+} encircling LTMR endings has significantly increased to approximately adult levels (Fig. 3B, 3G) and remains stable through at least P60 (Fig. 3C-F, 3G, Supplementary Table 1). C-LTMRs innervate the two families of non-tylotrich hairs, the zigzag hairs (~74% of hair follicles) and the awl/auchene hairs (Kuehn et al., 2019; Li and Ginty, 2014). At P1, Vglut3^{+} C-LTMR axons are present in the skin but there are few follicle-innervating nerve endings present (Fig. 3H, 3N). The proportion of C-LTMR-innervated hair follicles significantly increases between P1 and P3, with over half of hair follicles receiving innervation from a

C-LTMR axon ending (Fig. 3I, 3N). By P6 the proportion of C-LTMR innervated hair follicles has increased to approximately adult levels, where it remains stable (Fig. 3J-M, 3N, Table 1).

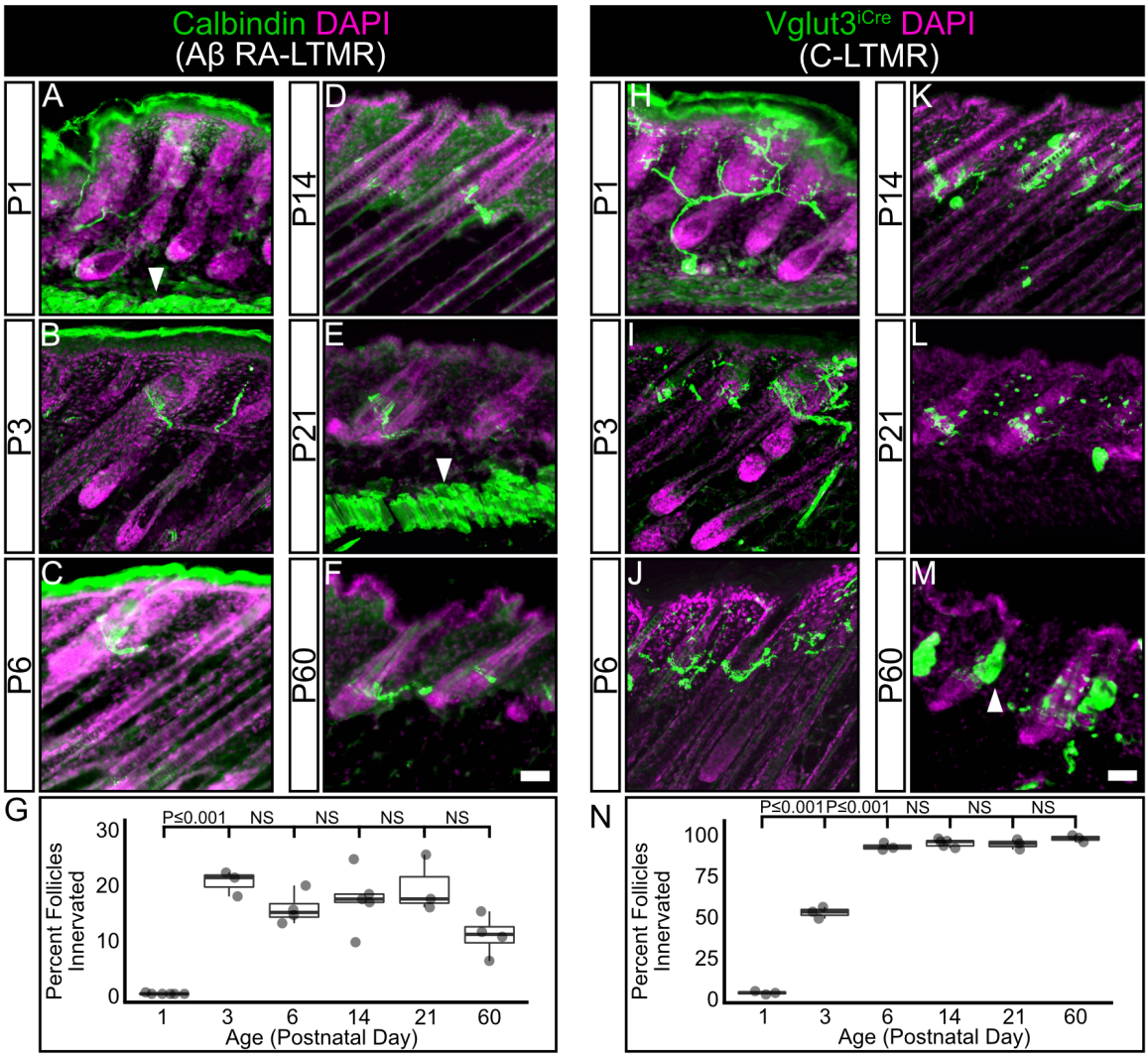

Figure 3 – Aβ RA-LTMR neurons complete innervation of hair follicles before C-LTMR neurons.

A-F) Representative images of hair follicle innervation labeled with a Aβ RA-LTMR specific marker (Calbindin, green) and DAPI (magenta). Mature longitudinal-lanceolate endings begin to appear by P3. Arrowheads (A, E) – Subcutaneous muscle autofluorescence, Scale bar – 50 μm

G) Quantification of the percentage of hair follicles innervated by a Calbindin positive Aβ RA-LTMR axon. The percentage of innervated hair follicles reaches its maximum level by P3. One-way ANOVA with Tukey's HSD post-hoc testing (ANOVA P≤ 0.001, P1-P3 P≤ 0.001). N= 6(P1), 3(P3), 4(P6), 5(P14), 3(P21), 4(P60)

H-M) Representative images of hair follicles innervated by Vglut3+ axons (*Vglut3^{iCre};TdTomato*, green) and DAPI (magenta). Mature longitudinal-lanceolate endings begin to appear by P3. Arrowhead (M) – Sebaceous gland autofluorescence, Scale bar – 50 μm

N) Quantification of the percentage of hair follicles innervated by a *Vglut3^{iCre};TdTomato* positive C-LTMR axon. The percentage of innervated hair follicles increases between P1 and P3, and reaches its maximum level by P6. One-way ANOVA with Tukey's HSD post-hoc testing (ANOVA P≤ 0.001, P1-P3 P≤ 0.001, P3-P6 P≤ 0.001). N= 3(P1), 3(P3), 3(P6), 5(P14), 3(P21), 3(P60)

To explore the timing of Aδ-LTMR receptive field development, I crossed the inducible *TrkB*^{CreERT2} line with a *Cre*-inducible GFP reporter line (*Ai140D*) to sparsely label Aδ-LTMRs, and imaged receptive fields at multiple time points (Daigle et al., 2018; Pomaville and Wright, 2021; Rutlin et al., 2014). The Aδ-LTMRs were ideal for developmental receptive field analysis as they were genetically accessible with prenatal tamoxifen administration and *TrkB*^{CreERT2} labels a stable population of cells throughout development. In the first 24 hours after birth, there are few follicle-innervating nerve endings present in the skin, though TrkB^{+} Aδ-LTMR axons are present and have begun to branch (Fig. 4A, 4E). At P3 the neurons have begun to form follicle-innervating endings (Fig. 4B, arrowheads, 4E), but still contain many non-follicle-innervating neurites (Fig. 4B, 4E). The transition from non-ending forming neurites to follicle-innervating endings continues at P6 (Fig. 4C, 4E). By P14 the receptive fields resemble those in mature animals, with few non-follicle-innervating neurites present, and hemicircular LLEs are present at most hair follicles in the innervated area (Fig. 4D, 4E, Supplementary Table 2). The completion of Aδ-LTMR development is further confirmed in sections of P14 skin co-labeled with β-III Tubulin and *TrkB*^{CreERT2}*;R26*^{iAP} driven with multiple high prenatal doses of tamoxifen (Fig. S2A-C). Quantification of the proportion of hair follicles innervated by a TrkB^{+}/β-III Tubulin $^{+}$ ending shows innervation matching expected proportions in adult animals (92.2% ± 3% s.e.m.). Taken together, these data show that innervation of hair follicles by LTMRs is an ongoing process during the first two postnatal weeks, and there is a subtype-specific temporal hierarchy of hair follicle innervation, with Calbindin^{+} Aβ RA-LTMRs preceding both Vglut3^{+} C-LTMRs and TrkB^{+} Aδ-LTMRs.

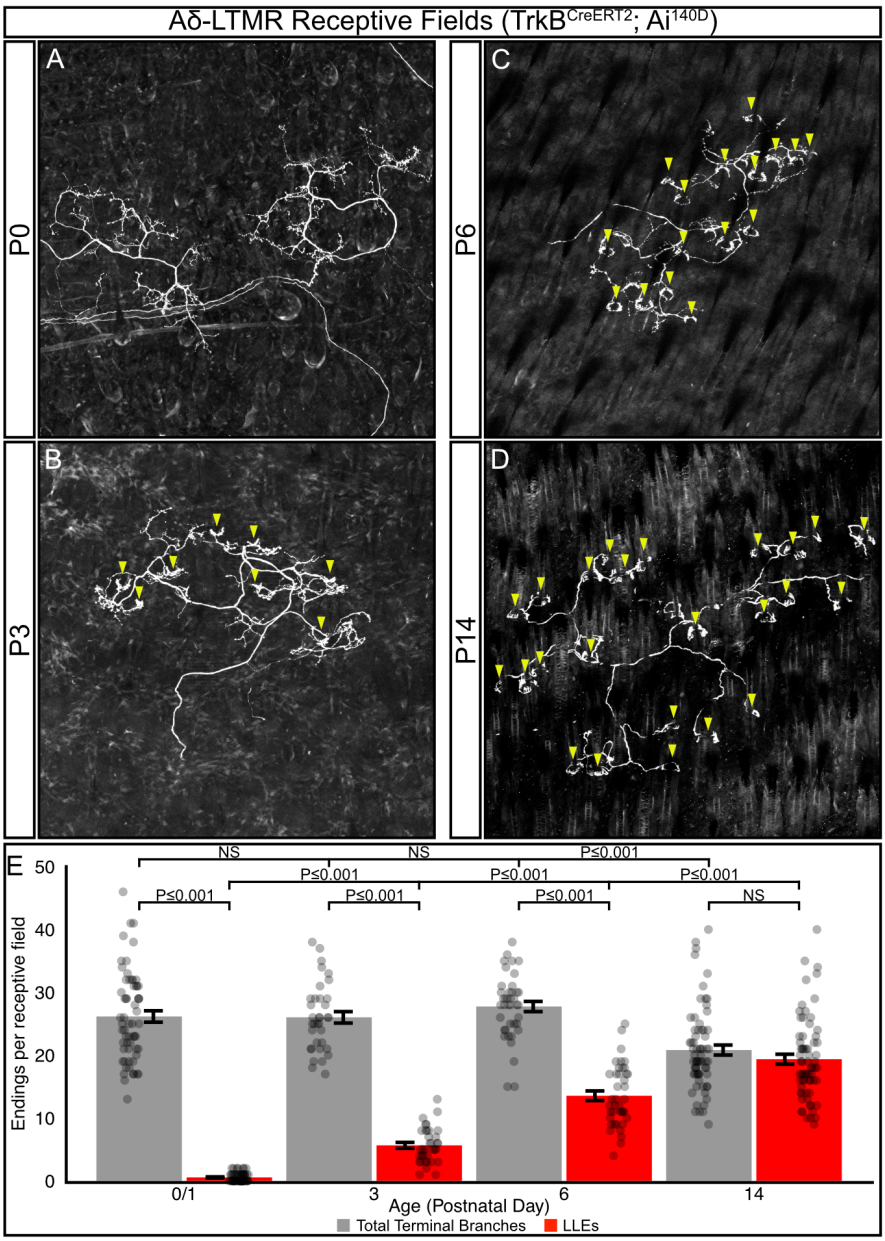

Figure 4 – Aδ-LTMRs develop longitudinal-lanceolate endings (LLEs) after elaboration/branching in the first postnatal week.

A-D) Representative images of sparsely labeled Aδ-LTMR receptive fields in mouse back skin. Aδ-LTMR axons are present in the skin at P0 (A, two distinct adjacent RFs shown). Follicle-innervating LLEs first appear by P3 (B); more follicle-innervating endings are present in P6 animals (C), and by P14 nearly all terminal branches end in LLEs (D). Arrowheads – Follicle-innervating LLEs. Scale bar – 100 μm

E) Quantification of the number of terminal branches per receptive field (grey) and the number of terminal LLEs per receptive field (red). Points represent individual receptive fields. Bars represent mean ± s.e.m. Total number of receptive fields quantified and (number of animals): P0/1: 61(4), P3: 35(3), P6: 40(3), P14: 68(3) Total branches: ANOVA P≤0.001, LLEs: ANOVA P≤0.001, Total branches vs LLEs: P0/1 Wilcoxon Rank Sum Test P≤0.001, P3 Wilcoxon Rank Sum Test P≤0.001, P6 Wilcoxon Rank Sum Test P≤0.001, P14 Wilcoxon Rank Sum Test P≥0.05

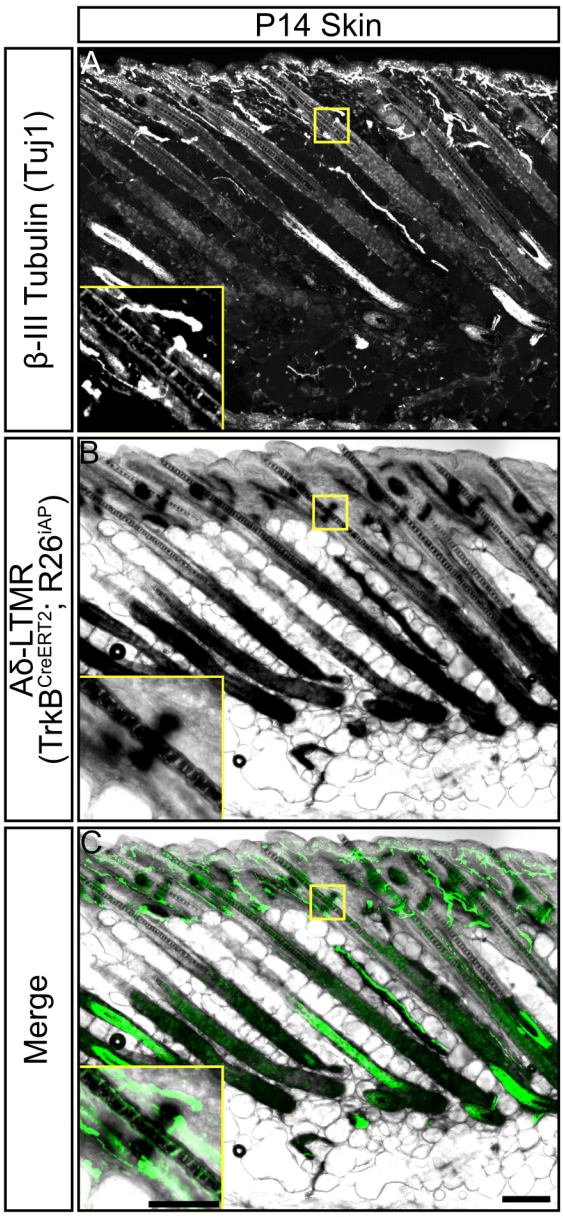

Supplemental Figure 2 – Aδ-LTMR neurons fully innervate hair follicles by P14.
A-C) Representative image of sagittal plane skin sections from a P14 mouse labeled with markers for all neurons (β-III Tubulin, A), Aδ-LTMRs (*TrkB^{CreERT2};iAP*), B), and merged channels (C). Insets – Higher magnification images of a β-III Tubulin^{+}/TrkB$^{CreERT2+}$ double positive longitudinal lanceolate ending. 92.2% ± 3% of follicles were innervated by a β-III Tubulin^{+}/TrkB^{+} LLE. This is similar to previously reported values. N = 4 animals. Scale bar – 100 μm, 50 μm inset.

Competition between Aδ-LTMRs shapes their receptive fields

Many sensory neurons tile their receptive fields in order to reduce homotypic overlap (Grueber et al., 2001; Grueber et al., 2002; Grueber et al., 2003; Sagasti et al., 2005). Of the hair follicles innervated by C-LTMRs, <30% are innervated by multiple C-LTMRs; for Aδ-LTMRs, <10% are innervated by multiple Aδ-LTMRs (Kuehn et al., 2019). I hypothesized that this near-exclusive pattern of receptive field innervation is the result of homotypic competition for territory. If this were true, I would expect individual

neurons of a given subtype to adjust their receptive field size in response to changes in neuronal subtype population. I developed a genetic strategy to test this hypothesis using deletion of the proapoptotic protein *Bax* to generate a model of neuronal overpopulation. Deletion of *Bax* blocks developmental programmed cell death in DRG neurons and results in 50-70% increases in the number of TrkA, TrkC, TrpV1, and CGRP-positive DRG neurons (Kinugasa et al., 2006; Sun et al., 2004; Suzuki et al., 2010). However, the effect of *Bax* deletion on LTMR populations has not previously been assessed.

To quantify the effect of *Bax* deletion on Aδ-LTMR and C-LTMR populations, I collected cryosections from the sixth thoracic DRG, which contains the neurons responsible for innervating the thoracic skin but contains no limb or glabrous skin innervating neurons(Takahashi and Nakajima, 1996). Sections were labeled with markers for sensory neurons (Islet 1/2, Fig. 5A, 5E), C-LTMRs (Tyrosine Hydroxylase (TH), Fig. 5B, 5F), and Aδ-LTMRs (*TrkB*^{CreERT2}*; R26*^{iAP}, (see methods) Fig. 5C, 5G), and the number of marker-positive cell bodies in the imaged sections was manually counted. Cell counts from wild-type and heterozygous mice showed no significant differences in any comparison and were pooled together for analysis (Fig. S3A-C). I found an overall 19% increase in the number of Islet 1/2-positive neurons in *Bax*$^{-/-}$ animals compared to control animals. The number of *TrkB*$^{CreERT2+}$ Aδ-LTMRs showed a significant increase (53%) in *Bax*$^{-/-}$ animals compared to control littermates. The number of TH^{+} C-LTMRs increased 33% in *Bax*$^{-/-}$ animals compared to control littermates, which was not statistically significant (Fig. 5I, Table 3). Deletion of *Bax* had no effect on hair follicle density in P21 mice, as measured using Oil Red O staining (Fig. S4A-D). Therefore,

Bax deletion results in a significant overpopulation of Aδ-LTMR neurons but does not significantly affect the number of C-LTMR neurons or the targets of LTMR innervation (hair follicles).

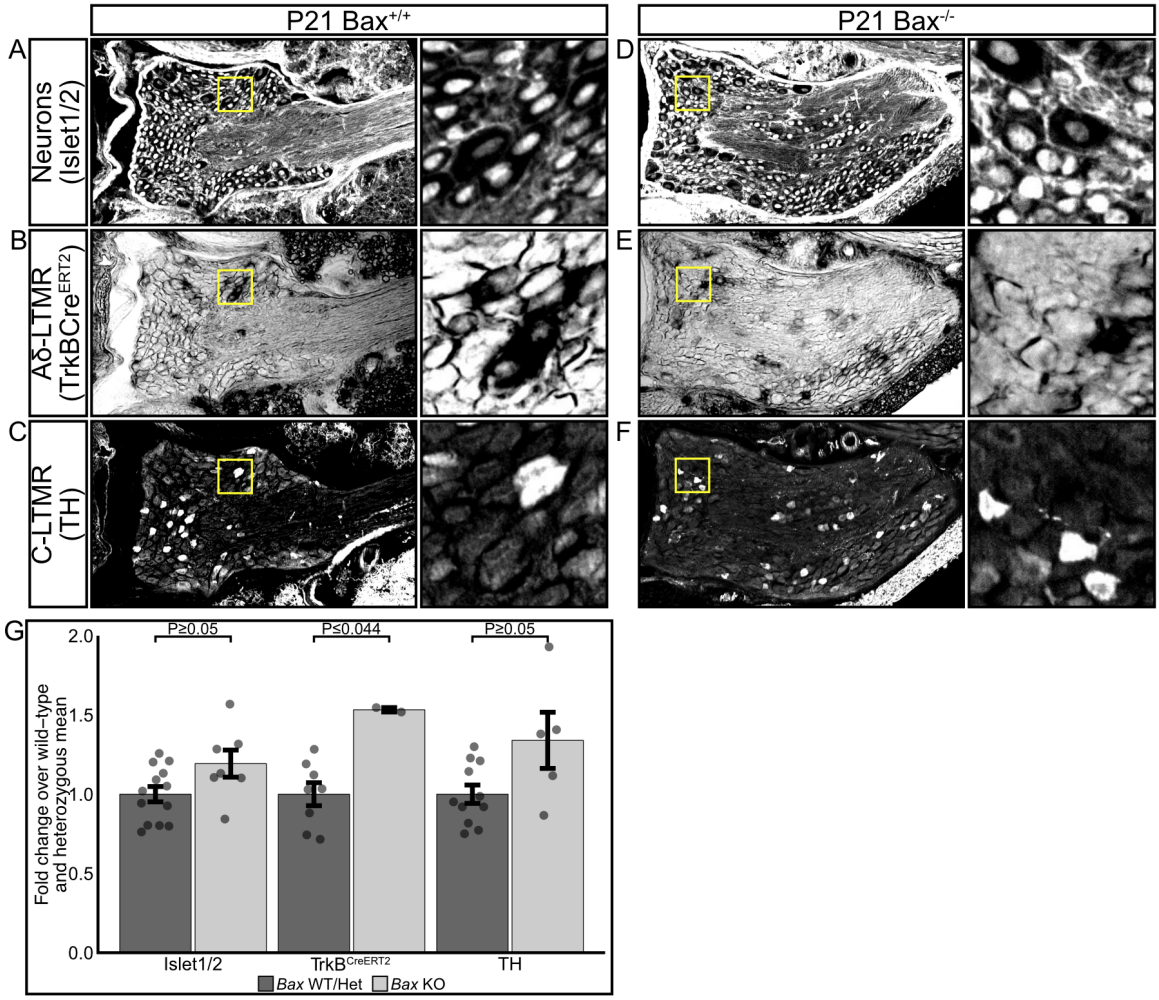

Figure 5 – Genetic deletion of the proapoptotic protein *Bax* has differential effects on LTMR populations

A-F) Representative sections of T6 dorsal root ganglia from 21-day old wild-type littermates (A-C) and *Bax* knockout (D-F) mice labeled with markers for neuronal nuclei (A, D Islet 1/2), Aδ-LTMR cell bodies (B, E TrkB^{CreERT2}; R26^{iAP}), C-LTMR cell bodies (C, F Tyrosine Hydroxylase). Scale bar – 50 μm. Insets show high-magnification of boxed regions.

E) Quantification of the change in T6 DRG LTMR neuron proportions in *Bax* knockout animals over wild-type and heterozygous animals. Bars represent mean ± s.e.m. N = Islet 1/2: WT/Het – 13, KO – 7, TrkB: WT/Het – 8, KO – 2, TH: WT/Het – 11, KO – 5. Islet 1/2 Wilcoxon Rank Sum: P=0.056, TrkB^{CreERT2} Wilcoxon Rank Sum: P≤0.044, TH Wilcoxon Rank Sum: P=0.089

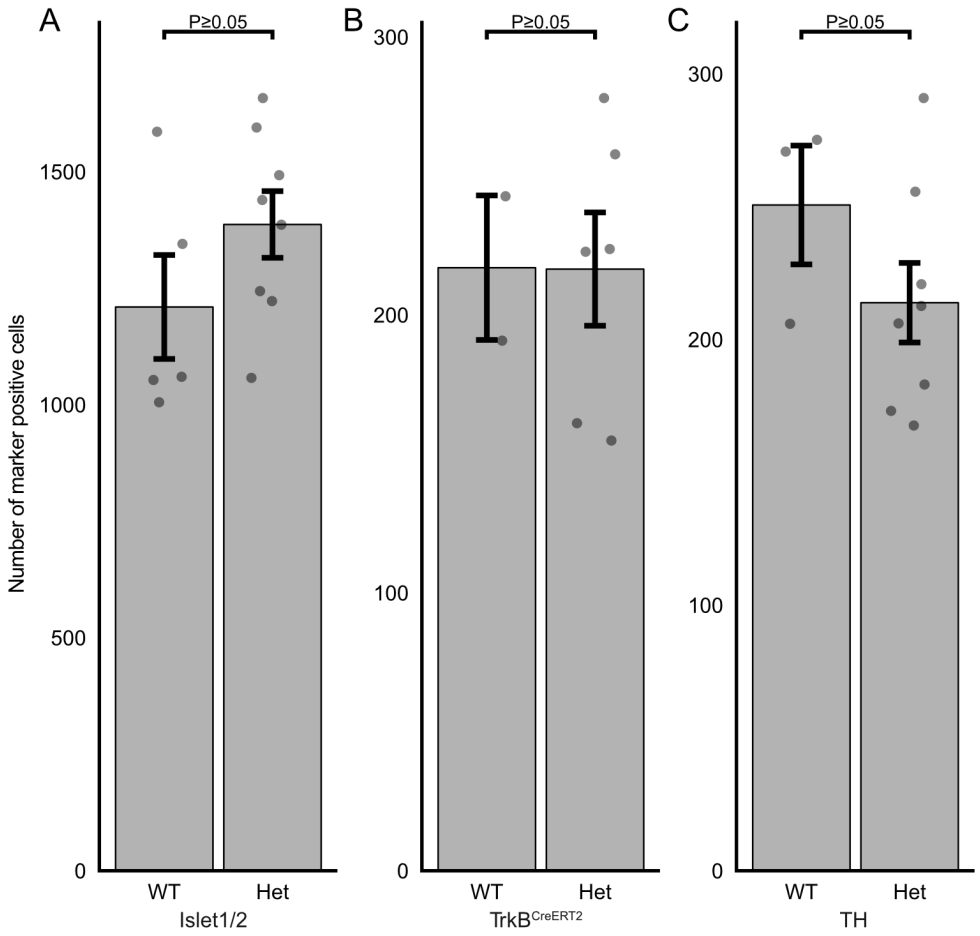

Supplemental Figure 3 – Mice with heterozygous *Bax* deletion have no significant change in the number of neuronal nuclei, Aδ-LTMRs or C-LTMRs compared to wild-type mice

A) Comparison of Islet 1/2^{+} nuclei in *Bax* wild-type and heterozygous mice shows no significant difference. Bars represent mean ± s.e.m. N = 5(WT), 8(Het). Wilcoxon rank sum P≥ 0.05

B) Comparison of TrkB$^{CreERT2+}$ cell bodies in *Bax* wild-type and heterozygous mice shows no significant difference. Bars represent mean ± s.e.m. N = 2(WT), 6(Het). Wilcoxon rank sum P≥ 0.05

C) Comparison of TH^{+} cell bodies in *Bax* wild-type and heterozygous mice shows no significant difference. Bars represent mean ± s.e.m. N = 3(WT), 8(Het). Wilcoxon rank sum P≥ 0.05

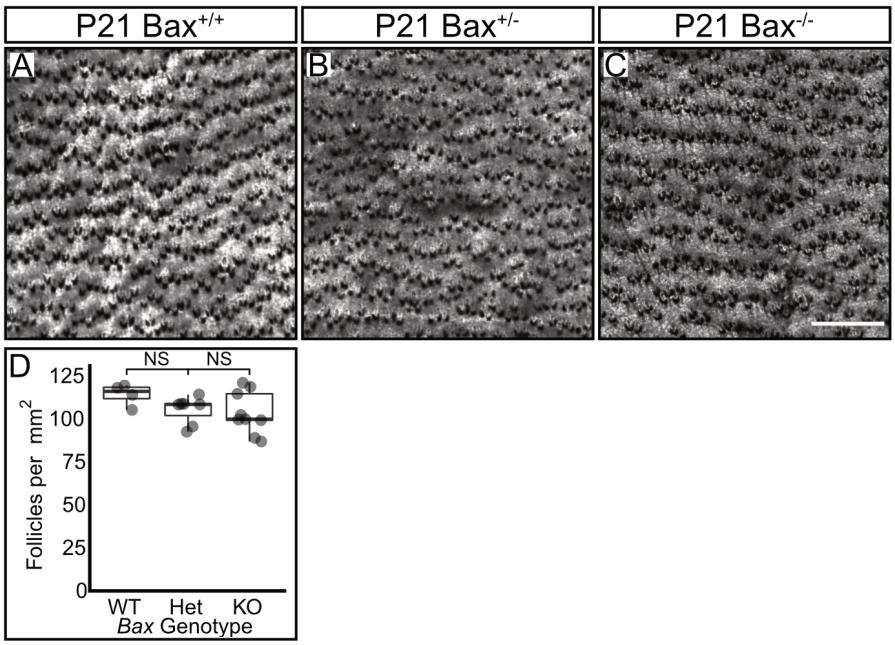

Supplemental Figure 4 – *Bax* deficiency does not change hair follicle density.

A-C) Representative images of P21 mouse back skin from *Bax* wild-type (A), heterozygous (B), and knockout (C) animals stained with the lipophilic marker Oil Red O to identify hair follicles. Scale bar – 500 μm

D) Quantification of the numbers of hair follicles per square millimeter of back skin. Wild-type: 113.2 ± 3.2 s.e.m. follicles/mm^2, Heterozygous: 104.3 ± 3 s.e.m. follicles/mm^2, Knockout: 102.5 ± 4.1 s.e.m. follicles/mm^2. N = 4(WT), 7(Het), 9(KO). One-way ANOVA P= 0.22

If LTMRs of the same subtype compete for territory, I would expect that the receptive fields of individual Aδ-LTMRs would become smaller in *Bax*$^{-/-}$ animals to accommodate the excess number of neurons, while the receptive fields of C-LTMRs would remain largely unchanged. To test this, I generated triple transgenic mice carrying 1: tamoxifen inducible *Cre* driver lines for Aδ-LTMRs (*TrkB*^{CreERT2}) or C-LTMRs (*TH*$^{IRES\text{-}CreER}$), 2: a *Cre*-dependent placental alkaline phosphatase reporter (*R26*^{iAP}), and 3: *Bax*$^{+/+}$, *Bax*$^{+/-}$, or *Bax*$^{-/-}$ (Badea et al., 2009; Knudson et al., 1995; Rotolo et al., 2008; Rutlin et al., 2014). I administered low doses of tamoxifen to timed-pregnant dams (Aδ-LTMRs) or juvenile mice (C-LTMRs) to sparsely label receptive fields and quantified the number of hair follicles in each receptive field of young adult animals (P21). Representative images

of Aδ-LTMR and C-LTMR receptive fields (Fig. 6A-6G) from *Bax*$^{+/+}$, *Bax*$^{+/-}$, and *Bax*$^{-/-}$ mice were traced using the FIJI plugin Simple Neurite Tracer (Fig. 6A'-G') to better illustrate the receptive field structure (Longair et al., 2011; Schindelin et al., 2012). Aδ-LTMRs showed a significant reduction in the number of hair follicles innervated by each neuron in *Bax*$^{-/-}$ animals (24.2 ± 0.5 s.e.m. follicles/neuron) compared with both wild-type (31.6 ± 0.8 s.e.m. follicles/neuron) and heterozygous (29.5 ± 0.5 s.e.m. follicles/neuron) animals (Fig. 6D). This represents a 23% decrease in the number of hair follicles innervated by single Aδ-LTMRs in *Bax*$^{-/-}$ animals. In contrast to the Aδ-LTMRs, there was no significant difference in the number of hair follicles innervated by each C-LTMR receptive field in *Bax*$^{-/-}$ (14.8 ± 0.7 s.e.m. follicles/neuron), heterozygous (16.6 ± 1.1 s.e.m. follicles/neuron), or wild-type (16.6 ± 0.5 s.e.m. follicles/neuron) animals (Fig. 6H). No significant differences were seen between mice of the same *Bax* genotype across litters for both Aδ-LTMRs and C-LTMRs (Fig. S5A-B). Therefore, I conclude that follicle-innervating LTMRs form their receptive fields in part through homotypic population-based competition.

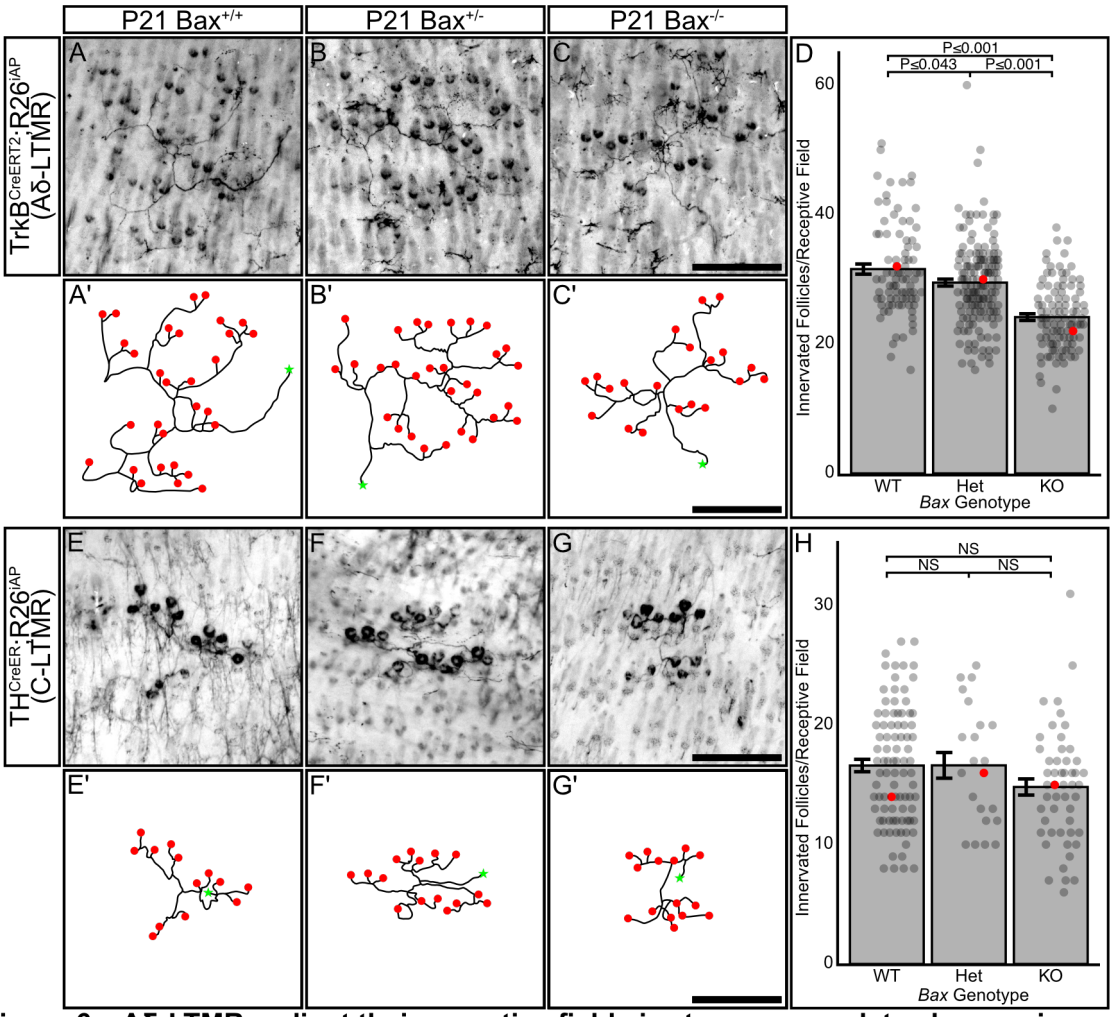

Figure 6 – Aδ-LTMRs adjust their receptive field size to accommodate changes in neuronal population due to *Bax* deletion.

A-C') Representative images and traced reconstructions of isolated Aδ-LTMR receptive fields from back skin of P21 *TrkB^{CreERT2}; R26^{iAP}*; *Bax* wild-type (A, A'), heterozygous (B, B'), and knockout (C, C') animals. Red dots in traces correspond with hair follicles, green stars indicate the axon segment from which the traced RF originates. Scale bar – 250 µm

D) Quantification of the number of hair follicles innervated by each Aδ-LTMR receptive field in *TrkB^{CreERT2};R26^{iAP}*; *Bax* wild-type, heterozygous, and knockout animals. Receptive fields in *Bax* knockout animals innervate fewer hair follicles than wild-type and heterozygous animals. Each dot represents one receptive field, red dots represent the data point from to the associated representative image. Bars represent mean ± s.e.m. One-way AONVA with Tukey's HSD post-hoc testing ANOVA P≤0.001, WT-KO P≤ 0.001, Het-KO P≤ 0.001, WT-Het P= 0.043. Number of individual receptive fields (number of animals): WT: 85(3), Het: 154(5), KO: 103(3)

E-G') Representative images and traced reconstructions of isolated C-LTMR receptive fields from back skin of P21 *TH^{CreERT2}; R26^{iAP}*;*Bax* wild-type (E, E'), heterozygous (F, F'), and knockout (G, G') animals. Red dots in traces correspond with hair follicles, green stars indicate the axon segment from which the traced RF originates. Scale bar – 250 µm

H) Quantification of the number of hair follicles innervated by each C-LTMR receptive field in *TH^{CreERT2}; R26^{iAP}*;*Bax* wild-type, heterozygous, and knockout animals. No significant difference was seen in the number of hair follicles innervated across *Bax* genotypes. Each dot represents one receptive field, the red dots represent the data point from to the associated representative image. Bars represent mean ± s.e.m. One-way AONVA, P= 0.098. Number of individual receptive fields (number of animals): WT: 90(6), Het: 22(4), KO: 51(3)

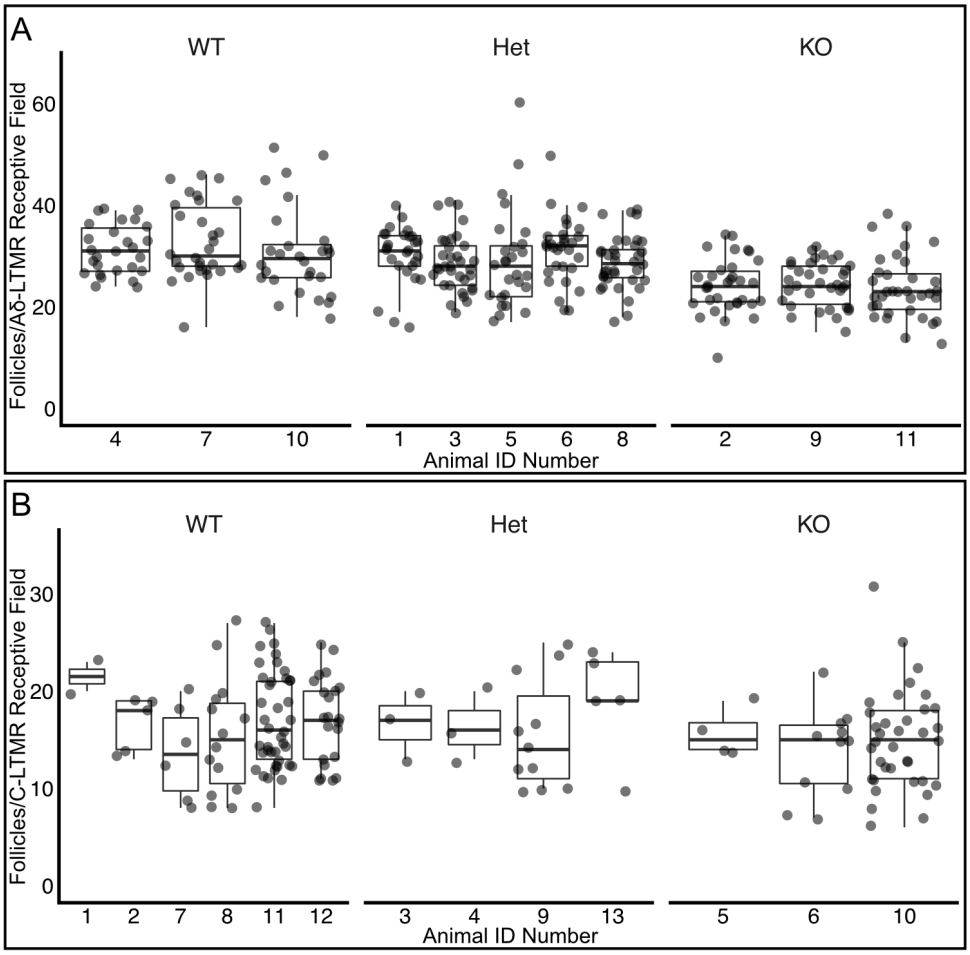

Supplemental Figure 5 – Lack of inter-animal variation in follicles innervated per receptive field between same-genotype animals.

A) Quantification of innervated hair follicles per Aδ-LTMR receptive field separated by animal. Each dot represents one quantified receptive field. No significant differences in number of innervated follicles per receptive field were seen between animals within genotype groups. Statistical analysis – One-way ANOVA Bax WT: P= 0.52, Bax Het: P= 0.49, Bax KO: P= 0.86

B) Quantification of innervated hair follicles per C-LTMR receptive field separated by animal. Each dot represents one quantified receptive field. No significant differences in number of innervated follicles per receptive field were seen between animals within genotype groups. Statistical analysis – One-way ANOVA Bax WT: P= 0.38, Bax Het: P= 0.70, Bax KO: P= 0.72

Discussion

The organized development of skin- and hair follicle-innervating sensory neurons is essential for communicating meaningful information about touch to the brain in order to moderate behavior. In this study I make use of multiple cell-type specific molecular and genetic tools to analyze the development of hair follicle innervation and explore the principles that govern follicle-innervating LTMR receptive field organization. I show innervation of hair follicles and initial LLE development occurs during the first two postnatal weeks, and that by P14, mice show an adult innervation pattern. I also show that LTMR subtypes have a differential dependence on Bax-mediated developmental apoptosis, with Aδ-LTMRs responding to deletion of *Bax* by significantly increasing their population, while the population of C-LTMRs increases only slightly. Finally, I demonstrate that in response to this change in population, Aδ-LTMR neurons shrink their receptive fields to accommodate their neighbors.

LTMR receptive fields undergo gradual refinement during the first two postnatal weeks

Previous work has described the tight association between hair follicles and the follicle-innervating LTMRs, showing PGP9.5 labeled axons wrapping hair follicles as early as E18, and describing the adult morphology of LTMRs in a population-specific manner (Bai et al., 2015; Li and Ginty, 2014; Li et al., 2011; Peters et al., 2002; Rutlin et al., 2014). Our work builds upon this by analyzing the development of follicle innervation during the first three postnatal weeks in an LTMR-subtype-specific manner. Specifically, I present a detailed timeline showing a gradual development of follicle innervation by Aβ RA-LTMRs and C-LTMRs during the first two postnatal weeks (Fig. 3). I also used a genetically-driven sparse labeling approach to examine the development of individual

Aδ-LTMR receptive fields, showing a gradual development of follicle-innervating endings and refinement of LTMR receptive field characteristics during the first two postnatal weeks (Fig. 4). These findings agree with recent work describing interactions between LTMR axons and terminal Schwann cells at the hair follicle during this time period (Meltzer et al., 2022b preprint).

Follicle Innervation Develops in a Temporally Ordered Manner

Our detailed examination of LTMR follicle innervation development revealed a temporal hierarchy for the different subtypes, with Aβ RA-LTMRs completing their innervation of hair follicles by P3, before C-LTMRs and Aδ-LTMRs do at P6 (Fig. 3). Recent comparison of the development of Aβ RA-LTMRs and Aδ-LTMRs supports this conclusion, showing Aβ RA-LTMRs maturing at P3 and Aδ-LTMRs maturing after P6 (Meltzer et al., 2022b preprint). This temporal hierarchy parallels the maturation of hair follicle subtypes. Guard hair placodes, which are innervated by Aβ RA-LTMRs, consolidate between E14 and E15, with the first guard hair shafts appearing between E16 and E18. The consolidation of other hair follicle placodes, which are innervated by C-LTMRs and Aδ-LTMRs, occurs in successive waves continuing until after birth (Hardy, 1949; Mann, 1962; Peters et al., 2002). This temporal hierarchy of innervation could also be due to the temporal order of LTMR differentiation. EdU birth dating studies have shown that Aβ RA-LTMR neurons are born as early as E9.5 and have a peak birth rate at E10.5 before sharply dropping off. In contrast, C-LTMRs and Aδ-LTMRs are born approximately one day later, peaking at E11.5 and gradually tapering off by E13.5 (Landy et al., 2021). Furthermore, single-cell transcriptomic analysis of the developing DRG shows that C-LTMRs are among the last populations to mature as transcriptionally distinct subtypes, mirroring their birthdate hierarchy (Sharma et al., 2020). It is tempting

to speculate that early-born Aβ RA-LTMRs could be a “pioneer” axon population in the periphery, functioning as a scaffold along which axons from Aδ-LTMRs and C-LTMRs grow before branching to form receptive fields. In invertebrate systems, pioneer axons play a critical role in establishing peripheral innervation patterns, and ablation of these cells leads to significant disruptions in follower axons (Bate, 1976; Edwards, 1977; Edwards et al., 1981; Keshishian, 1980; Klose and Bentley, 1989). In vertebrates, early extending axons often act as a permissive substrate upon which later-born neurons can extend their axons, but the necessity of these early-extending axons is less clear (Melançon et al., 1997; Pike et al., 1992; Pittman et al., 2008). In an interesting parallel, Ret is expressed in both early-born Aβ RA-LTMRs and in a population of pioneer axons in the zebrafish posterior lateral line (Tuttle et al., 2019). Future studies will be required to determine if early born Ret^+ Aβ RA-LTMRs function as pioneers in the mouse DRG.

Knockout of the proapoptotic protein *Bax* shows differential effects on LTMR populations

To understand how competition between LTMR neurons might influence receptive field development, I devised a genetic strategy to drive LTMR overpopulation by blocking developmental apoptosis. Multiple studies have demonstrated that sensory neurons are initially overproduced, followed by a wave of developmental apoptosis regulated by target-derived factors which ensures neurons and targets are appropriately matched (Reviewed in Buss et al., 2006; Fariñas et al., 1994; Oppenheim et al., 1991). Genetic deletion of the pro-apoptotic protein *Bax* blocks developmental apoptosis and results in significantly increased numbers of neurons in the DRG (Patel et al., 2000; White et al., 1998). While *Bax* knockout animals show a 1.5-fold to 1.8-fold increase in the population of proprioceptive and nociceptive DRG neurons and increased sensory

axon density in the paw, previous studies had not examined the effect of *Bax* deletion on populations of LTMRs (Suzuki et al., 2010). Our experiments specifically examining follicle-innervating LTMRs showed a significant increase in the number of Aδ-LTMR (*TrkB*$^{+}$) DRG neurons, but only a small, non-significant increase in C-LTMR (*TH*$^{+}$) DRG neurons. These results reveal an interesting difference in the dependence of different neuronal LTMR subtypes on developmental apoptosis to achieve their final numbers. The basis for this difference is unknown, but may involve mechanisms related to the specification, differentiation, and/or organization of LTMR neurons, such as the role for target-derived trophic cues in LTMR population determination and LLE maintenance.

Homotypic competition plays a role in LTMR receptive field organization

The development of tools for subtype-specific labeling of LTMRs revealed several interesting organizational properties. First, different LTMR subtypes have different hair follicle innervation patterns, with Aβ RA-LTMRs innervating guard and awl/auchene hairs, while Aδ-LTMRs and C-LTMRs innervate zigzag and awl/auchene hairs. Second, LTMRs have distinct, highly stereotyped receptive fields that typically innervate a fixed range of hair follicles (Bai et al., 2015; Li and Ginty, 2014; Li et al., 2011; Rutlin et al., 2014). In our study, I attempted to address these properties at a cellular level by examining the role of homotypic competition in the establishment of receptive fields. I reasoned that inducing overpopulation of LTMR subtypes with *Bax* deletion would lead to two potential outcomes. Either neurons would decrease their receptive field size to accommodate the increased number of neighbors and preserve homotypic tiling, or they would maintain their receptive field size at the expense of tiling. Aδ-LTMRs showed a clear preference for adjusting their receptive field size to accommodate the population increase, with each neuron in *Bax*$^{-/-}$ mice forming a

receptive field innervating significantly fewer hair follicles than in wild-type mice. In contrast, despite a small increase in the number of C-LTMRs in *Bax* deficient mice, these neurons did not adjust their receptive field size, suggesting they may overlap more than in *Bax* wild-type animals. This difference in response could be due to the stringency of the tiling behaviors of the two LTMR subtypes: approximately 10% of hair follicles in wild-type mice are innervated by two distinct Aδ-LTMRs, whereas 25% of hair follicles are innervated by two distinct C-LTMRs (Kuehn et al., 2019). I attempted a complementary approach, ablating a portion of the Aδ-LTMR population prenatally using the *TrkB*^{CreERT2} driver crossed to a *Cre*-dependent sensory neuron specific Diphtheria toxin receptor (*Avil*^{iDTR}), reasoning that population depletion before follicle innervation would result in larger receptive fields (Stantcheva et al., 2016). Unfortunately, these experiments resulted in perinatal lethality, potentially due to off-target effects of Diphtheria toxin administration.

At the molecular level, there is little known about the cues that regulate the targeting of LTMR subtypes to specific hair follicle types or the establishment of receptive fields. While BDNF derived from hair follicle-associated epithelial cells is important for the polarized innervation pattern and LLE maturation of TrkB^{+} Aδ-LTMR axonal endings, it is dispensable for the initial attraction of Aδ-LTMR axons to hair follicles, and it is unknown whether it regulates receptive field size (Rutlin et al., 2014). Similarly, recent work has shown that the GPI-linked receptor Netrin-G1 is required in LTMRs for the proper maturation of terminal endings around hair follicles, but not for terminal axon branching or receptive field size (Meltzer et al., 2022b preprint). In contrast, ɣ-Protocadherins are important for the peripheral branching and innervation of

non-guard hair follicles by Aβ-LTMRs, but not for the maturation of LLEs (Meltzer et al., 2022a preprint). Together, these data suggest that the initial innervation of hair follicles and the morphological maturation of their terminal endings are distinct events regulated by different molecular pathways. Interestingly, terminal Schwann cells are the source for ligands/binding partners for both Netrin-G1 and ɣ-Protocadherins in LTMRs, demonstrating that they play a critical role in regulating hair follicle innervation (Meltzer et al., 2022a preprint; Meltzer et al., 2022b preprint).

Why do distinct LTMR subtypes display different receptive field morphologies? Presumably, tight regulation of LTMR receptive field size and organization is intrinsically tied to their sensory functions. In order to allow for precise localization of a stimulus, cutaneous sensory neurons must innervate a constrained area of the skin and relay this information to the proper regions of the central nervous system. LTMR receptive field size and organization is also an important factor in determining the firing properties of individual neurons. Single neuron recordings from LTMRs have demonstrated significant sensory specialization across subtypes. The Aβ RA-LTMRs and C-LTMRs both fire action potentials in response to generalized skin indentation and skin stroking in the direction of hair growth (head to tail), differing in their specific response properties (Li et al., 2011). Aδ-LTMRs also fire action potentials in response to skin indentation, but selectively fire in response to skin stroking opposite the direction of hair growth (tail to head) due to their hemicircular arrangement on the caudal side of the hair follicle (Rutlin et al., 2014). Aβ RA-LTMRs, Aδ-LTMRs, and C-LTMRs can all fire action potentials through the stimulation of a single hair follicle. In contrast, the Aβ Field-LTMRs, which have significantly larger receptive fields than other LTMR subtypes, can

only fire action potentials through summation when multiple hairs are stimulated simultaneously (Bai et al., 2015). These unique properties result in a sensory system able to accurately localize higher magnitude stimuli through small receptive fields, while also detecting stimuli too faint to trigger action potentials through a single LLE.

The final factor potentially involved in LTMR tiling is an inherent characteristic of the LTMR receptive fields themselves. In adult mice, LTMR axons branch and form highly stereotyped receptive fields, with some subtypes such as the C-LTMRs forming fields innervating on average 15 hair follicles, while on the other extreme the Aβ Field-LTMRs can innervate over 150 hair follicles (Bai et al., 2015). Work examining the tiling of LTMR receptive fields has shown an interesting correlation between the number of hair follicles each individual receptive field innervates and the degree of overlap between neighboring homotypic receptive fields. Aβ Field-LTMRs, which have the largest receptive fields, show the least degree of overlap with homotypic neurons. C-LTMRs, which have the smallest receptive fields, show the highest degree of overlap (Kuehn et al., 2019).

The ordered development of follicle innervation and interactions between neighboring homotypic neurons during receptive field development raises the question of whether similar mechanisms regulate the organization of central DRG afferents in the spinal cord dorsal horn. The different LTMR subtypes target their axons to specific lamina in the dorsal spinal cord, somatotopically arrange their axons, and show a high degree of synaptic partner specificity (Abraira et al., 2017; Li et al., 2011; Odagaki et al., 2018). The cellular and molecular mechanisms that govern central afferent organization

remain largely unknown, but recent advancements in imaging and genetic tools may open this field to further investigation.

Age	Follicles/mm ± s.e.m. (Fig. 1B-G)	% $Tuj1^+$ ± s.e.m. (Fig. 2A-F)	% $Calbindin^+$ ± s.e.m. (Fig. 3A-F)	% TH^+ ± s.e.m. (Fig. 3H-M)	% $TrkB^+/Tuj1^+$ ± s.e.m. (Supp. Fig. 2A-C)
P1	10.66 ± 0.25	4.35 ± 1.28	0.05 ± 0.05	3.64 ± 0.59	
P3	9.90 ± 0.68	54.44 ± 1.50	20.16 ± 1.31	52.52 ± 2.03	
P6	11.25 ± 0.85	83.68 ± 6.17	15.44 ± 1.46	92.54 ± 1.26	
P14	8.85 ± 0.55	94.99 ± 0.94	17.07 ± 2.39	94.88 ± 1.07	92.2 ± 3.00
P21	8.37 ± 0.60	94.33 ± 0.95	19.30 ± 2.95	94.15 ± 1.77	
P60	5.04 ± 0.48	90.69 ± 2.88	10.59 ± 1.83	97.61 ± 1.20	

Table 1: Summary follicle innervation data shown in Figures 1-3.

Age	LLEs per Receptive Field ± s.e.m.	Terminal Branches per Receptive Field ± s.e.m.
P0/1	0.6 ± 0.08	26.2 ± 0.9
P3	5.7 ± 0.5	26.0 ± 0.9
P6	13.6 ± 0.8	27.8 ± 0.8
P14	19.4 ± 0.8	20.8 ± 0.8

Table 2: Summary Aδ-LTMR receptive field development data shown in Figure 4.

Cell Type	Marker	WT/Het Mean Cell Count ± s.e.m.	KO Mean Cell Count ± s.e.m.	KO normalized to WT/Het mean ± s.e.m.
Neurons	Islet 1/2	1318.8 ± 63.6	1573.4 ± 112.6	1.19 ± 0.09
Aδ-LTMR	$TrkB^{CreERT2}$	216.6 ± 15.7	332.0 ± 3.0	1.53 ± 0.01
C-LTMR	TH	223.9 ± 12.9	300.0 ± 39.7	1.34 ±0.18

Table 3: Summary of Bax knockout DRG cell count data shown in Figure 5.

Methods

Mouse Husbandry

Mice (*Mus musculus*) were housed in standard conditions, cared for by the Department of Comparative Medicine at Oregon Health & Science University. All animal experimental procedures were approved by OHSU Institutional Animal Care and Use Committee (Protocol # IS00000539) and adhered to the NIH *Guide for the care and use of laboratory animals*. Mice were maintained on a 12-hour light/dark cycle and were provided food and water *ad libitum*. For embryonic tamoxifen administration, the morning of vaginal plug observation was designated as E0.5. Mice were maintained on a mixed genetic background due to experiments being conducted with compound transgenic lines. Mice of both sexes were used, and littermates were used as controls.

Due to the estrogen inhibiting effects of tamoxifen during pregnancy, many female mice fail to initiate labor at the proper time resulting in fetal demise. For all female animals given tamoxifen during pregnancy, pups were delivered by cesarian section at embryonic day 19.5 after mild isoflurane-induced anesthesia and rapid cervical dislocation. After removal from the uterus and amniotic sac, pups were dried gently with a paper towel and warmed on a heating pad at 37° C. Viable pups breathe spontaneously within 1-2 minutes of removal from the amniotic sac and respond to gentle tactile stimuli within 2-3 minutes, becoming pink and actively moving within 5-10 minutes. Viable pups were placed with the litter of a nursing female mouse approximately 15 minutes after delivery and an equal number of pups were removed from the foster dam's litter. The day of birth or cross-fostering of animals was designated as P0.

Mouse Lines

Mouse lines used in this study have all been previously described (Table 4).

Table 4 - Mouse Lines Used:

Common name	Strain name	Reference	Jax/MGI Reference number
TH^{CreER}	B6;129-*Th*$^{tm1(cre/Esr1)Nat}$/J	(Rotolo et al., 2008)	JAX: 008532
$TrkB^{CreERT2}$	B6.129S6(Cg)-*Ntrk2*$^{tm3.1(cre/ERT2)Ddg}$/J	(Rutlin et al., 2014)	JAX: 027214
$Ret^{CreERT2}$	$Ret^{tm2(cre/ERT2)Ddg}$	(Luo et al., 2009)	MGI: 4437245
$Vglut3^{iCre}$	Tg(Slc17a8-icre)1Edw/SealJ	(Grimes et al., 2011)	JAX: 018147
Bax KO	B6.129X1-*Bax*^{tm1Sjk}/J	(Knudson et al., 1995)	JAX: 002994
Ai140D	B6.Cg-*Igs7tm140.1(tetO-EGFP,CAG-tTA2)Hze*/J	(Daigle et al., 2018)	JAX: 030220
R26-iAP	B6;129-Gt(ROSA)26Sor^{tm2Nat}/J	(Badea et al., 2003)	JAX: 009253

Tamoxifen Administration

Tamoxifen stock was made by dissolving tamoxifen powder in freshly opened 100% ethanol at a concentration of 150 mg/mL and stored at -80° C until needed. For tamoxifen administration to pregnant female mice, progesterone and β-estradiol were co-administered at a ratio of 1000:500:1, Tamoxifen:progesterone:β-estradiol. Administration timing and dosage are given in associated figure legends. For all administration methods and times, the Tamoxifen/ethanol stock solution was dissolved in sunflower seed oil by vortexing until an emulsion formed. The oil/ethanol mixture was then centrifuged in a heated vacuum centrifuge (SpeedVac) for 15 minutes to evaporate residual ethanol. Pregnant female mice were administered tamoxifen through oral gavage of 100 μL of sunflower seed oil with dissolved tamoxifen-progesterone-β-estradiol mixture. P12-16 pups were administered tamoxifen through oral gavage of 50 μL of sunflower seed oil with dissolved tamoxifen. P0-P11 pups were administered tamoxifen through IP injection of 10 μL of sunflower seed oil with dissolved tamoxifen.

Tamoxifen doses and timepoints for each use case can be found in Table 5.

Table 5 - Tamoxifen Administration Doses and Routes:

Experiment	Labeling Density	Associated Figure	Mouse Line	Tamoxifen Dose	Admin. Route	Admin. Age
Aδ-LTMR labeling in sections	High	Fig. S2	$TrkB^{CreERT2}$;$R26^{iAP}$	2 doses of 2 mg	P.O. (Maternal)	E12.5, E13.5
Aδ-LTMR fluorescent sparse labeling	Low	Fig. 4	$TrkB^{CreERT2}$;Ai140D	0.75 mg	P.O. (Maternal)	E13.5
Aδ-LTMR Cell Body Labeling	High	Fig. 5 B, E, F	$TrkB^{CreERT2}$;$R26^{iAP}$	3 doses of 0.5 mg	I.P.	P6, P7, P8
Aδ-LTMR RF sparse labeling	Low	Fig. 6 A-D	$TrkB^{CreERT2}$; $R26^{iAP}$	0.5 mg	P.O. (Maternal)	E13.5
C-LTMR RF sparse labeling	Low	Fig. 6 E-H	TH^{CreER}; $R26^{iAP}$	2 doses of 2 mg	P.O.	P14, P15

Tissue dissection and fixation

See (Pomaville and Wright, 2021) for a detailed description of histology methods. Briefly, animals were euthanized in accordance with IACUC approved protocols. Animals P6 and older were depilated using a commercial depilatory cream (Nair) and were washed with gentle soap and room temperature water. Skin was dissected away from the animal and placed onto a filter paper lined silicone-bottomed dish with a cover. Large fat deposits were trimmed away from the subcutaneous tissue using small scissors and the skin was pinned to the plate, subcutaneous side up, using fine insect pins. Skin was fixed 6 hours to overnight at 4° C in 4% paraformaldehyde with gentle agitation. After fixation, skin was washed with PBS for 30 minutes at room temperature with agitation before progressing to preparation for specific analysis methods. After washing the subcutaneous side of the fixed skin was scraped with a razor blade to remove remaining subcutaneous fat and muscle.

Spinal columns were dissected out and fixed overnight in 4% paraformaldehyde at 4° C with agitation. After fixation spinal columns were washed in PBS for 30 minutes at room temperature. Spinal columns were incubated overnight in 10% w/v EDTA/10% v/v glycerol in PBS to de-calcify the bones for sectioning through the spinal column (DRG section immunofluorescence and AP staining). Spinal columns were washed 4-5 hours in PBS at 4° C to remove EDTA and glycerol before further processing.

Whole Mount Skin Immunofluorescence

Fixed skin prepared as above was washed for 8 hours at room temperature in 0.2% v/v Triton X-100 in PBS with gentle agitation, changing the detergent every hour for the first 4 hours, then twice more. Skin was moved to blocking solution (5% v/v Normal Donkey Serum, 5% v/v DMSO, 0.25% v/v Triton X-100 in PBS) overnight at 4° C with gentle agitation. Skin was incubated in primary antibodies in blocking solution at the dilutions listed in Table 4 for 5 days at 4° C with gentle agitation. Skin was washed 2 hours with 0.2% v/v Triton X-100 in PBS, then 3 hours in PBS changing the PBS every hour at room temperature with agitation. Skin was moved to secondary antibodies in blocking solution at a 1:500 concentration for 2-3 days at 4° C with gentle agitation. Skin was washed 1 hour in 0.2% v/v Triton X-100, then 2-3 hours in PBS at room temperature before dehydration in a methanol gradient (30 minutes - 50% MeOH in PBS, 2 hours – 80% MeOH in PBS, overnight – 100% MeOH). After dehydration, skin was cleared in BABB and imaged.

Whole Mount Skin Oil Red O Staining and Imaging

Fixed and washed skin samples were incubated in 60% v/v isopropanol in water for 10 minutes at room temperature with agitation. Skin was then stained in 0.3% Oil Red O (ORO) in 60% isopropanol at room temperature until dark red staining of

sebaceous glands occurred (30 minutes to 3 hours). Skin was then washed twice with 60% isopropanol for 10 minutes each, then moved to water to store until imaging.

ORO stained skin was imaged by mounting epidermis side up on a glass slide with water and a standard coverslip. A 2 cm^2 area of skin was imaged using a 5x objective and the number of hair follicles were counted in 10 randomly selected 1 mm^2 fields. The counted field values were averaged together to generate an animal follicle density value.

Whole Mount Skin Alkaline Phosphatase Staining

Fixed, washed, and scraped skin was heat treated in 1 mM $MgCl_2$ in PBS at 70° C for 90 minutes with agitation every 15 minutes. Skin was allowed to cool to room temperature, then moved to a tube containing 0.1 M Tris/50 mM $MgCl_2$/0.1 M NaCl in water, pH 9.5 with 16.6 µg/mL BCIP and 33.3 µg/mL NBT and 12.5 mM Levamisole for the AP reaction. The AP staining was allowed to develop at room temperature with agitation until labeled neurons were clearly visible in the skin. Fresh buffer and substrate were added after 24 hours if staining wasn't satisfactory. After staining progressed to a satisfactory level, skin was pinned to silicone-bottomed dishes with insect pins and dehydrated for 30 minutes in 50% methanol in water, then 2 hours in 80% methanol in water, then overnight at room temperature in 100% methanol. Skin samples were cleared in a 2:1 mixture of Benzyl Benzoate:Benzyl Alcohol (BABB) for 15 minutes or until optically clear before mounting on a slide in BABB with a standard coverslip for imaging.

Whole Mount Skin Imaging and Receptive Field Quantification

Receptive fields in cleared AP-stained skin were imaged using a Zeiss AxioZoom V.16 Macroscope. The number of LLEs per receptive field were manually counted using

the Cell Counter plugin in FIJI/ImageJ. Receptive fields in representative images were semi-manually traced using the Simple Neurite Tracer plugin in Fiji/ImageJ (Longair et al., 2011). Receptive fields in cleared immunohistochemically labeled skin were imaged on a Zeiss AxioImager M.2 microscope with an Apotome.2 structured illumination module. The number of LLEs and non-LLE terminal branches were counted manually using the Cell Counter plugin in FIJI/ImageJ.

Skin Section Cryosection Preparation

A 1 cm x 1 cm square of back skin from the anterior midline was taken from fixed mouse skin. The small portion was cryoprotected in a sucrose gradient, 30 minutes in 10% sucrose in PBS, 2 hours in 15% sucrose in PBS, overnight at 4° C in 20% sucrose in PBS. Samples were mounted in OCT media and oriented with the sagittal plane as the cutting face. Samples were rapidly frozen in methylbutane chilled on dry ice. 50 μm sagittal sections were cut, every fifth section mounted on a slide, and allowed to dry at room temperature 2-3 hours before moving to a freezer or processing for immunohistochemistry or AP staining as described below.

Spinal Cord/DRG section preparation

The T5-T7 segment was dissected from fixed and decalcified spinal columns by cutting through the intervertebral disks between T4/5 and T7/8 with a sharp scalpel blade. The T5-T7 spinal column segment was cryoprotected with a sucrose/OCT gradient, 10% sucrose in PBS for 30 minutes, 15% sucrose in PBS for 1 hour, 20% sucrose in PBS for 2 hours, 30% sucrose on PBS for 2 hours, half 30% sucrose/half OCT overnight at 4° C with gentle agitation. Samples were mounted in OCT and rapidly frozen in methylbutane cooled on dry ice. 20 μm sections were cut and mounted on slides, collecting every third section, and allowed to dry for 2 hours at room temperature

before freezing or processing for AP staining then immunohistochemistry as described below.

Section Alkaline Phosphatase Staining

Slide mounted cryosections were washed 3 times for 10 minutes in PBS at room temperature, then were incubated for 30 minutes in 1 mM $MgCl_2$ at 70° C. Sections were moved to a humidified slide staining chamber and were stained with 0.1 M Tris/50 mM $MgCl_2$/0.1 M NaCl in water, pH 9.5 with 16.6 µg/mL BCIP and 33.3 µg/mL NBT and 1.25 mM Levamisole until sufficient staining had developed, 4-48 hours. Once sufficient staining had developed sections were incubated for 15 minutes in 1.25 mM levamisole, 0.25 M EDTA in PBS to stop the AP reaction. Sections were then coverslipped with Fluoromount-G or were processed for fluorescence immunohistochemistry.

Section Immunohistochemistry

Slide mounted cryosections were washed 3 times for 10 minutes in PBS at room temperature, then were incubated for 30 minutes in blocking solution (5% v/v Normal Donkey Serum, 5% v/v DMSO, 0.25% v/v Triton X-100 in PBS). Slides were incubated in primary antibodies diluted in blocking solution at the concentrations listed in Table 4 overnight at 4° C in a humidified staining box. Slides were washed 3 times for 10 minutes each with PBS, then incubated for 4 hours at room temperature in secondary antibodies diluted at 1:500 in blocking solution. Slides were washed 3 times for 10 minutes each in PBS, adding 1:5000 Hoescht to the first wash. Slides were coverslipped with Fluoromount-G and imaged.

Skin Section Image quantification

Immunohistochemically labeled and AP-stained skin sections were imaged on a Zeiss AxioImager M.2 microscope with an Apotome.2 structured illumination module.

For each animal, a tiled image field approximately 4500 μm wide was captured on a series of 5 nonconsecutive skin sections. The number of hair follicle structures in each section was counted using the DAPI channel. The number of hair follicles with a marker-positive LLE was counted using either the IHC labels described in the text, or AP staining. The proportion of innervated follicles and follicle density measurements from each section were averaged together to generate an average follicle density and follicle innervation proportion value for each animal.

DRG section Image Quantification

AP stained and immunohistochemically labeled DRG sections were imaged on a Zeiss AxioImager M.2 microscope with an Apotome.2 structured illumination module. Cell counting was performed manually using the Cell Counter plugin in FIJI/ImageJ.

Statistical Analysis

All statistics were performed in R v4.1.1. Statistical tests, N values, and P-values are described in the text/figure legends where relevant.

Table 6 – Antibodies Used:

Antibody	Supplier	Item Number	RRID	Use concentration
Rb α-Calbindin	Swant	CB 38	AB_10000340	1:1000
Rb α-TH	Millipore	AB152	AB_390204	1:1000
Sh α-TH	Millipore	AB1542	AB_90755	1:500
Ms α-Isl1/2	DSHB	39.4D5	AB_2314683	1:250
Gt α-TdTomato	Biorbyt	orb182397	AB_2687917	1:1000
Ck α-GFP	Abcam	ab13970	AB_300798	1:1000
Dk α-Rb IgG 488	ThermoFisher	A-21206		1:500
Dk α-Rb IgG 546	ThermoFisher	A10040		1:500
Dk α-Rb IgG 647	ThermoFisher	A-31573		1:500
Dk α-Ms IgG 647	ThermoFisher	A-31571		1:500
Dk α-Ck IgY 488	Jackson Immuno Research	NC0215979		1:500
Dk α-Ck IgY Cy3	Millipore Sigma	AP194C		1:500
Dk α-Sh 488	ThermoFisher	A-11015		1:500
Dk α-Gt 546	ThermoFisher	A-11056		1:500

Acknowledgements

We thank the Ginty, Badea, and Nathans Labs for the mouse lines used in the preparation of this manuscript. We would also like to thank the members of the Lumpkin Lab for their help with refining the whole-mount skin immunohistochemistry protocol. Finally, we would like to thank the members of the Wright Lab, Murthy Lab, and Kerstein lab for their feedback on the experiments presented in this manuscript.

Competing Interests

No competing interests declared

Funding

This work was supported by the National Institutes of Health [R01NS091027 to K.M.W., T32GM071338 to M.B.P.] and a Whitehall Foundation Research Grant [to K.M.W.].

Data Availability

Data used in the preparation of this manuscript will be made available upon request.

Chapter 4: Assessing the role of the cell adhesion protein teneurin transmembrane protein 3 in spinal cord somatotopic organization

Matthew B. Pomaville, Kevin M. Wright

*This chapter contains an incomplete story and is recorded here in the hope of serving as a foundation for future projects in the Wright Lab.

Chapter Introduction

While the peripheral receptive fields of the follicle-innervating LTMR neurons have been heavily studied and some molecular cues which regulate their development have been identified, there is still relatively little known about the cues which regulate the development of the central synaptic fields of LTMR neurons. The central projections of sensory neurons originating in the DRG form complex synaptic fields, also referred to as synaptic glomeruli, with dorsal horn interneurons as well as central projections of other sensory neurons. Early work on the central projections of peripheral sensory neurons showed organization into laminae within the dorsal horn of the spinal cord, and into dermatome-associated regions in the rostral-caudal axis (Arvidsson and Pfaller, 1990; Rexed, 1952; Rexed, 1954; Takahashi et al., 2003). Experiments using various retrograde tracers injected into the skin showed a dorsal-ventral division of the dorsal horn laminae by innervating neuron type, with more small diameter sensory neurons innervating the superficial laminae (I-III) and medium and large diameter sensory neurons innervating deeper laminae (III-V) (Maslany et al., 1992). This work has been confirmed and expanded upon in recent years using molecular and genetic tools. The central projections of DRG neurons form overlapping layers, with peptidergic nociceptors in the most superficial lamina, followed by non-peptidergic nociceptors, C-LTMRs, Aδ-LTMRs, Aβ-LTMRs, and finally proprioceptors (Abraira et al., 2017; Li et al., 2011). In addition to the dorsal-ventral lamination and rostral-caudal segmentation of the spinal cord, multiple studies demonstrated medial-lateral somatotopic organization using injections of retrograde tracers into different regions of the skin. Experiments on cats, then in non-human primates, rats, and humans showed that for skin regions within any given dermatome the neurons innervating regions further from the rostral-caudal

midline formed synaptic fields more medially in the dorsal horn than neurons innervating skin regions more proximal to the rostral-caudal midline (Brown et al., 1991; Florence et al., 1988; Florence et al., 1989; Florence et al., 1991; Maslany et al., 1992; Nyberg and Blomqvist, 1985). Experiments using retrograde tracers labeled with two different fluorescent markers showed that adjacent areas of skin form largely non-overlapping columns in the dorsal horn which are aligned relative to the location of the injections (Li et al., 2011; Odagaki et al., 2018). While markers exist which segment the various populations of the dorsal horn laminae dorsal-ventrally, thus far no markers exist which would suggest a molecular pathway responsible for medio-lateral somatotopic localization (Abraira et al., 2017; Häring et al., 2018).

Multiple studies demonstrate that an assortment of cell adhesion molecules, transcription factors, and growth factor receptors are involved in targeting central projections of DRG neurons to the proper locations in the dorsal horn. Knockout of the Pou domain, class 4, transcription factor 1 (Pou4f1/Brn3a) showed marked misprojection of TrkA-positive and TrkC-positive central projections into the spinal cord dorsal horn (Zou et al., 2012). Studies have also identified Ret, Runx1, and Runx3 as necessary factors for DRG central projection targeting (Fleming et al., 2015; Honma et al., 2010; Inoue et al., 2002; Yoshikawa et al., 2007). Of particular interest to our group was the potential role of the transmembrane glycoprotein teneurin transmembrane protein 3 (Tenm3) in the mediolateral organization of the spinal cord. Mouse Tenm3 is an approximately 300 kDa transmembrane protein with significant homology to the *Drosophila odd Oz* protein, perturbation of which causes the loss of odd number body segments in mutant fly embryos (Levine et al., 1994). Tenm3 interacts homotypically in

both cis and trans configurations with other members of the teneurin family, functioning as both a cell adhesion molecule and an intracellular signaling molecule (Beckmann et al., 2013; Depew et al., 2018; Jackson et al., 2018).This homophilic adhesion mechanism is essential for topographic patterning in multiple neuronal systems, including projecting axons in the hippocampus and targeting of optic nerve axons to proper retinoreceptive regions of the brain (Antinucci et al., 2013; Berns et al., 2018; Leamey et al., 2007). Tenm3 can also interact both adhesively and repulsively with Latrophilin 2 (Lphn2) depending on alternative splicing of both proteins(Boucard et al., 2014; del Toro et al., 2020). This combination of push and pull interactions is essential for construction and refinement of hippocampal networks (Pederick et al., 2021). Based on these roles in targeting other projecting axons to precise locations I hypothesized that Tenm3 may have a role in the mediolateral targeting of DRG central projections.

Methods

Mouse lines

Mouse lines used in these experiments were maintained in accordance with OHSU IACUC guidelines under standard housing conditions. The mouse lines used in this study are described in Table 1.

Common name	Strain name	Reference	Jax/MGI Reference number
$Wnt1^{Cre}$	$H2az2^{Tg(Wnt1\text{-}cre)11Rth}$ Tg(Wnt1-GAL4)11Rth/J	(Danielian et al., 1998)	JAX: 003829
$Tenm3^{Flox}$	$Tenm3^{em2.1Luo/J}$	(Berns et al., 2018)	JAX: 031705

Table 1: Mouse lines

Glass needle and paired injection apparatus construction

Glass needles were pulled from WPI 1B250F-4 capillary tubes using the following settings: Temp: Ramp+3, Pull: 0, Vel: 46, Time: 110. Pulled needles were beveled on a modified hard drive pipette beveler before use as needed.

The dual injection apparatus was constructed from a plastic base with 2 beveled needles attached using cyanoacrylate glue with 5 mm between the needle tips. Before attaching the needles to the plastic base, the non-beveled end of each needle was bent using a flame to allow attachment of the pressure injection apparatus

Subcutaneous CTB Injection

P4 mouse pups were anesthetized by cooling on ice until nonresponsive before injection. Both needles were inserted 4-5 mm into the skin, maintaining as shallow an angle as possible to keep the injections in the subcutaneous tissue. A Toohey Pressure System IIc Pressure injector with two channels was used to deliver roughly 200 nL (7 ms, 30 psi) of CTB from each needle. The needles were withdrawn before pups were rewarmed and returned to the dam.

Choleratoxin subunit B conjugated to Alexafluor488 and Alexafluor555 (ThermoFisher C34775 and C34776, respectively) were injected, one tracer in each needle.

Imaging

At P10 injected mice were euthanized with standard procedures, and the hair removed with commercial depilatory cream (Nair). Skin and spinal cords were collected in ice cold PBS and acutely dissected, removing excess fat and subcutaneous tissue from skin and exposing the dorsal spinal cord. Tissues were imaged on a Zeiss AxioZoom without fixation for whole mount preparations. After acute imaging spinal cords were trimmed to include only the labeled region ± 1 vertebrae segment and were fixed for 1

hour at 4°C in 4% PFA protected from light. Spinal cords were dissected out from the spinal column and mounted in 3% low-melt agarose before vibratome sectioning into 50 µm sections. Sections were mounted on slides and images on a Zeiss AxioImager.M2 with Apotome.2 structures illumination module.

Results

Tenm3 is expressed in a mediolateral gradient in the dorsal horn during development

I first examined the expression of *Tenm3* in the spinal cord. Due to the unavailability of a reliable antibody against Tenm3 protein I chose to look at the Allen Mouse Spinal Cord and Allen Developing Mouse Brain *in situ* hybridization atlases. Sections from E15.5 mice show high expression of *Tenm3* RNA in both the dorsal spinal cord and DRG during embryonic development, before the earliest born DRG neurons are beginning to project axons into the dorsal horn (Fig. 1A) (Allen Institute for Brain Science, 2008a; Thompson et al., 2014). Sections from the spinal cord taken at postnatal day 4 show a marked mediolateral gradient of *Tenm3* expression in the spinal cord dorsal horn and varying *Tenm3* expression in the DRG somas (Fig. 1B). Interestingly, *in situ* hybridization for *Lphn2* RNA shows an inverse gradient in the dorsal horn (Fig. 1C) (Allen Institute for Brain Science, 2008b; Henry and Hohmann, 2012).

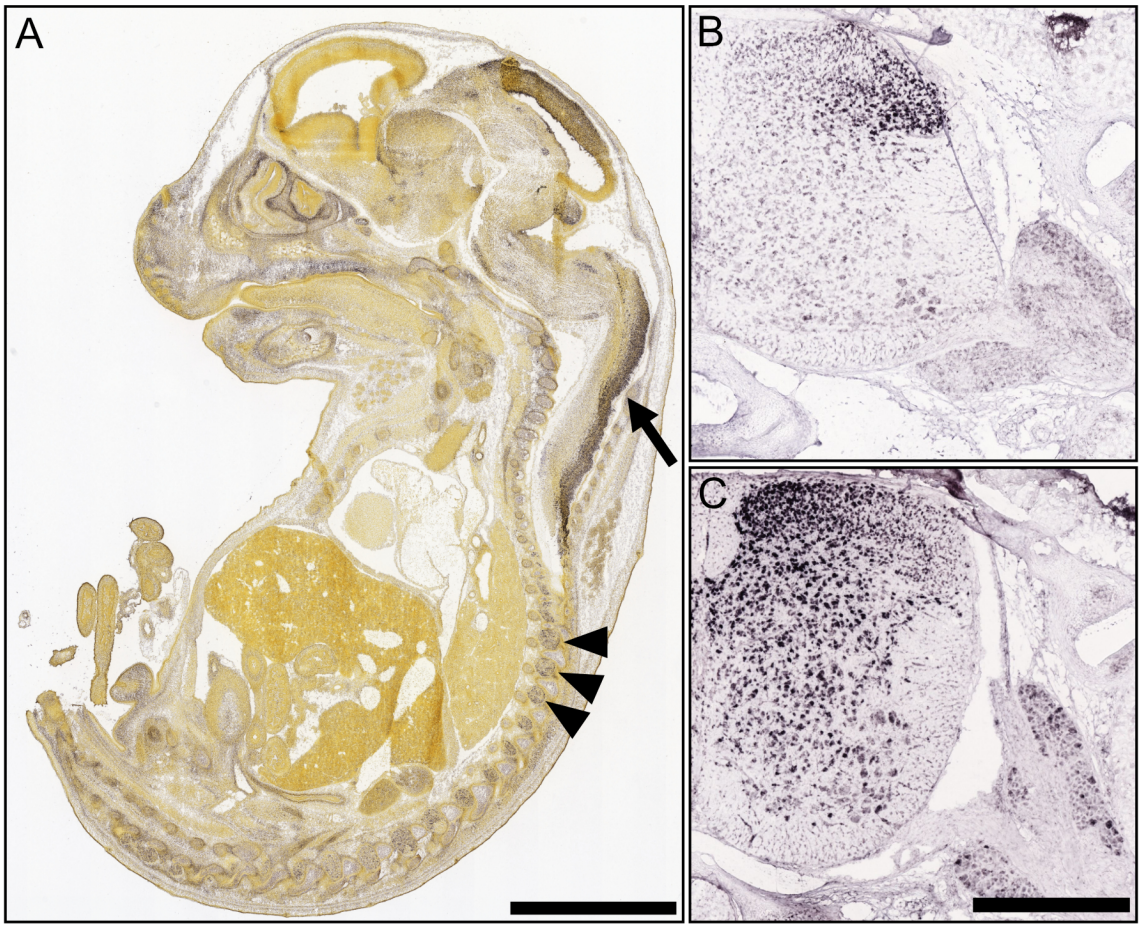

Figure 1 - Tenm3 and Lphn2 are expressed in mediolateral gradients in the spinal cord dorsal horn.
A) *In situ* hybridization for Tenm3 in E15.5 mouse embryos from the Allen Developing Mouse Brain Atlas shows expression of Tenm3 mRNA in the dorsal spinal cord (arrow) and the DRGs (arrowheads). Scale bar - 2500 μm
B-C) *In situ* hybridization for Tenm3 (B) and Lphn2 (C) in P4 mouse spinal cord from the Allen Mouse Spinal Cord Atlas show opposing gradients of expression in the dorsal horn. Scale bar - 500 μm

Paired injection of retrograde tracers into the skin reliably labels somatotopic columns in the dorsal horn

Previous studies have shown subcutaneous injection of retrograde tracers into the skin reliably labels the dorsal horn columns in the spinal cord associated with the injection site (Li et al., 2011; Odagaki et al., 2018). To assess the potential role of Tenm3 in the somatotopic organization of the dorsal horn I needed a way to perform two subcutaneous injections on neonatal mice with a known and reproducible distance between the injection site centers. I developed an injection apparatus to reproducibly

inject cholera toxin B subunit (CTB) tagged with two different fluorescent reporters using a pair of beveled glass needles spaced 5 mm apart (Fig. 2A). Small volumes of CTB were injected into the skin of lightly anesthetized P4 wild-type mouse pups using the needle apparatus and two air-driven injection systems. At 7 days post injection (d.p.i.) skin from injected animals was collected, transferred to cold phosphate buffered saline, and imaged without fixation. In most animals two labeled patches of skin could be clearly visualized (Fig. 2B). The spinal cords from injected animals were also collected, transferred to cold phosphate buffered saline with heparin, and the dorsal lamina of the spinal column was carefully dissected away exposing the dorsal spinal cord and DRGs. Fluorescently labeled somatotopic columns were clearly visible in most animals in a spinal cord segment associated with the injected skin dermatome (Fig. 2C).

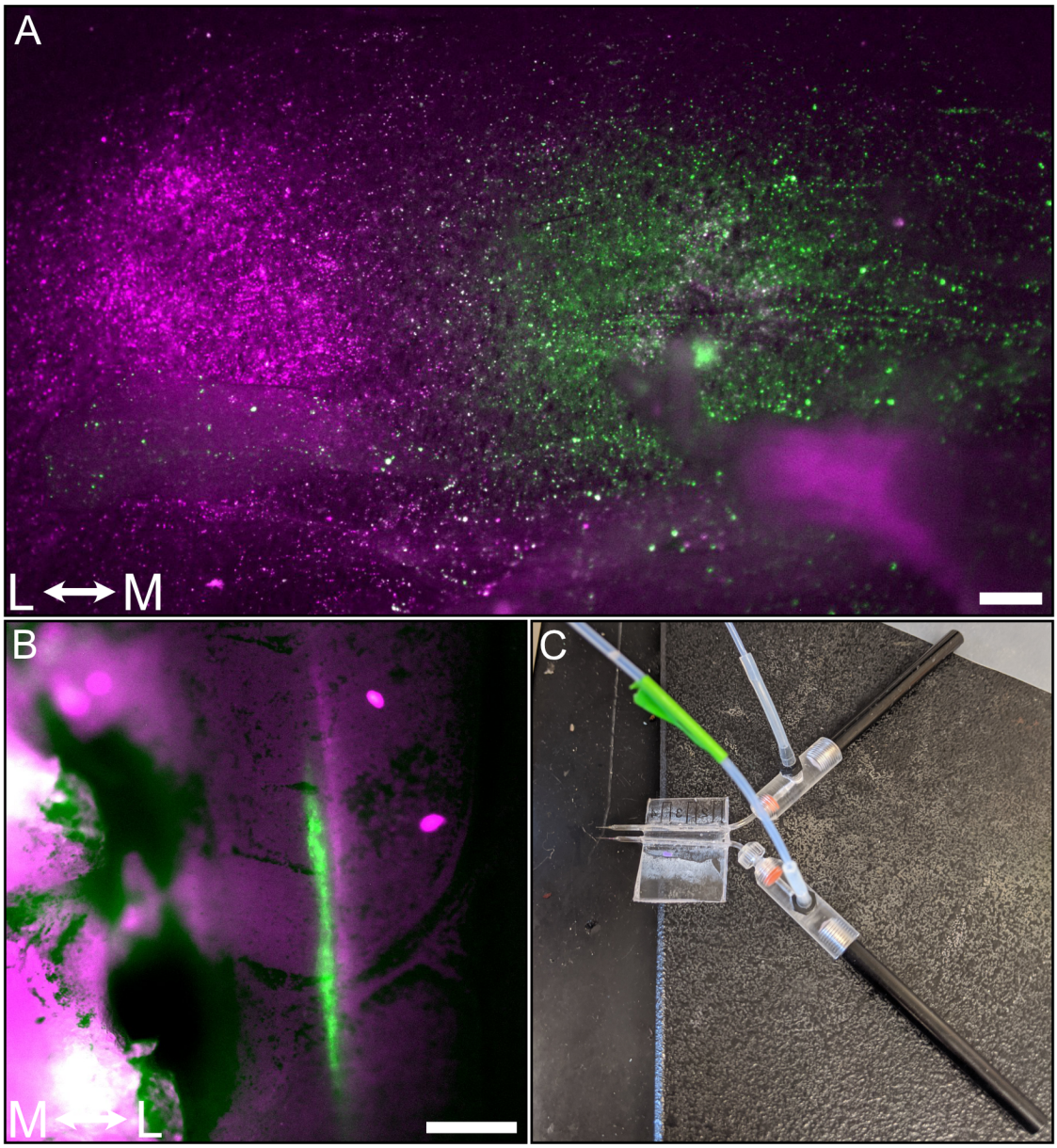

Figure 2 - Paired injection of fluorescent retrograde tracers labels somatotopically arranged DRG central projections.

A) Double tracer injected skin from a P11 mouse pup 7 d.p.i. showing two labeled skin patches. Magenta tracer was injected from the lateral needle, and green tracer was injected from the medial needle. Scale bar - 500 μm

B) Labeled central projection columns in a hemisected spinal cord from the animal shown in (A). More medial skin innervating neurons (green) project laterally in the dorsal horn, and more lateral skin innervating neurons (magenta) project medially in the dorsal horn. Scale bar - 250 μm

C) The prototype apparatus for repeatable paired subcutaneous injection of retrograde tracers. Two beveled glass needles are glued to a plastic base with the needle tips 5 mm apart.

Tenm3 conditional knockout disrupts dorsal horn somatotopic columns

To assess the role of Tenm3 in dorsal horn somatotopic patterning I utilized a conditional knockout of *Tenm3* driven throughout the midbrain and early neural crest progenitors by $Wnt1^{Cre}$. *Wnt1* is a secreted signaling protein expressed throughout the neural tube and neural crest beginning around E8.5 and continuing throughout development (Danielian et al., 1998). I crossed $Wnt1^{Cre}$ mice with mice carrying floxed *Tenm3* alleles ($Tenm^{F/F}$) to generate $Wnt1^{Cre};Tenm3^{F/+}$ and $Wnt1^{Cre};Tenm3^{F/F}$ offspring (Berns et al., 2018). Lightly anesthetized pups of unknown genotype from these crosses were injected with fluorescently labeled CTB using the double injection apparatus in figure 2. At P10 (6 d.p.i.) skin and spinal cords were collected and acutely imaged. Labeled adjacent dorsal horn columns can be seen in the $Wnt1^{Cre};Tenm3^{F/+}$ spinal cord (Fig. 3A), while in $Wnt1^{Cre};Tenm3^{F/F}$ animals the dorsal horn columns are disrupted and overlapping (Fig. 3B). To further analyze the degree of overlap in the dorsal horn columns the labeled spinal cords were lightly fixed with paraformaldehyde and sectioned on a vibratome. Imaged sections showed the characteristic “flame-like” projections in the dorsal horn formed by the labeled neurons (Fig. 3C). In $Tenm3^{F/F}$ animals, the labeled projections show more overlap in the dorsal horn (Fig. 3D). Thresholded section images show little overlap between projections in $Wnt1^{Cre};Tenm3^{F/+}$ and increased overlap between labeled projections in $Wnt1^{Cre};Tenm3^{F/F}$ (Fig. 3C’-D’).

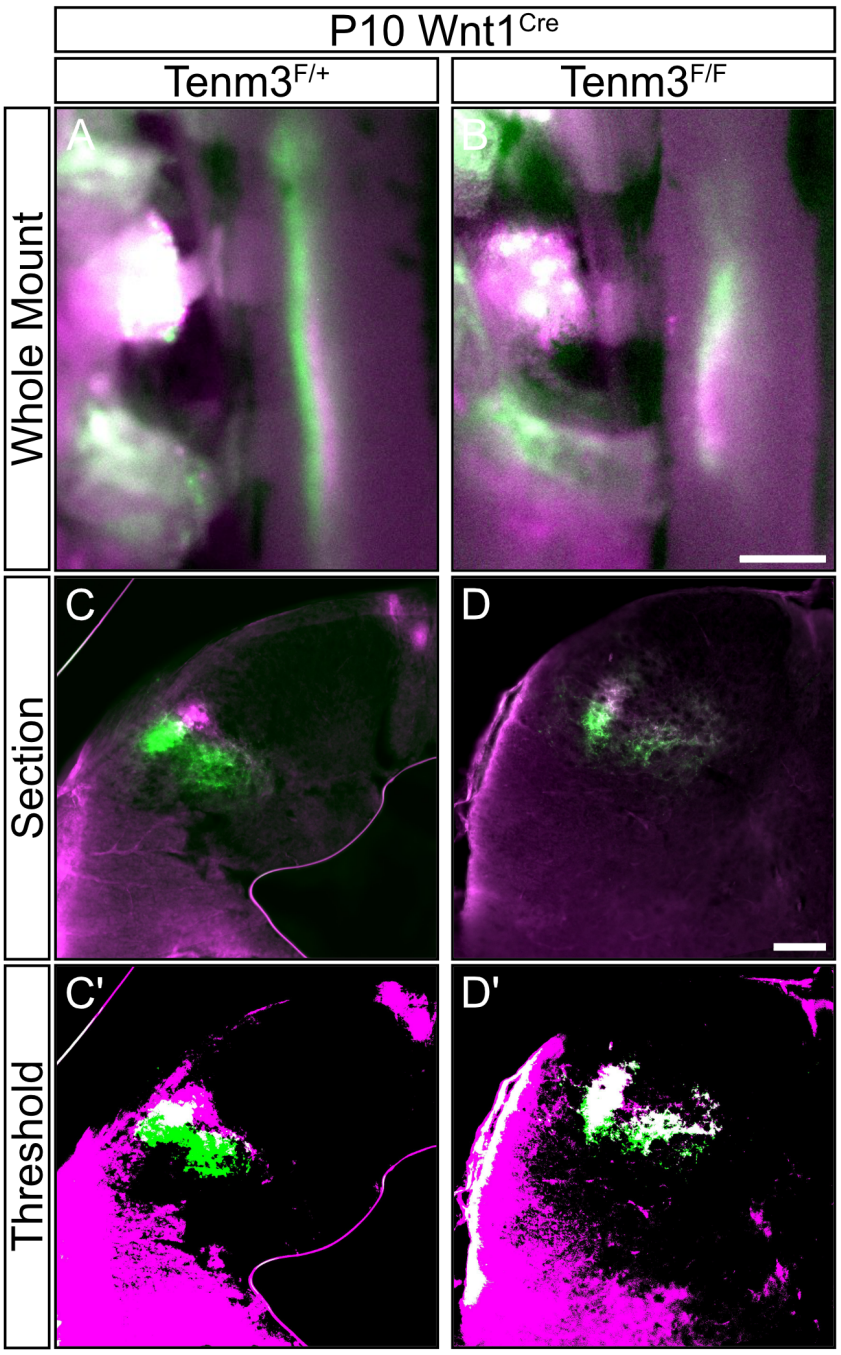

Figure 3 - Knockout of Tenm3 in the peripheral nervous system disrupts dorsal horn somatotopic arrangement.

A-B) Whole mount images of spinal cords from P10 $Wnt1^{Cre}$; $Tenm3^{F/+}$ (A) and $Wnt1^{Cre}$; $Tenm3^{F/F}$ (B) mouse pups double tracer-injected with fluorescently-labeled CTB. Scale bar: 300 μm

C-D) Sections through retrolabeled spinal cords in (A) and (B). Somatotopic columns in (D) show more overlap than those of wild-type mice in (C). Scale bar: 100 μm

C'-D') Thresholded section images from (C) and (D) showing increased overlap (white) in Tenm3 cKO animals.

Discussion

The preliminary findings presented in this chapter form a foundation for future research into the role of various cell adhesion proteins, including Tenm3 and Lphn2, in the somatotopic patterning of the spinal cord dorsal horn. Using paired subcutaneous injection of fluorescently tagged retrograde tracer (CTB) Ishowed distinct and repeatable labeling of adjacent central projection columns in the dorsal horn of the spinal cord (Fig. 2). This injection paradigm can be used on nearly any skin surface of the mouse, providing a more flexible alternative to previous injection techniques used to assess somatotopy such as injecting adjacent digits or the palmar and dorsal surfaces of the paws. Our preliminary findings regarding the effects of *Tenm3* knockout in the spinal cord and DRG neurons suggest *Tenm3* plays an important role in organizing DRG central projections into somatotopic columns (Fig. 3). From this Ideveloped a preliminary model where *Tenm3* expression gradients in both the dorsal horn and DRG act together to arrange central projections (Fig. 4).

Further exploration into the role of cell adhesion molecules such as Tenm3 in patterning the central projections of DRG neurons are needed to better understand the mechanisms by which the dorsal horn laminates as well as arranges somatotopic columns. These preliminary data presented a method for addressing the role of potential homophilic adhesion molecules in the establishment of dorsal horn patterning using $Wnt1^{Cre}$ to ablate expression in all neural crest-derived neurons. By combining this tool with genetic tools targeted to the spinal cord dorsal horn interneurons ($Ptf1a^{Cre}$) or DRG neurons ($Avil^{Cre}$) specifically the role of adhesion molecules on both sides of the dorsal horn synapse can be evaluated (Hasegawa et al., 2007; Nakhai et al., 2007). Furthermore, inducible genetic tools for both *Ptf1a* and *Avil* have been generated,

allowing analysis of cell-intrinsic mechanisms of central projection targeting (Kopinke et al., 2012; Lau et al., 2011). Similar conditional tools can be used to explore the role of *Lphn2* which is expressed in the spinal cord dorsal horn and DRG in an opposing gradient to that of *Tenm3* (Anderson et al., 2017).

Potential Concerns

While the preliminary date presented in this chapter shows a potentially interesting avenue for future research there are multiple concerns that should be addressed. The primary concern is the off-target effects reported in the $Wnt1^{Cre}$ genetic driver line used in this study (Danielian et al., 1998). This Cre-line has a high propensity to recombine in spermatogonia cells causing germ-line deletion when male mice are carriers for the Cre-driver. This recombination occurred in mice maintained after these experiments were performed generating $Tenm3^{+/\Delta}$ heterozygous animals. These animals are healthy and reproduce without issues as heterozygotes. Other issues relating to off-target effects and ectopic expression of *Wnt1* in the $Wnt1^{Cre}$ mice have been reported, including significant expansion of the midbrain even when the line is maintained as heterozygous animals. A new *Wnt1* genetic driver line ($Wnt1^{Cre2}$) has been generated which reduces these off-target effects through removal of the remaining *Wnt1* gene elements left in the original transgene (Lewis et al., 2013).

A separate potential concern with future experiments based on the model presented here is the difficulty encountered fixing and imaging CTB labeled tissue. While conducting the preliminary experiments shown here, Ifound the injected CTB to be difficult to fix without dispersion of the signal. Extremely light fixation helped maintain tissue integrity without complete loss of signal, but the tissue was unable to be immunolabeled with any other markers and was unable to be cleared using BABB. This

is likely due to the disruption of the membrane and other lipid-heavy structures during both tissue permeabilization for immunohistochemistry and solvent-based tissue clearing. Fixable retrograde tracers such as fluorescently-tagged amino dextran, which contains free amines amenable to formaldehyde fixation, exist and may be an option worth pursuing in future experiments. Additionally, the use of fluorescent protein cassette via Adeno-associated viruses (AAV), as has been done in other work, may provide a more targeted and controllable method to retrogradely label sensory neurons in the skin (Kuehn et al., 2019).

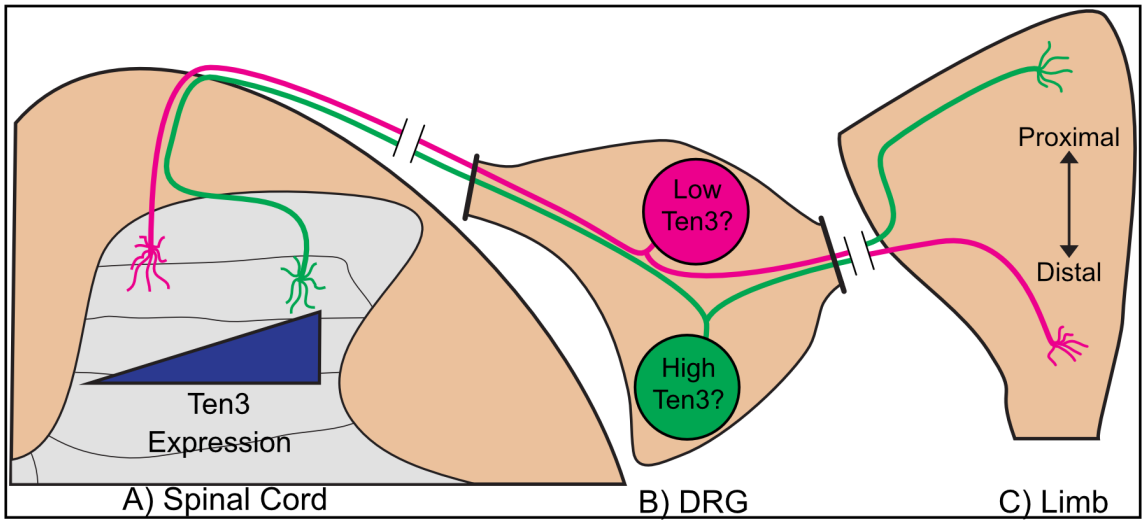

Figure 4 - A gradient of Tenm3 expression could play a role in dorsal horn somatotopic patterning.
A-C) In our proposed model the gradient of Tenm3 expression in the dorsal horn (A) and DRG neurons (B) drive somatotopic arrangement of limb innervating neurons (C) through alignment of homophilic interactions of Tenm3. DRG neurons expressing high levels of Tenm3 (green) innervate proximal limb regions and establish central projections in the lateral dorsal horn where Tenm3 expression is high. DRG neurons expressing low levels of Tenm3 (magenta) innervate distal limb regions and establish central projections in the medial dorsal horn where Tenm3 expression is low.

Chapter 5: Conclusions and Extended Discussion

Summary of Results

While the sensory neurons that innervate the skin have long been a topic of interest to neuroscientists there is still very little known about how these neurons develop and organize themselves in both the periphery and the central nervous system. In this dissertation I explored the development of the follicle-innervating LTMR neurons, a family of highly specialized sensory neurons which detect the faintest tactile stimuli in our environment and tested the hypothesis that the periphery receptive fields of these neurons tile in a homotypically exclusive manner. To this end, I also developed a comprehensive set of protocols for immunohistochemical labeling and histological staining of glabrous and hairy skin in section and whole mount preparations. Finally, I collected preliminary data suggesting the cell adhesion molecule Teneurin 3 (*Tenm3*) may have a role in the organization and targeting of the central projections of skin innervating neurons.

In chapter 2 of this dissertation, I present a collection of detailed protocols for immunofluorescent labeling and histological staining of hairy and glabrous skin in both section and whole mount formats. One of the many functions of the skin is to serve as a barrier, separating conditions inside the body from those outside the body. As a part of this function the skin is highly hydrophobic and contains multiple layers of epithelial cells held together with tight junctions (Kirschner and Brandner, 2012; Niessen, 2007). This makes immunohistological and immunofluorescent labeling, which rely on even tissue penetration by antibodies suspended in an aqueous buffer, challenging. Additionally, in non-albino mice the pigmentation density of the skin changes as mice progress through the hair follicle cycle, decreasing the amount of light transmission that can be achieved

even in tissue cleared using solvent clearing (Müller-Röver et al., 2001). These two issues were overcome in whole mount skin preparations through the use of appropriate detergents during the permeabilization and antigen blocking phases of tissue processing and through careful choice of experimental timepoints to avoid processing skin during anagen, when it is most pigmented and thickest. These protocols made the detailed analysis of follicle-innervating neurons development and structure in chapter 3 possible, as well as enabling collaboration projects with groups studying mechanisms of neuropathy and neurodevelopmental disorders.

Chapter 3 of this dissertation focused on characterizing the development of the three subtypes of LLE-forming follicle-innervating LTMR neurons and the role of competition for innervation targets in determining receptive field size in these neurons. Using a combination of molecular markers for follicle-innervating LTMR populations and conditional genetic labeling I demonstrated that follicle-innervating neurons are present in the skin at birth, but do not begin to form follicle-innervating LLEs until P3. Based on these experiments, I showed that Aβ RA-LTMR neurons complete their innervation of hair follicles before Aδ-LTMR and C-LTMR neurons. I also characterized the development of individual Aδ-LTMR neurons in whole mount skin preparations, showing that these neurons develop their follicle-innervating LLEs gradually, and prune away free branches that do not innervate follicles. Finally, I used a model of sensory neuron overpopulation driven by knockout of the pro-apoptotic gene *Bax* to assess the role of sensory neuron overpopulation on the receptive field tiling seen in follicle-innervating LTMRs. Using sparse genetic labeling approaches to examine isolated receptive fields from C-LTMR and Aδ-LTMR neurons I showed that in *Bax* knockout animals the

increase in population results in significant reductions in receptive field size in Aδ-LTMR neurons but not C-LTMR neurons.

In chapter 4 of this dissertation, I present preliminary work exploring a potential molecular mechanism regulating the somatotopic arrangement of central projections of DRG sensory neurons. Using paired subcutaneous injection of retrograde neuronal tracers, I was able to label adjacent somatotopic columns in a repeatable manner. Furthermore, using a neural crest-wide conditional knockout of the gene coding for *Tenm3*, a cell adhesion protein expressed in a gradient in the dorsal horn of the spinal cord, I showed that Tenm3 expression may play a role in dorsal horn somatotopic arrangement.

These findings demonstrate a high degree of patterning and refinement in the mouse somatosensory system. The mechanisms that enable this patterning and organization remain relatively unclear, but the ongoing development and refinement of molecular and genetic tools for exploring the various subtypes of cutaneous neurons will create a fertile field for future research.

Basic Science Implications

What mechanisms regulate LTMR receptive field tiling?

Previous studies have shown that follicle-innervating LTMRs form receptive fields in the skin with varying degrees of homotypic tiling (Kuehn et al., 2019). Aδ-LTMRs tile with near exclusivity, with only 5-10% of hair follicles innervated by more than one neuron, while C-LTMRs tile less stringently, with approximately 20% of neurons receiving innervation from more than one neuron. The data presented in this dissertation show that in one population of LTMR neurons, the Aδ-LTMRs, neurons adjust their receptive field size to accommodate an increased number of sensory

neurons, while another population, the C-LTMRs, do not appear to adjust their receptive fields in response to population changes. This suggests there may be multiple mechanisms at play regulating the development of LTMR receptive fields.

Much of the early work exploring molecular markers for skin innervating neurons focused on the neurotrophic growth factors and their canonical receptors. Most DRG neurons express at least one neurotrophin receptor during their development, and disruption of the expression of growth factors or receptors has been shown to significantly alter sensory neuron development (Crowley et al., 1994; Fundin et al., 1997a; Klein et al., 1993; Klein et al., 1994). Additionally, extensive work has shown expression of neurotrophins and their receptors in the hair follicle epithelium at various points during follicle development and hair follicle cycling (Botchkarev et al., 1998a; Botchkarev et al., 1998b; Botchkarev et al., 2004; Botchkareva et al., 1999; Botchkareva et al., 2000). Detailed examination of the Aδ-LTMRs has shown that expression of BDNF from the hair follicle epithelial cells is essential for proper formation of a hemicircular LLE, with targeted BDNF knockout resulting in a loss of LLE polarization and a significant reduction in the number of lanceolate endings formed per follicle (Rutlin et al., 2014). This, in conjunction with the tiling phenotype shown in chapter 3 of this dissertation, suggests that Aδ-LTMR neurons may use expression of BDNF at hair follicles for targeting and that some level of competition for trophic factors at hair follicles may control receptive field morphology. While such direct interactions have not been shown for the other follicle-innervating LTMR neurons the developing hair follicle niche has been shown to express multiple canonical neurotrophins and other axon guidance/cell adhesion molecules in highly specific patterns, suggesting an

expanded role for these signaling molecules in LTMR receptive field formation (Sennett et al., 2015).

The receptive fields of follicle-innervating LTMR neurons show varying degrees of isoneuronal exclusion in addition to the varying degrees of homotypic tiling seen in their receptive fields. Aδ-LTMRs very rarely have multiple axon branches that innervate a given hair follicle, while in C-LTMRs over 70% of hair follicles are innervated by multiple branches from the same neurons (Kuehn et al., 2019). Isoneuronal exclusion in Aδ-LTMRs is similar to the isoneuronal tiling seen in class IV DA neurons of *Drosophila* larvae, while the lack of isoneuronal tiling but maintained homotypic tiling in C-LTMRs is similar to the patterns seen in class III DA neurons (Grueber et al., 2002; Grueber et al., 2003). This similarity in patterns suggests a similar mechanism may be at play. It is known that mammalian DSCAM is involved in multiple self-recognition and avoidance mechanisms in retinal neurons (Garrett et al., 2018; Simmons et al., 2017). It has also been shown that *Dscam* transcripts are present in DRG neurons during embryonic development, with low levels of expression into adulthood, suggesting a role in isoneuronal tiling in LTMR neurons (Sharma et al., 2020).

Does activity play a role in LTMR receptive field development and refinement?

The findings presented in chapter 3 of this dissertation demonstrate that skin innervation in mice is still immature at birth and heavily refines during the first two postnatal weeks, coincident with hair follicle cycling and significant growth. This aligns with growth and development patterns seen in other mammalian sensory systems, such as the retina which matures after the first postnatal week (Bassett and Wallace, 2012; Tworig and Feller, 2022). This gradual development of skin innervation during the first two postnatal weeks, concurrent with hair follicle development and maturation, suggests

the potential for an activity-dependent mechanism for LTMR receptive field refinement. Multiple sensory systems require activity during development to organize and refine their synaptic connections, including: 1) spontaneous patterned cholinergic and glutamatergic waves that refine eye-specific organization of retinal ganglion cells axons in retinorecipient areas of the brain prior to eye opening, 2) glabrous skin innervating somatosensory neurons which expand and remap their dorsal horn synaptic fields and brainstem representations before adulthood, and 3) auditory neurons in the cochlea which depend on calcium bursts initiated in hair cells to promote synaptic pruning (Burbridge et al., 2014; Ge et al., 2021; Lehnert et al., 2021; Tiriac et al., 2022; Tritsch et al., 2010). In LTMR neurons, the terminal Schwann cells or skin movements experienced by pups could provide an extrinsic source of stimulation to help drive RF refinement and LLE formation. Activity could play an even larger role in the organization of DRG central projections, refining a rough somatotopic map established through gradients of cell adhesion proteins like Tenm3 and Lphn2. Simultaneous activity between central projections of adjacent neurons onto interneurons could serve to strengthen these connections, while lack of simultaneous activity could serve as a cue for synapse removal, as in a classical Hebbian synapse model (Hebb, 1949).

The role of glia in follicle innervation

While cutaneous neurons have been studied since the beginnings of modern neuroscience it has only been very recently that attention has been paid to the glial cells which support specialized cutaneous nerve endings, the terminal Schwann cells (TSCs). Two to three of these specialized non-myelinating Schwann cells settle near the base of each LLE and form projections which sandwich the lanceolate projections of LTMR neurons (Kaidoh and Inoué, 2000; Li and Ginty, 2014). These cells were initially

thought to function as an insulator and support structure for neighboring lanceolate projections, as they leave the side of each neuron projection facing the hair follicle basal lamina exposed (Kaidoh and Inoué, 2000; Li and Ginty, 2014; Takahashi-Iwanaga, 2000). Recent work examining TSCs associated with free nerve endings in the skin has shown these cells to have a direct nociceptive function, causing increased pain response in mice when TSCs were stimulated optogenetically (Abdo et al., 2019). Recent work examining the development and refinement of LLEs has shown further roles for TSCs as the source of ligands for Netrin G1 and γ-Protocadherins (Pcdhg) in hair follicle innervation (Meltzer et al., 2022a preprint; Meltzer et al., 2022b preprint). Netrin G1 is present in follicle-innervating neurons, and its expression of its ligand Lrrc4c in TSCs has been shown to be necessary for LLE formation but not targeting axons to hair follicles initially (Meltzer et al., 2022b preprint). Similar mechanisms have been shown to target microglia to axons of layer V cortical neurons and promote neuronal survival (Fujita et al., 2020). Deletion of various γ-Protocadherin isoforms from LTMR neurons or from TSCs showed defects in both branching and LLE formation, with different isoforms playing specific roles in central synapse formation (Pcdhg3) and peripheral axon branching (Pcdgh7), but nor apparent role In LLE formation or maintenance (Meltzer et al., 2022a preprint).

Given that a single TSC encompasses lanceolate endings from multiple LTMR subtypes, it is unlikely that TSCs are responsible for the selective innervation of hair follicles by specific LTMR subtypes or for the homotypic tiling of LTMR receptive fields. However, given their role in LLE maturation and potential activation of intracellular

signaling cascades through a GPI-linked co-receptor TSCs may play a role in blocking apoptosis and pruning in LTMR neurons which successfully innervate a hair follicle.

Translational Implications

Human hair follicle innervation

Despite our growing understanding of mammalian skin innervation through the study of mice, our specific knowledge of cutaneous innervation in humans is relatively underdeveloped. Like all mammals, human skin is entirely covered with hair follicles, though at a much lower density than in common research models like mice. A study examining hair follicle innervation in skin specimens from human embryos shows hair follicles innervated by LLEs similar to those seen in mice developing between 22 and 35 weeks of gestation (Payne et al., 1991). Similar examination of skin innervation in Rhesus macaque embryos showed sensory neurons present in the skin early in the second trimester of gestation, with LLEs present at hair follicles by the late third trimester or birth (Bressler and Munger, 1983). This work also showed flattened projections adjacent to LLE forming axons, thought to be TSCs, present early in the second trimester. These data suggest human hair follicles receive innervation similar to that seen in mice and that this innervation develops prenatally, appearing mature at birth. Human hair follicles have also been shown to express NGF and NT-3, as well as their receptors TrkA and TrkC, though these factors have primarily only been studied with regard to their regulation of the hair follicle cycle and hair loss (Adly et al., 2005; Adly et al., 2006). However minimal this data may be, these factors suggest that human hair follicle innervation may develop through similar mechanisms and processes to mouse hair follicle innervation.

Hairy skin innervation in humans has not been studied to the extent that glabrous skin innervation has, and thus the sensory neuron types that innervate hairy skin are less well defined. One study examining innervation of the inner forearm using single fiber recordings identified myelinated, rapidly adapting neurons which formed receptive fields innervating at least twenty hair follicles and responded with increased intensity when hair follicles were moved against the direction of hair growth (Vallbo et al., 1995). While this is far from a comprehensive analysis, it does suggest that human hair follicles may be innervated by at least one population of mechanoreceptive neurons similar to the follicle-innervating LTMRs in mice. The presence of human sensory neuron populations like those seen in mice is further supported by a recent spatial transcriptomic study of human DRGs which showed, among other things, that clusters of cells with molecular profiles similar to those of mouse Aβ RA-LTMR and Aδ-LTMR are clearly identifiable, and that a distinct cluster resembling mouse C-LTMRs was also present (Tavares-Ferreira et al., 2022). Because there have been no studies examining the patterning and interactions of multiple hair follicle-innervating neurons in humans it is impossible to definitively say if they form exclusively tiled receptive fields like their counterparts in mice or if the follicle innervating receptive fields that exist are consistent across the body. Given the wide variation in tactile acuity across body regions in humans it is reasonable to assume that follicle-innervating neurons may have different field sizes depending on the body region they innervate. Regions of the skin needing more tactile acuity (the face, backs of the hands, etc.) may have smaller follicle-innervating receptive fields, while regions needing less acuity may have fields which innervate many more hair follicles.

The role of cutaneous innervation in sensory processing disorders

One key role thought to be played by LTMR neurons in hairy skin of humans is the encoding of pleasurable touch. While the Aβ-LTMR neurons are commonly thought to be primarily involved in discriminative touch, the act of identifying objects and surfaces, pleasurable touch, also called affective touch or social touch, is thought to be communicated primarily by a population of unmyelinated sensory neurons called the C-mechanoreceptors in humans. These neurons fire in response to slow, gentle skin stroking and increase their response when thermal stimulus approximating human skin temperature is applied (Ackerley et al., 2014b; Ackerley et al., 2014c). Analysis of the effects of this form of touch using emotional descriptors found a strong positive association with terms like “comfort” and “positive affect” (Ackerley et al., 2014a). In functional MRI studies of the cortical processing of touch, affective touch was found to increase activity in the insular cortex and decrease activity in the sensory cortex (Olausson et al., 2002; Olausson et al., 2008). This suggests that C-mechanoreceptor activity may be more directly involved in emotional coding of touch than discriminative touch. Presently, no study has examined whether hair follicles are innervated by C-mechanoreceptors in humans, though with the recent identification of molecular markers that could identify putative C-LTMR neurons in humans this analysis may soon be possible.

Human hair follicle innervation may also play a role in how sensory processing disorders and conditions like autism spectrum disorder (ASD) effect the perception of touch. Many ASD patients report increased sensitivity to tactile stimuli, often including hypersensitivity to stimuli normally considered low-threshold (Blakemore et al., 2006; Cascio, 2010; Tomchek and Dunn, 2007). Functional MRI studies of subjects with and

without ASD showed decreased cortical response to cutaneous stimuli associated with affective touch and C-mechanoreceptors in patients with ASD, suggesting a potential miswiring of the pathways responsible for this important element of human social interactions (Voos et al., 2013). While most research into the biological effects of ASD risk genes and known ASD-associated mutations has focused on the cortical effects of these mutations, a handful of studies have examined the peripheral sensory effects of ASD-associated mutations. Mice lacking the ASD-associated gene methyl-CpG-binding protein 2 (*Mecp2*) in sensory neurons only showed general sensory disfunction caused by a loss of pre-synaptic inhibition of these neurons (Orefice et al., 2016). Rats with partial loss of *Mecp2* had increased nonpeptidergic nociceptor density in their skin, a finding that correlates with findings of skin innervation studies of patients with *Mecp2* mutations, suggesting overgrowth of sensory neurons may play a role in sensory processing disorders (Bhattacherjee et al., 2017; Symons et al., 2019).

This idea that the sensory disorders seen in ASD and ASD-like syndromes are due, at least in part, to disruptions in peripheral sensory innervation is further supported by the effects seen in mice with mutations in phosphatase and tensin homolog (*Pten*) a gene strongly associated with ASD cases. *Pten* is known to regulate neuronal arbor size during development, and disruption of its expression is correlated with behavioral and social interaction abnormalities in mice (Kwon et al., 2006). Ongoing work from the Wright lab has shown mice heterozygous for *Pten* have abnormal DRG neuron development and differentiation, suggesting abnormal innervation of the skin may also be present (Wright Lab, Unpublished Data). Given the high degree of refinement present in the normally-functioning somatosensory system, it is reasonable to suspect

that gross changes to the proportions of sensory neurons present, the sizes of their receptive fields, or physiological changes to the receptors they express could cause gross sensory processing changes as well.

Conclusion

The high degree of organization and patterning demonstrated in the mouse somatosensory system is possibly an inherent part of its function. To properly respond to tactile stimuli animals must be able to localize these stimuli on their body. Without strict patterning of sensory neuron receptive fields in the skin and a meaningful organization of the central projections in the spinal cord and higher nervous system structures, communicating localization of sensory stimuli suddenly becomes much more complicated. The work presented in this dissertation examines the development of hair follicle sensory innervation at a previously unstudied level of detail and presents a new potential mechanism for LTMR receptive field patterning and organization.

References

Abdo, H., Calvo-Enrique, L., Lopez, J. M., Song, J., Zhang, M.-D. M.-D., Usoskin, D., Manira, A. E., Adameyko, I., Hjerling-Leffler, J., Ernfors, P., et al. (2019). Specialized cutaneous Schwann cells initiate pain sensation. *Science (1979)* **365**, 695–699.

Abraira, V. E. and Ginty, D. D. (2013). The Sensory Neurons of Touch. *Neuron* **79**, 618–639.

Abraira, V. E., Kuehn, E. D., Chirila, A. M., Springel, M. W., Toliver, A. A., Zimmerman, A. L., Orefice, L. L., Bai, L., Song, B. J., Bashista, K. A., et al. (2017). The Cellular and Synaptic Architecture of the Mechanosensory Dorsal Horn. *Cell* **168**, 295-310.e19.

Ackerley, R., Saar, K., McGlone, F. and Backlund Wasling, H. (2014a). Quantifying the sensory and emotional perception of touch: Differences between glabrous and hairy skin. *Front Behav Neurosci* **8**, 34.

Ackerley, R., Carlsson, I., Wester, H., Olausson, H. and Backlund Wasling, H. (2014b). Touch perceptions across skin sites: Differences between sensitivity, direction discrimination and pleasantness. *Front Behav Neurosci* **8**,.

Ackerley, R., Backlund Wasling, H., Liljencrantz, J., Olausson, H., Johnson, R. D. and Wessberg, J. (2014c). Human C-tactile afferents are tuned to the temperature of a skin-stroking caress. *Journal of Neuroscience* **34**, 2879–2883.

Adly, M. A., Assaf, H. A., Nada, E. A., Soliman, M. and Hussein, M. R. (2005). Human scalp skin and hair follicles express neurotrophin-3 and its high-affinity receptor tyrosine kinase C, and show hair cycle-dependent alterations in expression. *British Journal of Dermatology* **153**, 514–520.

Adly, M. A., Assaf, H. A., Nada, E. A., Soliman, M. and Hussein, M. (2006). Expression of nerve growth factor and its high-affinity receptor, tyrosine kinase A proteins, in the human scalp skin. *J Cutan Pathol* **33**, 559–568.

Adrian, E. D. (1926). The impulses produced by sensory nerve endings: Part I. *J Physiol* **61**, 49–72.

Agarwala, K. L., Ganesh, S., Amano, K., Suzuki, T. and Yamakawa, K. (2001). DSCAM, a highly conserved gene in mammals, expressed in differentiating mouse brain. *Biochem Biophys Res Commun* **281**, 697–705.

Allen Institute for Brain Science (2008a). Allen Developing Mouse Brain Atlas.

Allen Institute for Brain Science (2008b). Allen Mouse Spinal Cord Atlas.

Alonso, L. (2006). The hair cycle. *J Cell Sci* **119**, 391–393.

Alvarez-Buylla, R. and de Arellano, J. R. (1952). Local Responses in Pacinian Corpuscles. *American Journal of Physiology-Legacy Content* **172**, 237–244.

Anderson, G. R., Maxeiner, S., Sando, R., Tsetsenis, T., Malenka, R. C. and Südhof, T. C. (2017). Postsynaptic adhesion GPCR latrophilin-2 mediates target recognition in entorhinal-hippocampal synapse assembly. *Journal of Cell Biology* **216**, 3831–3846.

Antinucci, P., Nikolaou, N., Meyer, M. P. and Hindges, R. (2013). Teneurin-3 Specifies Morphological and Functional Connectivity of Retinal Ganglion Cells in the Vertebrate Visual System. *Cell Rep* **5**, 582–592.

Arimura, N., Okada, M., Taya, S., Dewa, K. I., Tsuzuki, A., Uetake, H., Miyashita, S., Hashizume, K., Shimaoka, K., Egusa, S., et al. (2020). DSCAM regulates delamination of neurons in the developing midbrain. *Sci Adv* **6**,.

Arvidsson, J. and Pfaller, K. (1990). Central projections of C4–C8 dorsal root ganglia in the rat studied by anterograde transport of WGA-HRP. *Journal of Comparative Neurology* **292**, 349–362.

Badea, T. C., Wang, Y. and Nathans, J. (2003). A noninvasive genetic/pharmacologic strategy for visualizing cell morphology and clonal relationships in the mouse. *The Journal of Neuroscience* **23**, 2314–22.

Badea, T. C., Hua, Z. L., Smallwood, P. M., Williams, J., Rotolo, T., Ye, X. and Nathans, J. (2009). New Mouse Lines for the Analysis of Neuronal Morphology Using CreER(T)/loxP-Directed Sparse Labeling. *PLoS One* **4**, e7859.

Bai, L., Lehnert, B. P., Liu, J., Neubarth, N. L., Dickendesher, T. L., Nwe, P. H., Cassidy, C., Woodbury, C. J. and Ginty, D. D. (2015). Genetic Identification of an Expansive Mechanoreceptor Sensitive to Skin Stroking. *Cell* **163**, 1783–1795.

Bandell, M., Story, G. M., Hwang, S. W., Viswanath, V., Eid, S. R., Petrus, M. J., Earley, T. J. and Patapoutian, A. (2004). Noxious cold ion channel TRPA1 is activated by pungent compounds and bradykinin. *Neuron* **41**, 849–857.

Bassett, E. A. and Wallace, V. A. (2012). Cell fate determination in the vertebrate retina. *Trends Neurosci* **35**, 565–573.

Bate, C. M. (1976). Pioneer neurones in an insect embryo. *Nature* **260**, 54–56.

Bautista, D. M., Movahed, P., Hinman, A., Axelsson, H. E., Sterner, O., Högestätt, E. D., Julius, D., Jordt, S. E. and Zygmunt, P. M. (2005). Pungent products from garlic activate the sensory ion channel TRPA1. *Proc Natl Acad Sci U S A* **102**, 12248–12252.

Bautista, D. M., Jordt, S. E., Nikai, T., Tsuruda, P. R., Read, A. J., Poblete, J., Yamoah, E. N., Basbaum, A. I. and Julius, D. (2006). TRPA1 Mediates the Inflammatory Actions of Environmental Irritants and Proalgesic Agents. *Cell* **124**, 1269–1282.

Bautista, D. M., Siemens, J., Glazer, J. M., Tsuruda, P. R., Basbaum, A. I., Stucky, C. L., Jordt, S. E. and Julius, D. (2007). The menthol receptor TRPM8 is the principal detector of environmental cold. *Nature* **448**, 204–208.

Beckmann, J., Schubert, R., Chiquet-Ehrismann, R. and Müller, D. J. (2013). Deciphering teneurin domains that facilitate cellular recognition, cell-cell adhesion, and neurite outgrowth using atomic force microscopy-based single-cell force spectroscopy. *Nano Lett* **13**, 2937–2946.

Berns, D. S., DeNardo, L. A., Pederick, D. T. and Luo, L. (2018). Teneurin-3 controls topographic circuit assembly in the hippocampus. *Nature* **554**, 328–333.

Bhattacherjee, A., Mu, Y., Winter, M. K., Knapp, J. R., Eggimann, L. S., Gunewardena, S. S., Kobayashi, K., Kato, S., Krizsan-Agbas, D. and Smith, P. G. (2017). Neuronal cytoskeletal gene dysregulation and mechanical hypersensitivity in a rat model of Rett syndrome. *Proc Natl Acad Sci U S A* **114**, E6952–E6961.

Blackshaw, S. E. (1981). Morphology and distribution of touch cell terminals in the skin of the leech. *J Physiol* **320**, 219–228.

Blackshaw, S. E., Nicholls, J. G. and Parnas, I. (1982). Expanded receptive fields of cutaneous mechanoreceptor cells after single neurone deletion in leech central nervous system. *J Physiol* **326**, 261–268.

Blair, E. A. and Erlanger, J. (1933). A COMPARISON OF THE CHARACTERISTICS OF AXONS THROUGH THEIR INDIVIDUAL ELECTRICAL RESPONSES. *American Journal of Physiology-Legacy Content* **106**, 524–564.

Blakemore, S. J., Tavassoli, T., Calò, S., Thomas, R. M., Catmur, C., Frith, U. and Haggard, P. (2006). Tactile sensitivity in Asperger syndrome. *Brain Cogn* **61**, 5–13.

Bodmer, R. and Jan, Y. N. (1987). Morphological differentiation of the embryonic peripheral neurons in Drosophila. *Roux's Archives of Developmental Biology* **196**, 69–77.

Bonnet, R. (1878). Studien über die Innervation der Haarbälge der Hausthiere. *Morphologisches Jahrbuch* **4**, 329–398.

Botchkarev, V. A., Welker, P., Albers, K. M., Botchkareva, N. v., Metz, M., Lewin, G. R., Bulfone-Paus, S., Peters, E. M. J., Lindner, G. and Paus, R. (1998a). A new role for neurotrophin-3: Involvement in the regulation of hair follicle regression (catagen). *American Journal of Pathology* **153**, 785–799.

Botchkarev, V. A., Botchkareva, N. v., Albers, K. M., van der Veen, C., Lewin, G. R. and Paus, R. (1998b). Neurotrophin-3 involvement in the regulation of hair follicle morphogenesis. *Journal of Investigative Dermatology* **111**, 279–285.

Botchkarev, V. A., Botchkareva, N. v., Peters, E. M. J. and Paus, R. (2004). Epithelial growth control by neurotrophins: Leads and lessons from the hair follicle. In *Progress in Brain Research*, pp. 493–513. Elsevier.

Botchkareva, N. v., Botchkarev, V. A., Chen, L. H., Lindner, G. and Paus, R. (1999). A role for p75 neurotrophin receptor in the control of hair follicle morphogenesis. *Dev Biol* **216**, 135–153.

Botchkareva, N. v., Botchkarev, V. A., Albers, K. M., Metz, M. and Paus, R. (2000). Distinct roles for nerve growth factor and brain-derived neurotrophic factor in controlling the rate of hair follicle morphogenesis. *Journal of Investigative Dermatology* **114**, 314–320.

Boucard, A. A., Maxeiner, S. and Südhof, T. C. (2014). Latrophilins function as heterophilic cell-adhesion molecules by binding to teneurins: Regulation by alternative splicing. *Journal of Biological Chemistry* **289**, 387–402.

Bressler, M. and Munger, B. L. (1983). Embryonic maturation of sensory terminals of primate facial hairs. *Journal of Investigative Dermatology* **80**, 245–260.

Brown, P. B. and Fuchs, J. L. (1975). Somatotopic representation of hindlimb skin in cat dorsal horn. *J Neurophysiol* **38**, 1–9.

Brown, A. G. and Iggo, A. (1967). A quantitative study of cutaneous receptors and afferent fibres in the cat and rabbit. *J Physiol* **193**, 707–733.

Brown, P. B., Gladfelter, W. E., Culberson, J. C., Covalt-Dunning, D., Sonty, R. v., Pubols, L. M. and Millecchia, R. J. (1991). Somatotopic organization of single primary afferent axon projections to cat spinal cord dorsal horn. *Journal of Neuroscience* **11**, 298–309.

Brumovsky, P., Villar, M. J. and Hökfelt, T. (2006). Tyrosine hydroxylase is expressed in a subpopulation of small dorsal root ganglion neurons in the adult mouse. *Exp Neurol* **200**, 153–165.

Burbridge, T. J., Xu, H. P., Ackman, J. B., Ge, X., Zhang, Y., Ye, M. J., Zhou, Z. J., Xu, J., Contractor, A. and Crair, M. C. (2014). Visual circuit development requires

patterned activity mediated by retinal acetylcholine receptors. *Neuron* **84**, 1049–1064.

Burgess, P. R., Petit, D. and Warren, R. M. (1968). Receptor types in cat hairy skin supplied by myelinated fibers. *J Neurophysiol* **31**, 833–848.

Buss, R. R., Sun, W. and Oppenheim, R. W. (2006). Adaptive roles of programmed cell death during nervous system development. *Annu Rev Neurosci* **29**, 1–35.

Cain, D. M., Khasabov, S. G. and Simone, D. A. (2001). Response properties of mechanoreceptors and nociceptors in mouse glabrous skin: An in vivo study. *J Neurophysiol* **85**, 1561–1574.

Carroll, S. L., Silos-Santiago, I., Frese, S. E., Ruit, K. G., Milbrandt, J. and Snider, W. D. (1992). Dorsal root ganglion neurons expressing trk are selectively sensitive to NGF deprivation in utero. *Neuron* **9**, 779–788.

Cascio, C. J. (2010). Somatosensory processing in neurodevelopmental disorders. *J Neurodev Disord* **2**, 62–69.

Caterina, M. J., Schumacher, M. A., Tominaga, M., Rosen, T. A., Levine, J. D. and Julius, D. (1997). The capsaicin receptor: A heat-activated ion channel in the pain pathway. *Nature* **389**, 816–824.

Conover, J. C., Erickson, J. T., Katz, D. M., Bianchi, L. M., Poueymirou, W. T., McClain, J., Pan, L., Helgren, M., Ip, N. Y., Boland, P., et al. (1995). Neuronal deficits, not involving motor neurons, in mice lacking BDNF and/or NT4. *Nature 1995 375:6528* **375**, 235–238.

Coste, B., Mathur, J., Schmidt, M., Earley, T. J., Ranade, S., Petrus, M. J., Dubin, A. E. and Patapoutian, A. (2010). Piezo1 and Piezo2 are essential components of distinct mechanically activated cation channels. *Science (1979)* **330**, 55–60.

Crowley, C., Spencer, S. D., Nishimura, M. C., Chen, K. S., Pitts-Meek, S., Armaninl, M. P., Ling, L. H., McMahon, S. B., Shelton, D. L., Levinson, A. D., et al. (1994). Mice lacking nerve growth factor display perinatal loss of sensory and sympathetic neurons yet develop basal forebrain cholinergic neurons. *Cell* **76**, 1001–1011.

Daigle, T. L., Madisen, L., Hage, T. A., Valley, M. T., Knoblich, U., Larsen, R. S., Takeno, M. M., Huang, L., Gu, H., Larsen, R., et al. (2018). A Suite of Transgenic Driver and Reporter Mouse Lines with Enhanced Brain-Cell-Type Targeting and Functionality. *Cell* **174**, 465-480.e22.

Danielian, P. S., Muccino, D., Rowitch, D. H., Michael, S. K. and McMahon, A. P. (1998). Modification of gene activity in mouse embryos in utero by a tamoxifen-inducible form of Cre recombinase. *Current Biology* **8**, 1323–1326.

Deckwerth, T. L., Elliott, J. L., Knudson, C. M., Johnson, E. M., Snider, W. D. and Korsmeyer, S. J. (1996). BAX is required for neuronal death after trophic factor deprivation and during development. *Neuron* **17**, 401–411.

del Toro, D., Carrasquero-Ordaz, M. A., Chu, A., Ruff, T., Shahin, M., Jackson, V. A., Chavent, M., Berbeira-Santana, M., Seyit-Bremer, G., Brignani, S., et al. (2020). Structural Basis of Teneurin-Latrophilin Interaction in Repulsive Guidance of Migrating Neurons. *Cell* **180**, 323-339.e19.

Depew, A. T., Aimino, M. A. and Mosca, T. J. (2018). The Tenets of Teneurin : Conserved Mechanisms Regulate Diverse Developmental Processes in the Drosophila Nervous System.

Dhaka, A., Earley, T. J., Watson, J. and Patapoutian, A. (2008). Visualizing cold spots: TRPM8-expressing sensory neurons and their projections. *Journal of Neuroscience* **28**, 566–575.

Dong, X., Han, S. K., Zylka, M. J., Simon, M. I. and Anderson, D. J. (2001). A diverse family of GPCRs expressed in specific subsets of nociceptive sensory neurons. *Cell* **106**, 619–632.

Durbec, P., Marcos-Gutierrez, C. v., Kilkenny, C., Grigoriou, M., Wartiowaara, K., Suvanto, P., Smith, D., Ponder, B., Costantini, F., Saarma, M., et al. (1996). GDNF signalling through the Ret receptor tyrosine kinase. *Nature* **381**, 789–793.

Edwards, J. S. (1977). Pathfinding by Arthropod Sensory Nerves. In *Identified Neurons and Behavior of Arthropods*, pp. 483–493. Boston, MA: Springer US.

Edwards, J. S., Chen, S. W. and Berns, M. W. (1981). Cercal sensory development following laser microlesions of embryonic apical cells in Acheta domesticus. *Journal of Neuroscience* **1**, 250–258.

Emoto, K., He, Y., Ye, B., Grueber, W. B., Adler, P. N., Jan, L. Y. and Jan, Y. N. (2004). Control of Dendritic Branching and Tiling by the Tricornered-Kinase/Furry Signaling Pathway in Drosophila Sensory Neurons. *Cell* **119**, 245–256.

Emoto, K., Parrish, J. Z., Jan, L. Y. and Jan, Y. N. (2006). The tumour suppressor Hippo acts with the NDR kinases in dendritic tiling and maintenance. *Nature 2006 443:7108* **443**, 210–213.

Ernfors, P., Lee, K. F. and Jaenisch, R. (1994a). Mice lacking brain-derived neurotrophic factor develop with sensory deficits. *Nature* **368**, 147–150.

Ernfors, P., Lee, K.-F., Kucera, J. and Jaenisch, R. (1994b). Lack of neurotrophin-3 leads to deficiencies in the peripheral nervous system and loss of limb proprioceptive afferents. *Cell* **77**, 503–512.

Farajian, R., Raven, M. A., Cusato, K. and Reese, B. E. (2004). Cellular positioning and dendritic field size of cholinergic amacrine cells are impervious to early ablation of neighboring cells in the mouse retina. *Vis Neurosci* **21**, 13–22.

Fariñas, I., Jones, K. R., Backus, C., Wang, X. Y. and Reichardt, L. F. (1994). Severe sensory and sympathetic deficits in mice lacking neurotrophin-3. *Nature* **369**, 658–661.

Fariñas, I., Yoshida, C. K., Backus, C. and Reichardt, L. F. (1996). Lack of neurotrophin-3 results in death of spinal sensory neurons and premature differentiation of their precursors. *Neuron* **17**, 1065–1078.

Faure, L., Wang, Y., Kastriti, M. E., Fontanet, P., Cheung, K. K. Y., Petitpré, C., Wu, H., Sun, L. L., Runge, K., Croci, L., et al. (2020). Single cell RNA sequencing identifies early diversity of sensory neurons forming via bi-potential intermediates. *Nature Communications 2020 11:1* **11**, 1–15.

Fleming, M. S., Vysochan, A., Paixão, S., Niu, J., Klein, R., Savitt, J. M. and Luo, W. (2015). Cis and trans RET signaling control the survival and central projection growth of rapidly adapting mechanoreceptors. *Elife* **2015**,.

Florence, S. L., Wall, J. T. and Kaas, J. H. (1988). The somatotopic pattern of afferent projections from the digits to the spinal cord and cuneate nucleus in macaque monkeys. *Brain Res* **452**, 388–392.

Florence, S. L., Wall, J. T. and Kaas, J. H. (1989). Somatotopic organization of inputs from the hand to the spinal gray and cuneate nucleus of monkeys with observations on the cuneate nucleus of humans. *Journal of Comparative Neurology* **286**, 48–70.

Florence, S. L., Wall, J. T. and Kaas, J. H. (1991). Central projections from the skin of the hand in squirrel monkeys. *Journal of Comparative Neurology* **311**, 563–578.

Fujita, Y., Nakanishi, T., Ueno, M., Itohara, S. and Yamashita, T. (2020). Netrin-G1 Regulates Microglial Accumulation along Axons and Supports the Survival of Layer V Neurons in the Postnatal Mouse Brain. *Cell Rep* **31**,.

Fundin, B. T., Arvidsson, J., Aldskogius, H., Johansson, O., Rice, S. N. and Rice, F. L. (1997a). Comprehensive immunofluorescence and lectin binding analysis of intervibrissal fur innervation in the mystacial pad of the rat. *Journal of Comparative Neurology* **385**, 185–206.

Fundin, B. T., Silos-Santiago, I., Ernfors, P., Fagan, A. M., Aldskogius, H., Dechiara, T. M., Phillips, H. S., Barbacid, M., Yancopoulos, G. D. and Rice, F. L. (1997b). Differential Dependency of Cutaneous Mechanoreceptors on Neurotrophins, trk Receptors, and P75 LNGFR. *Dev Biol* **190**, 94–116.

Garrett, A. M., Khalil, A., Walton, D. O. and Burgess, R. W. (2018). DSCAM promotes self-avoidance in the developing mouse retina by masking the functions of cadherin superfamily members. *Proc Natl Acad Sci U S A* **115**, E10216–E10224.

Gasser, H. S. and Erlanger, J. (1927). THE RÔLE PLAYED BY THE SIZES OF THE CONSTITUENT FIBERS OF A NERVE TRUNK IN DETERMINING THE FORM OF ITS ACTION POTENTIAL WAVE. *American Journal of Physiology-Legacy Content* **80**, 522–547.

Ge, X., Zhang, K., Gribizis, A., Hamodi, A. S., Sabino, A. M. and Crair, M. C. (2021). Retinal waves prime visual motion detection by simulating future optic flow. *Science (1979)* **373**,.

Gray, H. and Carter, H. v. (2010). *Anatomy, descriptive and surgical.* 15th ed. (ed. Pick, T. P.) and Howden, R.) New York: Barnes & Noble.

Green, D. P. (2021). The role of Mrgprs in pain. *Neurosci Lett* **744**, 135544.

Grimes, W. N., Seal, R. P., Oesch, N., Edwards, R. H. and Diamond, J. S. (2011). Genetic targeting and physiological features of VGLUT3+ amacrine cells. *Vis Neurosci* **28**, 381–392.

Grueber, W. B., Graubard, K. and Truman, J. W. (2001). Tiling of the body wall by multidendritic sensory neurons in Manduca sexta. *Journal of Comparative Neurology* **440**, 271–283.

Grueber, W. B., Jan, L. Y. and Jan, Y. N. (2002). Tiling of the Drosophila epidermis by multidendritic sensory neurons. *Development* **129**, 2867–78.

Grueber, W. B., Ye, B., Moore, A. W., Jan, L. Y. and Jan, Y. N. (2003). Dendrites of Distinct Classes of Drosophila Sensory Neurons Show Different Capacities for Homotypic Repulsion. *Current Biology* **13**, 618–626.

Halata, Z. (1993). Sensory innervation of the hairy skin (light-and electronmicroscopic study). *Journal of Investigative Dermatology* **101**,.

Han, C., Wang, D., Soba, P., Zhu, S., Lin, X., Jan, L. Y. and Jan, Y. N. (2012). Integrins Regulate Repulsion-Mediated Dendritic Patterning of Drosophila Sensory Neurons by Restricting Dendrites in a 2D Space. *Neuron* **73**, 64–78.

Han, L., Ma, C., Liu, Q., Weng, H. J., Cui, Y., Tang, Z., Kim, Y., Nie, H., Qu, L., Patel, K. N., et al. (2013). A subpopulation of nociceptors specifically linked to itch. *Nat Neurosci* **16**, 174–182.

Hardy, M. H. (1949). The development of mouse hair in vitro with some observations on pigmentation. *J Anat* **83**, 364–84, 3 pl.

Häring, M., Zeisel, A., Hochgerner, H., Rinwa, P., Jakobsson, J. E. T., Lönnerberg, P., la Manno, G., Sharma, N., Borgius, L., Kiehn, O., et al. (2018). Neuronal atlas of the dorsal horn defines its architecture and links sensory input to transcriptional cell types. *Nat Neurosci* 1.

Hasegawa, H., Abbott, S., Han, B. X., Qi, Y. and Wang, F. (2007). Analyzing somatosensory axon projections with the sensory neuron-specific Advillin gene. *Journal of Neuroscience* **27**, 14404–14414.

Hebb, D. O. (1949). *The Organization of Behavior; A Neuropsychological Theory*. 1st ed. Wiley.

Henry, A. M. and Hohmann, J. G. (2012). High-resolution gene expression atlases for adult and Developing Mouse Brain and Spinal Cord. *Mammalian Genome* **23**, 539–549.

Honma, Y., Kawano, M., Kohsaka, S. and Ogawa, M. (2010). Axonal projections of mechanoreceptive dorsal root ganglion neurons depend on Ret. *Development* **137**, 2319–2328.

Horch, K. W., Tuckett, R. P. and Burgess, P. R. (1977). A key to the classification of cutaneous mechanoreceptors. *Journal of Investigative Dermatology* **69**, 75–82.

Huckfeldt, R. M., Schubert, T., Morgan, J. L., Godinho, L., di Cristo, G., Huang, Z. J. and Wong, R. O. L. (2009). Transient neurites of retinal horizontal cells exhibit columnar tiling via homotypic interactions. *Nat Neurosci* **12**, 35–43.

Hunt, C. C. and McIntyre, A. K. (1960). An analysis of fibre diameter and receptor characteristics of myelinated cutaneous afferent fibres in cat. *J Physiol* **153**, 99–112.

Hursh, J. B. (1939). CONDUCTION VELOCITY AND DIAMETER OF NERVE FIBERS. *American Journal of Physiology-Legacy Content* **127**, 131–139.

Huxley, A. F. and Stämpfli, R. (1949). Evidence for saltatory conduction in peripheral myelinated nerve fibres. *J Physiol* **108**, 315–39.

Iggo, A. (1960). Cutaneous mechanoreceptors with afferent C fibres. *J Physiol* **152**, 337–353.

Iggo, A. and Muir, A. R. (1969). The structure and function of a slowly adapting touch corpuscle in hairy skin. *J Physiol* **200**, 763–796.

Inoue, K. I., Ozaki, S., Shiga, T., Ito, K., Masuda, T., Okado, N., Iseda, T., Kawaguchi, S., Ogawa, M., Bae, S. C., et al. (2002). Runx3 controls the axonal projection of proprioceptive dorsal root ganglion neurons. *Nat Neurosci* **5**, 946–954.

Jackson, V. A., Meijer, D. H., Carrasquero, M., van Bezouwen, L. S., Lowe, E. D., Kleanthous, C., Janssen, B. J. C. and Seiradake, E. (2018). Structures of Teneurin adhesion receptors reveal an ancient fold for cell-cell interaction. *Nat Commun* **9**, 1–9.

Jenkins, B. A. and Lumpkin, E. A. (2017). Developing a sense of touch. *Development* **144**, 4078–4090.

Johnson, K. O. and Hsiao, S. S. (1992). Neural Mechanisms of Tactual form and Texture Perception. *Annu Rev Neurosci* **15**, 227–250.

Jones, K. R., Fariñas, I., Backus, C. and Reichardt, L. F. (1994). Targeted disruption of the BDNF gene perturbs brain and sensory neuron development but not motor neuron development. *Cell* **76**, 989–999.

Joong Woo Leem, Willis, W. D. and Jin Mo Chung (1993). Cutaneous sensory receptors in the rat foot. *J Neurophysiol* **69**, 1684–1699.

Kaidoh, T. and Inoué, T. (2000). Intercellular Junctions Between Palisade Nerve Endings and Outer Root Sheath Cells of Rat Vellus Hairs. *J. Comp. Neurol* **420**, 419–427.

Keeley, P. W., Lebo, M. C., Vieler, J. D., Kim, J. J., st. John, A. J. and Reese, B. E. (2020). Interrelationships between Cellular Density, Mosaic Patterning, and Dendritic Coverage of VGluT3 Amacrine Cells. *The Journal of Neuroscience* JN-RM-1027-20.

Keshishian, H. (1980). The origin and morphogenesis of pioneer neurons in the grasshopper metathoracic leg. *Dev Biol* **80**, 388–397.

Kim, M. E., Shrestha, B. R., Blazeski, R., Mason, C. A. and Grueber, W. B. (2012). Integrins Establish Dendrite-Substrate Relationships that Promote Dendritic Self-Avoidance and Patterning in Drosophila Sensory Neurons. *Neuron* **73**, 79–91.

Kinugasa, T., Kudo, N. and Ozaki, S. (2006). Peripheral targets influence sensory-motor connectivity in the neonatal spinal cord: Sciatic nerve axotomy in Bax-deficient mice. *Neurosci Res* **54**, 30–37.

Kirschner, N. and Brandner, J. M. (2012). Barriers and more: Functions of tight junction proteins in the skin. *Ann N Y Acad Sci* **1257**, 158–166.

Klein, R., Smeyne, R. J., Wurst, W., Long, L. K., Auerbach, B. A., Joyner, A. L. and Barbacid, M. (1993). Targeted disruption of the trkB neurotrophin receptor gene results in nervous system lesions and neonatal death. *Cell* **75**, 113–122.

Klein, R., Silos-Santiago, I., Smeyne, R. J., Lira, S. A., Brambilla, R., Bryant, S., Zhang, L., Snider, W. D. and Barbacid, M. (1994). Disruption of the neurotrophin-3 receptor gene trkC eliminates la muscle afferents and results in abnormal movements. *Nature* **368**, 249–251.

Klose, M. and Bentley, D. (1989). Transient pioneer neurons are essential for formation of an embryonic peripheral nerve. *Science (1979)* **245**, 982–984.

Knibestöl, M. (1973). Stimulus—response functions of rapidly adapting mechanoreceptors in the human glabrous skin area. *J Physiol* **232**, 427–452.

Knudson, C. M., Tung, K. S. K., Tourtellotte, W. G., Brown, G. A. J. and Korsmeyer, S. J. (1995). Bax-deficient mice with lymphoid hyperplasia and male germ cell death. *Science (1979)* **270**, 96–99.

Koike-Kumagai, M., Yasunaga, K. I., Morikawa, R., Kanamori, T. and Emoto, K. (2009). The target of rapamycin complex 2 controls dendritic tiling of Drosophila sensory neurons through the Tricornered kinase signalling pathway. *EMBO Journal* **28**, 3879–3892.

Koltzenburg, M., Stucky, C. L. and Lewin, G. R. (1997). Receptive properties of mouse sensory neurons innervating hairy skin. *J Neurophysiol* **78**, 1841–1850.

Kopinke, D., Brailsford, M., Pan, F. C., Magnuson, M. A., Wright, C. V. E. and Murtaugh, L. C. (2012). Ongoing Notch signaling maintains phenotypic fidelity in the adult exocrine pancreas. *Dev Biol* **362**, 57–64.

Kramer, A. P. and Kuwada, J. Y. (1983). Formation of the receptive fields of leech mechanosensory neurons during embryonic development. *Journal of Neuroscience* **3**, 2474–2486.

Kramer, I., Sigrist, M., de Nooij, J. C., Taniuchi, I., Jessell, T. M. and Arber, S. (2006). A Role for Runx Transcription Factor Signaling in Dorsal Root Ganglion Sensory Neuron Diversification. *Neuron* **49**, 379–393.

Kuehn, E. D., Meltzer, S., Abraira, V. E., Ho, C.-Y. C.-Y. and Ginty, D. D. (2019). Tiling and somatotopic alignment of mammalian low-threshold mechanoreceptors. *Proceedings of the National Academy of Sciences* **116**, 9168–9177.

Kwon, C. H., Luikart, B. W., Powell, C. M., Zhou, J., Matheny, S. A., Zhang, W., Li, Y., Baker, S. J. and Parada, L. F. (2006). Pten Regulates Neuronal Arborization and Social Interaction in Mice. *Neuron* **50**, 377–388.

Lamballe, F., Klein, R. and Barbacid, M. (1991). trkC, a new member of the trk family of tyrosine protein kinases, is a receptor for neurotrophin-3. *Cell* **66**, 967–979.

Landy, M. A., Goyal, M. and Lai, H. C. (2021). Nociceptor subtypes are born continuously over DRG development. *Dev Biol* **479**, 91–98.

Lau, J., Minett, M. S., Zhao, J., Dennehy, U., Wang, F., Wood, J. N. and Bogdanov, Y. D. (2011). Temporal control of gene deletion in sensory ganglia using a tamoxifen-inducible Advillin-Cre-ERT2 recombinase mouse. *Mol Pain* **7**,.

Lawson, S. N. and Biscoe, T. J. (1979). Development of mouse dorsal root ganglia: an autoradiographic and quantitative study. *J Neurocytol* **8**, 265–274.

Leamey, C. A., Merlin, S., Lattouf, P., Sawatari, A., Zhou, X., Demel, N., Glendining, K. A., Oohashi, T., Sur, M. and Fässler, R. (2007). Ten_m3 Regulates Eye-Specific Patterning in the Mammalian Visual Pathway and Is Required for Binocular Vision. *PLoS Biol* **5**, e241.

Lee, T. and Luo, L. (1999). Mosaic analysis with a repressible neurotechnique cell marker for studies of gene function in neuronal morphogenesis. *Neuron* **22**, 451–461.

Lee, S. C. S., Cowgill, E. J., Al-Nabulsi, A., Quinn, E. J., Evans, S. M. and Reese, B. E. (2011). Homotypic Regulation of Neuronal Morphology and Connectivity in the Mouse Retina. *Journal of Neuroscience* **31**, 14126–14133.

Lehnert, B. P., Santiago, C., Huey, E. L., Emanuel, A. J., Renauld, S., Africawala, N., Alkislar, I., Zheng, Y., Bai, L., Koutsioumpa, C., et al. (2021). Mechanoreceptor synapses in the brainstem shape the central representation of touch. *Cell* **184**, 5608-5621.e18.

Lentz, S. I., Knudson, C. M., Korsmeyer, S. J. and Snider, W. D. (1999). Neurotrophins support the development of diverse sensory axon morphologies. *J Neurosci* **19**, 1038–1048.

Levine, A., Bashan-Ahrend, A., Budai-Hadrian, O., Gartenberg, D., Menasherow, S. and Wides, R. (1994). odd Oz: A novel Drosophila pair rule gene. *Cell* **77**, 587–598.

Lewin, G. R. and McMahon, S. B. (1991). Physiological properties of primary sensory neurons appropriately and inappropriately innervating skin in the adult rat. *J Neurophysiol* **66**, 1205–1217.

Lewis, A. E., Vasudevan, H. N., O'Neill, A. K., Soriano, P. and Bush, J. O. (2013). The widely used Wnt1-Cre transgene causes developmental phenotypes by ectopic activation of Wnt signaling. *Dev Biol* **379**, 229–234.

Li, L. and Ginty, D. D. (2014). The structure and organization of lanceolate mechanosensory complexes at mouse hair follicles. *Elife* **3**, e01901.

Li, L., Rutlin, M., Abraira, V. E., Cassidy, C., Kus, L., Gong, S., Jankowski, M. P., Luo, W., Heintz, N., Koerber, H. R., et al. (2011). The Functional Organization of Cutaneous Low-Threshold Mechanosensory Neurons. *Cell* **147**, 1615–1627.

Li, C. L., Li, K. cheng, Wu, D., Chen, Y., Luo, H., Zhao, J. R., Wang, S. shuang, Sun, M. ming, Lu, Y. J., Zhong, Y. qing, et al. (2016). Somatosensory neuron types identified by high-coverage single-cell RNA-sequencing and functional heterogeneity. *Cell Res* **26**, 83–102.

Liu, X., Ernfors, P., Wu, H. and Jaenisch, R. (1995). Sensory but not motor neuron deficits in mice lacking NT4 and BDNF. *Nature* **375**, 238–241.

Liu, Q., Vrontou, S., Rice, F. L., Zylka, M. J., Dong, X. and Anderson, D. J. (2007). Molecular genetic visualization of a rare subset of unmyelinated sensory neurons that may detect gentle touch. *Nat Neurosci* **10**, 946–948.

Liu, Q., Tang, Z., Surdenikova, L., Kim, S., Patel, K. N., Kim, A., Ru, F., Guan, Y., Weng, H. J., Geng, Y., et al. (2009). Sensory Neuron-Specific GPCR Mrgprs Are Itch Receptors Mediating Chloroquine-Induced Pruritus. *Cell* **139**, 1353–1365.

Liu, Q., Sikand, P., Ma, C., Tang, Z., Han, L., Li, Z., Sun, S., LaMotte, R. H. and Dong, X. (2012). Mechanisms of itch evoked by β-alanine. *Journal of Neuroscience* **32**, 14532–14537.

Loewenstein, W. R. (1961). ON THE 'SPECIFICITY' OF A SENSORY RECEPTOR. *J Neurophysiol* **24**, 150–158.

Longair, M. H., Baker, D. A. and Armstrong, J. D. (2011). Simple Neurite Tracer: open source software for reconstruction, visualization and analysis of neuronal processes. *Bioinformatics* **27**, 2453–2454.

Lou, S., Duan, B., Vong, L., Lowell, B. B. and Ma, Q. (2013). Runx1 Controls Terminal Morphology and Mechanosensitivity of VGLUT3-expressing C-Mechanoreceptors. *Journal of Neuroscience* **33**, 870–882.

Lou, S., Pan, X., Huang, T., Duan, B., Yang, F.-C., Yang, J., Xiong, M., Liu, Y. and Ma, Q. (2015). Incoherent Feed-Forward Regulatory Loops Control Segregation of C-Mechanoreceptors, Nociceptors, and Pruriceptors. *Journal of Neuroscience* **35**, 5317–5329.

Luo, W., Wickramasinghe, S. R., Savitt, J. M., Griffin, J. W., Dawson, T. M. and Ginty, D. D. (2007). A Hierarchical NGF Signaling Cascade Controls Ret-Dependent and Ret-Independent Events during Development of Nonpeptidergic DRG Neurons. *Neuron* **54**, 739–754.

Luo, W., Enomoto, H., Rice, F. L., Milbrandt, J. and Ginty, D. D. (2009). Molecular Identification of Rapidly Adapting Mechanoreceptors and Their Developmental Dependence on Ret Signaling. *Neuron* **64**, 841–856.

Lynn, B. and Carpenter, S. E. (1982). Primary afferent units from the hairy skin of the rat hind limb. *Brain Res* **238**, 29–43.

Ma, Q. (2010). Labeled lines meet and talk: Population coding of somatic sensations. *Journal of Clinical Investigation* **120**, 3773–3778.

Ma, Q., Fode, C., Guillemot, F. and Anderson, D. J. (1999). NEUROGENIN1 and NEUROGENIN2 control two distinct waves of neurogenesis in developing dorsal root ganglia. *Genes Dev* **13**, 1717–1728.

Mann, S. J. (1962). Prenatal formation of hair follicle types. *Anat Rec* **144**, 135–141.

Marmigère, F. and Ernfors, P. (2007). Specification and connectivity of neuronal subtypes in the sensory lineage. *Nat Rev Neurosci* **8**, 114–127.

Maslany, S., Crockett, D. P. and David Egger, M. (1992). Organization of cutaneous primary afferent fibers projecting to the dorsal horn in the rat: WGA-HRP versus B-HRP. *Brain Res* **569**, 123–135.

McKemy, D. D., Neuhausser, W. M. and Julius, D. (2002). Identification of a cold receptor reveals a general role for TRP channels in thermosensation. *Nature* **416**, 52–58.

Melançon, E., Liu, D. W. C., Westerfield, M. and Eisen, J. S. (1997). Pathfinding by identified zebrafish motoneurons in the absence of muscle pioneers. *Journal of Neuroscience* **17**, 7796–7804.

Meltzer, S., Comeau, K., Chirila, A., Osei-Asante, E., DeLisle, M., Zhang, Q., Kalish, B. T., Tasnim, A., Huey, E., Fuller, L. C., et al. (2022a). γ-Protocadherins control synapse formation and peripheral branching of touch sensory neurons. *bioRxiv* 2022.05.25.493080.

Meltzer, S., Comeau, K., Osei-Asante, E., Handler, A., Zhang, Q., Sano, C., Itohara, S. and Ginty, D. D. (2022b). A role for axon-glial interactions and Netrin-G1 signaling in the formation of low-threshold mechanoreceptor end organs. *bioRxiv* 2022.06.16.496261.

Merkel, Fr. (1875). Tastzellen und Tastkörperchen bei den Hausthieren und beim Menschen. *Archiv für Mikroskopische Anatomie* **11**, 636–652.

Metzger, D. and Chambon, P. (2001). Site- and time-specific gene targeting in the mouse. *Methods* **24**, 71–80.

Millard, C. L. and Woolf, C. J. (1988). Sensory innervation of the hairs of the rat hindlimb: A light microscopic analysis. *Journal of Comparative Neurology* **277**, 183–194.

Molliver, D. C., Wright, D. E., Leitner, M. L., Parsadanian, A. S., Doster, K., Wen, D., Yan, Q. and Snider, W. D. (1997). IB4-binding DRG neurons switch from NGF to GDNF dependence in early postnatal life. *Neuron* **19**, 849–861.

Müller-Röver, S., Handjiski, B., van der Veen, C., Eichmüller, S., Foitzik, K., McKay, I. A., Stenn, K. S. and Paus, R. (2001). A comprehensive guide for the accurate classification of murine hair follicles in distinct hair cycle stages. *Journal of Investigative Dermatology* **117**, 3–15.

Nagy, J. I. and Hunt, S. P. (1982). Fluoride-resistant acid phosphatase-containing neurones in dorsal root ganglia are separate from those containing substance P or somatostatin. *Neuroscience* **7**, 89–97.

Nakhai, H., Sel, S., Favor, J., Mendoza-Torres, L., Paulsen, F., Duncker, G. I. W. and Schmid, R. M. (2007). Ptf1a is essential for the differentiation of GABAergic and glycinergic amacrine cells and horizontal cells in the mouse retina. *Development* **134**, 1151–1160.

Niessen, C. M. (2007). Tight junctions/adherens junctions: Basic structure and function. *Journal of Investigative Dermatology* **127**, 2525–2532.

Nolte, J. (2009). *The Human Brain: An Introduction To Its Functional Anatomy*. 6th ed. Philadelphia: Mosby-Elsevier.

Norrsell, U. (2000). Magnus Gustaf Blix (1849-1904); neurophysiological, physiological, and engineering virtuoso. *J Hist Neurosci* **9**, 238–249.

Nowak, J. A., Polak, L., Pasolli, H. A. and Fuchs, E. (2008). Hair follicle stem cells are specified and function in early skin morphogenesis. *Cell Stem Cell* **3**, 33–43.

Nyberg, G. and Blomqvist, A. (1985). The somatotopic organization of forelimb cutaneous nerves in the brachial dorsal horn: An anatomical study in the cat. *Journal of Comparative Neurology* **242**, 28–39.

Odagaki, K., Kameda, H., Hayashi, T. and Sakurai, M. (2018). Mediolateral and dorsoventral projection patterns of cutaneous afferents within transverse planes of the mouse spinal dorsal horn. *Journal of Comparative Neurology* 1–13.

Olausson, H., Lamarre, Y., Backlund, H., Morin, C., Wallin, B. G., Starck, G., Ekholm, S., Strigo, I., Worsley, K., Vallbo, B., et al. (2002). Unmyelinated tactile afferents signal touch and project to insular cortex. *Nat Neurosci* **5**, 900–904.

Olausson, H. W., Cole, J., Vallbo, Å., McGlone, F., Elam, M., Krämer, H. H., Rylander, K., Wessberg, J. and Bushnell, M. C. (2008). Unmyelinated tactile afferents have opposite effects on insular and somatosensory cortical processing. *Neurosci Lett* **436**, 128–132.

Olson, W. and Luo, W. (2018). Somatotopic organization of central arbors from nociceptive afferents develops independently of their intact peripheral target innervation. *Journal of Comparative Neurology*.

Olson, W., Dong, P., Fleming, M. and Luo, W. (2016). The specification and wiring of mammalian cutaneous low-threshold mechanoreceptors. *Wiley Interdiscip Rev Dev Biol* **5**, 389–404.

Oppenheim, R. (1991). Cell Death During Development Of The Nervous System. *Annu Rev Neurosci* **14**, 453–501.

Oppenheim, R. W., Prevette, D., Qin-Wei, Y., Collins, F. and MacDonald, J. (1991). Control of embryonic motoneuron survival in vivo by ciliary neurotrophic factor. *Science (1979)* **251**, 1616–1618.

Orefice, L., Zimmerman, A., Chirila, A., Sleboda, S. J., Head, J. P. and Ginty, D. D. (2016). Peripheral Mechanosensory Neuron Dysfunction Underlies Tactile and Behavioral Deficits in Mouse Models of ASDs. *Cell* **166**, 299–313.

Pacini, F. (1835). Sopra un particolare genere di piccoli corpi globulosi scorpeti nel corpo umano da Filippo Pacini Aluno interna degli spedali riunti di Pistoia. *Sopra un*

Particolar Genere di Piccoli Corpi Globulosi Scoperti Nel Corpo Umano Da Filippo Pacini Alunno Interno degli Spedali Riunti di Pistoia.

Paré, M., Smith, A. M. and Rice, F. L. (2002). Distribution and terminal arborizations of cutaneous mechanoreceptors in the glabrous finger pads of the monkey. *Journal of Comparative Neurology* **445**, 347–359.

Patel, T. D., Jackman, A., Rice, F. L., Kucera, J. and Snider, W. D. (2000). Development of sensory neurons in the absence of NGF/TrkA signaling in vivo. *Neuron* **25**, 345–357.

Paus, R., Müller-Röver, S., van der Veen, C., Maurer, M., Eichmüller, S., Ling, G., Hofmann, U., Foitzik, K., Mecklenburg, L. and Handjiski, B. (1999). A comprehensive guide for the recognition and classification of distinct stages of hair follicle morphogenesis. *Journal of Investigative Dermatology* **113**, 523–532.

Payne, J., Middleton, J. and Fitzgerald, M. (1991). The pattern and timing of cutaneous hair follicle innervation in the rat pup and human fetus. *Developmental Brain Research* **61**, 173–182.

Pearce, J. M. S. (2005). The law of specific nerve energies and sensory spots. *Eur Neurol* **54**, 115–117.

Pederick, D. T., Lui, J. H., Gingrich, E. C., Xu, C., Wagner, M. J., Liu, Y., He, Z., Quake, S. R. and Luo, L. (2021). Reciprocal repulsions instruct the precise assembly of parallel hippocampal networks. *Science (1979)* **372**, 1068–1073.

Perl, E. R. (1968). Myelinated afferent fibres innervating the primate skin and their response to noxious stimuli. *J Physiol* **197**, 593–615.

Peters, E. M. J., Botchkarev, V. A., Müller-Röver, S., Moll, I., Rice, F. L. and Paus, R. (2002). Developmental timing of hair follicle and dorsal skin innervation in mice. *J Comp Neurol* **448**, 28–52.

Pike, S. H., Melancon, E. F. and Eisen, J. S. (1992). Pathfinding by zebrafish motoneurons in the absence of normal pioneer axons. *Development* **114**, 825–831.

Pittman, A. J., Law, M. Y. and Chien, C. bin (2008). Pathfinding in a large vertebrate axon tract: Isotypic interactions guide retinotectal axons at multiple choice points. *Development* **135**, 2865–2871.

Polansky, R. (2009). The Sorts of Intelligible Objects. In *Aristotle's De Anima*, pp. 473–480. Cambridge University Press.

Pomaville, M. B. and Wright, K. M. (2021). Immunohistochemical and Genetic Labeling of Hairy and Glabrous Skin Innervation. *Curr Protoc* **1**, 1–31.

Ranade, S. S., Woo, S. H., Dubin, A. E., Moshourab, R. A., Wetzel, C., Petrus, M., Mathur, J., Bégay, V., Coste, B., Mainquist, J., et al. (2014). Piezo2 is the major transducer of mechanical forces for touch sensation in mice. *Nature* **516**, 121–125.

Reese, B. E., Raven, M. A. and Stagg, S. B. (2005). Afferents and homotypic neighbors regulate horizontal cell morphology, connectivity, and retinal coverage. *Journal of Neuroscience* **25**, 2167–2175.

Rexed, B. (1952). The cytoarchitectonic organization of the spinal cord in the cat. *Journal of Comparative Neurology* **96**, 415–495.

Rexed, B. (1954). A cytoarchitectonic atlas of the spinal coed in the cat. *Journal of Comparative Neurology* **100**, 297–379.

Rice, F. L. and Albrecht, P. J. (2008). Cutaneous Mechanisms of Tactile Perception: Morphological and Chemical Organization of the Innervation to the Skin. In *The Senses: A Comprehensive Reference*, pp. 1–31.

Rotolo, T., Smallwood, P. M., Williams, J. and Nathans, J. (2008). Genetically-Directed, Cell Type-Specific Sparse Labeling for the Analysis of Neuronal Morphology. *PLoS One* **3**, e4099.

Rutlin, M., Ho, C. Y., Abraira, V. E., Cassidy, C., Bai, L., Woodbury, C. J. and Ginty, D. D. (2014). The Cellular and Molecular Basis of Direction Selectivity of Aδ-LTMRs. *Cell* **159**, 1640–1651.

Sagasti, A., Guido, M. R., Raible, D. W. and Schier, A. F. (2005). Repulsive Interactions Shape the Morphologies and Functional Arrangement of Zebrafish Peripheral Sensory Arbors. *Current Biology* **15**, 804–814.

Sauer, B. and Du, E. I. (1987). Functional expression of the cre-lox site-specific recombination system in the yeast Saccharomyces cerevisiae. *Mol Cell Biol* **7**, 2087.

Sauer, B. and Henderson, N. (1988). Site-specific DNA recombination in mammalian cells by the Cre recombinase of bacteriophage P1. *Proc Natl Acad Sci U S A* **85**, 5166.

Schindelin, J., Arganda-Carreras, I., Frise, E., Kaynig, V., Longair, M., Pietzsch, T., Preibisch, S., Rueden, C., Saalfeld, S., Schmid, B., et al. (2012). Fiji: An open-source platform for biological-image analysis. *Nat Methods* **9**, 676–682.

Schmucker, D., Clemens, J. C., Shu, H., Worby, C. A., Xiao, J., Muda, M., Dixon, J. E. and Zipursky, S. L. (2000). Drosophila Dscam is an axon guidance receptor exhibiting extraordinary molecular diversity. *Cell* **101**, 671–684.

Seal, R. P., Wang, X., Guan, Y., Raja, S. N., Woodbury, C. J., Basbaum, A. I. and Edwards, R. H. (2009). Injury-induced mechanical hypersensitivity requires C-low threshold mechanoreceptors. *Nature* **462**, 651–655.

Sennett, R., Wang, Z., Rezza, A., Grisanti, L., Roitershtein, N., Sicchio, C., Mok, K. W., Heitman, N. J., Clavel, C., Ma'ayan, A., et al. (2015). An Integrated Transcriptome Atlas of Embryonic Hair Follicle Progenitors, Their Niche, and the Developing Skin. *Dev Cell* **34**, 577–591.

Serbedzija, G. N., Fraser, S. E. and Bronner-Fraser, M. (1990). Pathways of trunk neural crest cell migration in the mouse embryo as revealed by vital dye labelling. *Development* **108**, 605–612.

Sharma, N., Flaherty, K., Lezgiyeva, K., Wagner, D. E., Klein, A. M. and Ginty, D. D. (2020). The emergence of transcriptional identity in somatosensory neurons. *Nature* **577**, 392–398.

Shehab, S. A. S. and Hughes, D. I. (2011). Simultaneous identification of unmyelinated and myelinated primary somatic afferents by co-injection of isolectin B4 and Cholera toxin subunit B into the sciatic nerve of the rat. *J Neurosci Methods* **198**, 213–221.

Shinohara, T., Harada, M., Ogi, K., Maruyama, M., Fujii, R., Tanaka, H., Fukusumi, S., Komatsu, H., Hosoya, M., Noguchi, Y., et al. (2004). Identification of a G

protein-coupled receptor specifically responsive to β-alanine. *Journal of Biological Chemistry* **279**, 23559–23564.

Silos-Santiago, I., Jeng, B. and Snider, W. D. (1995). Sensory afferents show appropriate somatotopy at the earliest stage of projection to dorsal horn. *Neuroreport* **6**, 861–865.

Silverman, J. D. and Kruger, L. (1990). Selective neuronal glycoconjugate expression in sensory and autonomic ganglia: relation of lectin reactivity to peptide and enzyme markers. *J Neurocytol* **19**, 789–801.

Simmons, A. B., Bloomsburg, S. J., Sukeena, J. M., Miller, C. J., Ortega-Burgos, Y., Borghuis, B. G. and Fuerst, P. G. (2017). DSCAM-mediated control of dendritic and axonal arbor outgrowth enforces tiling and inhibits synaptic plasticity. *Proceedings of the National Academy of Sciences* 201713548.

Smeyne, R. J., Klein, R., Schnapp, A., Long, L. K., Bryant, S., Lewin, A., Lira, S. A. and Barbacid, M. (1994). Severe sensory and sympathetic neuropathies in mice carrying a disrupted Trk/NGF receptor gene. *Nature 1994 368:6468* **368**, 246–249.

Soba, P., Zhu, S., Emoto, K., Younger, S., Yang, S. J., Yu, H. H., Lee, T., Jan, L. Y. and Jan, Y. N. (2007). Drosophila Sensory Neurons Require Dscam for Dendritic Self-Avoidance and Proper Dendritic Field Organization. *Neuron* **54**, 403–416.

Squinto, S. P., Stitt, T. N., Aldrich, T. H., Davis, S., Blanco, S. M., RadzieJewski, C., Glass, D. J., Masiakowski, P., Furth, M. E., Valenzuela, D. M., et al. (1991). trkB encodes a functional receptor for brain-derived neurotrophic factor and neurotrophin-3 but not nerve growth factor. *Cell* **65**, 885–893.

Stantcheva, K. K., Iovino, L., Dhandapani, R., Martinez, C., Castaldi, L., Nocchi, L., Perlas, E., Portulano, C., Pesaresi, M., Shirlekar, K. S., et al. (2016). A subpopulation of itch-sensing neurons marked by Ret and somatostatin expression. *EMBO Rep* **17**, 585–600.

Story, G. M., Peier, A. M., Reeve, A. J., Eid, S. R., Mosbacher, J., Hricik, T. R., Earley, T. J., Hergarden, A. C., Andersson, D. A., Hwang, S. W., et al. (2003). ANKTM1, a TRP-like channel expressed in nociceptive neurons, is activated by cold temperatures. *Cell* **112**, 819–829.

Stucky, C. L. and Lewin, G. R. (1999). Isolectin B4-positive and -negative nociceptors are functionally distinct. *Journal of Neuroscience* **19**, 6497–6505.

Sun, W., Gould, T. W., Vinsant, S., Prevette, D. and Oppenheim, R. W. (2003). Neuromuscular development after the prevention of naturally occurring neuronal death by Bax deletion. *Journal of Neuroscience* **23**, 7298–7310.

Sun, W., Winseck, A., Vinsant, S., Park, O. H., Kim, H. and Oppenheim, R. W. (2004). Programmed cell death of adult-generated hippocampal neurons is mediated by the proapoptotic gene bax. *Journal of Neuroscience* **24**, 11205–11213.

Sundberg, J. P., Peters, E. M. J. and Paus, R. (2005). Analysis of hair follicles in mutant laboratory mice. *The journal of investigative dermatology. Symposium proceedings / the Society for Investigative Dermatology, Inc. [and] European Society for Dermatological Research* **10**, 264–270.

Suzuki, H., Aoyama, Y., Senzaki, K., Vincler, M., Wittenauer, S., Yoshikawa, M., Ozaki, S., Oppenheim, R. W. and Shiga, T. (2010). Characterization of sensory neurons in the dorsal root ganglia of Bax-deficient mice. *Brain Res* **1362**, 23–31.

Symons, F. J., Barney, C. C., Byiers, B. J., McAdams, B. D., Foster, S. X. Y. L., Feyma, T. J., Wendelschafer-Crabb, G. and Kennedy, W. R. (2019). A clinical case–control comparison of epidermal innervation density in Rett syndrome. *Brain Behav* **9**,.

Takahashi, Y. and Nakajima, Y. (1996). Dermatomes in the rat limbs as determined by antidromic stimulation of sensory C-fibers in spinal nerves. *Pain* **67**, 197–202.

Takahashi, Y., Chiba, T., Kurokawa, M. and Aoki, Y. (2003). Dermatomes and the central organization of dermatomes and body surface regions in the spinal cord dorsal horn in rats. *Journal of Comparative Neurology* **462**, 29–41.

Takahashi-Iwanaga, H. (2000). Three-dimensional microanatomy of longitudinal lanceolate endings in rat vibrissae. *Journal of Comparative Neurology* **426**, 259–269.

Tasaki, I. (1939). THE ELECTRO-SALTATORY TRANSMISSION OF THE NERVE IMPULSE AND THE EFFECT OF NARCOSIS UPON THE NERVE FIBER. *American Journal of Physiology-Legacy Content* **127**, 211–227.

Tavares-Ferreira, D., Shiers, S., Ray, P. R., Wangzhou, A., Jeevakumar, V., Sankaranarayanan, I., Cervantes, A. M., Reese, J. C., Chamessian, A., Copits, B. A., et al. (2022). Spatial transcriptomics of dorsal root ganglia identifies molecular signatures of human nociceptors. *Sci Transl Med* **14**, eabj8186.

Thompson, C. L., Ng, L., Menon, V., Martinez, S., Lee, C. K., Glattfelder, K., Sunkin, S. M., Henry, A., Lau, C., Dang, C., et al. (2014). A high-resolution spatiotemporal atlas of gene expression of the developing mouse brain. *Neuron* **83**, 309–323.

Tiriac, A., Bistrong, K., Pitcher, M. N., Tworig, J. M. and Feller, M. B. (2022). The influence of spontaneous and visual activity on the development of direction selectivity maps in mouse retina. *Cell Rep* **38**, 110225.

Todd, A. J. (2010). Neuronal circuitry for pain processing in the dorsal horn. *Nature Reviews Neuroscience 2010 11:12* **11**, 823–836.

Tomchek, S. D. and Dunn, W. (2007). Sensory processing in children with and without autism: a comparative study using the short sensory profile. *American Journal of Occupational Therapy* **61**, 190–200.

Tritsch, N. X., Rodríguez-Contreras, A., Crins, T. T. H., Wang, H. C., Borst, J. G. G. and Bergles, D. E. (2010). Calcium action potentials in hair cells pattern auditory neuron activity before hearing onset. *Nat Neurosci* **13**, 1050–1052.

Trupp, M., Arenas, E., Fainzilber, M., Nilsson, A.-S., Sieber, B.-A., Grigoriou, M., Kilkenny, C., Salazar-Grueso, E., Pachnis, V., Arumäe, U., et al. (1996). Functional receptor for GDNF encoded by the c-ret proto-oncogene. *Nature* **381**, 785–789.

Tuckett, R. P., Horch, K. W. and Burgess, P. R. (1978). Response of cutaneous hair and field mechanoreceptors in cat to threshold stimuli. *J Neurophysiol* **41**, 138–149.

Tuttle, A., Drerup, C. M., Marra, M., McGraw, H. and Nechiporuk, A. v. (2019). Retrograde ret signaling controls sensory pioneer axon outgrowth. *Elife* **8**,.

Tworig, J. M. and Feller, M. B. (2022). Müller Glia in Retinal Development: From Specification to Circuit Integration. *Front Neural Circuits* **15**, 173.

Usoskin, D., Furlan, A., Islam, S., Abdo, H., Lönnerberg, P., Lou, D., Hjerling-Leffler, J., Haeggström, J., Kharchenko, O., Kharchenko, P. v., et al. (2015).

Unbiased classification of sensory neuron types by large-scale single-cell RNA sequencing. *Nat Neurosci* **18**, 145–153.

Vallbo, A. B., Olausson, H., Wessberg, J. and Kakuda, N. (1995). Receptive field characteristics of tactile units with myelinated afferents in hairy skin of human subjects. *J Physiol* **483**, 783–795.

Vogelbaum, M. A., Long, J. X. and Rich, K. M. (1998). Developmental regulation of apoptosis in dorsal root ganglion neurons. *J Neurosci* **18**, 8928–8935.

von Frey, M. (1894). Beiträge zur Physiologie des Schmerzsinns. *Ber Kgl Sächs Ges Wiss* **46**, 185–196.

von Frey, M. (1896). Untersuchungen über die Sinnesfunctionen der menschlichen Haut. *Abh. Sachs. Ges. Wiss.* **23**, 175–266.

Voos, A. C., Pelphrey, K. A. and Kaiser, M. D. (2013). Autistic traits are associated with diminished neural response to affective touch. *Soc Cogn Affect Neurosci* **8**, 378–386.

Vrontou, S., Wong, A. M., Rau, K. K., Koerber, H. R. and Anderson, D. J. (2013). Genetic identification of C fibres that detect massage-like stroking of hairy skin in vivo. *Nature* **493**, 669–673.

Wagner, R. and Meissner, G. (1852). Uber das Vorhandensein bisher unbekannter eigenthumlicher tastkorperchen (corpuscula tactus) in den gefuhlswarzchen der menschlichen haut und über die endausbreitung sensitiver nerven. *Nachrichten Georg-August-Uni. Konigl Ges Wiss Gotttingen* **2**, 17–30.

Weddell, G., Taylor, D. A. and Williams, C. M. (1955). Studies on the innervation of skin. III. The patterned arrangement of the spinal sensory nerves to the rabbit ear. *J Anat* **89**, 317–42.

Weston, J. A. (1970). The Migration and Differentiation of Neural Crest Cells. *Adv Morphog* **8**, 41–114.

White, F. A., Keller-Peck, C. R., Michael Knudson, C., Korsmeyer, S. J. and Snider, W. D. (1998). Widespread elimination of naturally occurring neuronal death in Bax-deficient mice. *Journal of Neuroscience* **18**, 1428–1439.

Winkelmann, R. K. (1959). THE INNERVATION OF A HAIR FOLLICLE. *Ann N Y Acad Sci* **83**, 400–407.

Wojtowicz, W. M., Flanagan, J. J., Millard, S. S., Zipursky, S. L. and Clemens, J. C. (2004). Alternative splicing of Drosophila Dscam generates axon guidance receptors that exhibit isoform-specific homophilic binding. *Cell* **118**, 619–633.

Woolf, C. J. and Fitzgerald, M. (1986). Somatotopic organization of cutaneous afferent terminals and dorsal horn neuronal receptive fields in the superficial and deep laminae of the rat lumbar spinal cord. *Journal of Comparative Neurology* **251**, 517–531.

Wu, H., Williams, J. and Nathans, J. (2012). Morphologic diversity of cutaneous sensory afferents revealed by genetically directed sparse labeling. *Elife* **1**, 1–20.

Yamaguchi, S. and Otsuguro, K. ichi (2017). A mechanically activated ion channel is functionally expressed in the MrgprB4 positive sensory neurons, which detect stroking of hairy skin in mice. *Neurosci Lett* **653**, 139–145.

Yau, K. W. (1976). Receptive fields, geometry and conduction block of sensory neurones in the central nervous system of the leech. *J Physiol* **263**, 513–538.

Yoshikawa, M., Senzaki, K., Yokomizo, T., Takahashi, S., Ozaki, S. and Shiga, T. (2007). Runx1 selectively regulates cell fate specification and axonal projections of dorsal root ganglion neurons. *Dev Biol* **303**, 663–674.

Zotterman, Y. (1939). Touch, pain and tickling: an electro-physiological investigation on cutaneous sensory nerves. *J Physiol* **95**, 1–28.

Zou, M., Li, S., Klein, W. H. and Xiang, M. (2012). Brn3a/Pou4f1 regulates dorsal root ganglion sensory neuron specification and axonal projection into the spinal cord. *Dev Biol* **364**, 114–127.